CR-73122

ME-TR-033-1

28

HEAT TRANSFER BETWEEN SURFACES IN CONTACT:

THE EFFECT OF LOW CONDUCTANCE INTERSTITIAL MATERIALS

PART I

EXPERIMENTAL VERIFICATION OF NASA TEST APPARATUS

by

P.A. Smuda, L.S. Fletcher, D.A. Gyorog

Research Sponsored by

AMES RESEARCH CENTER

NATIONAL AERONAUTICS AND SPACE ADMINISTRATION

under Grant NGR 03-001-033

Mechanical Engineering Department
Arizona State University
Tempe, Arizona

June, 1967

HEAT TRANSFER BETWEEN SURFACES IN CONTACT:

THE EFFECT OF LOW CONDUCTANCE INTERSTITIAL MATERIALS

PART I

EXPERIMENTAL VERIFICATION OF NASA TEST APPARATUS

by

P.A. Smuda, L.S. Fletcher, D.A. Gyorog

Revised pages

ME-TR-033-1

NASA-CR-73122

Research Sponsored by
Ames Research Center

NATIONAL AERONAUTICS AND SPACE ADMINISTRATION
under Grant NGR 03-001-~~003~~ 033

Mechanical Engineering Department
Arizona State University
Tempe, Arizona

June, 1967
(Revised April, 1968)

HEAT TRANSFER BETWEEN SURFACES IN CONTACT:

THE EFFECT OF LOW CONDUCTANCE INTERSTITIAL MATERIALS

PART I

EXPERIMENTAL VERIFICATION OF NASA TEST APPARATUS

Revised Pages

by

P.A. Smuda, L.S. Fletcher, D.A. Gyorog

ME-TR-033-1

NASA-CR-73122

Research Sponsored by
Ames Research Center

NATIONAL AERONAUTICS AND SPACE ADMINISTRATION
under Grant NGR 03-001-~~003~~ 033

Mechanical Engineering Department
Arizona State University
Tempe, Arizona

June, 1967
(Revised April, 1968)

ACKNOWLEDGMENTS

The authors gratefully acknowledge the financial support for this program which was furnished by the National Aeronautics and Space Administration.

The laboratory and vacuum facility were provided by Arizona State University, and the test apparatus was loaned by Ames Research Center.

The supervision and construction of substantial portions of the test facility were performed through the efforts of Jim Abbott, Jim Heywood, Joe Smith, Rod McIntyre, and the Arizona State University Development Shop.

The authors wish to express their appreciation to Dr. Joseph Galloway for his assistance with test specimen X-rays, and to AiResearch Manufacturing Company for assistance with surface roughness measurements.

Finally, sincere thanks are due Mrs. Shirley Lodwick, Mrs. Linda Williams, and Mrs. Esther Taylor for their assistance with the typing and publication of this report.

TABLE OF CONTENTS

LIST OF TABLES

LIST OF FIGURES

NOMENCLATURE

A	Area, sq ft
E	Voltage drop across heater, volts
F	Shape factor
h_c	Thermal contact conductance, Btu/hr sq ft ^{o}F
I	Current, amps
k	Thermal conductivity, Btu/hr ft ^{o}F
L	Load, lbs
P	Pressure, psi
q	Heat flux, Btu/hr
R_c	Thermal contact resistance, hr sq ft ^{o}F/Btu
T	Temperature, ^{o}F
ΔT	Temperature difference, ^{o}F
x	Axial length along specimen, in
Δx	Increment of length, in
δ	Uncertainty increment
ε	Emissivity
σ	Stephan-Boltzmann constant

Subscripts

0	Ambient conditions
1	Surface or Specimen 1
2	Surface or Specimen 2
a	Apparent contact area
i	Input value
j	Junction
m	Mean junction value

n	Net value
α	Specimen surface
β	Radiation shield surface

CHAPTER I

INTRODUCTION

Heat transfer within and between spacecraft components and structures presents a problem because the nature, magnitude, and direction of such transfer is difficult to predict accurately. Electronic components are directly mounted to liquid cooled panels in the Saturn V vehicle to provide for the disposal of generated heat. Similarly, the complete space vehicle with its environmental control sub-systems must be designed for adequate transfer of heat or for adequate thermal isolation. Because thermal control design requires information on the conductance of joints, the thermal conductance between metallic surfaces, with and without interstitial fillers, has become an important problem.

The prediction of thermal conductivity and heat flows in solids has been sufficiently established; in contrast, however, very little is known about the prediction of thermal conductance between contacting solids. A large number of investigations have been carried out in the field of thermal contact conductance, as evidenced by the bibliographies of Atkins (2)*, Gex (22), and Vidoni (35). In addition, critical reviews of the status of experimental and analytical developments in the area of heat transfer across interfaces of solids in contact have been presented by Hudack (24) and Minges (29). The results of these investigations and comparative studies indicate several different theories for predicting

*Numbers in parentheses designate references.

the thermal conductance of metallic contacts; but only two of these theories (9, 28) consider the effect of interstitial materials.

Specific results of experimental investigations of thermal conductance of metallic contacts with interstitial fillers are rather limited. The majority of the investigations on this subject have emphasized the improvement of the contact conductance by the use of high conductivity metal foils and greases. The limited availability of design information for contact heat transfer calculations with insulating interstitial filler materials suggests that additional studies are needed. The present experimental investigation will provide these conductance data in a vacuum environment for a number of low thermal conductance interstitial filler materials over a wide range of junction temperatures and loads.

The modes of heat transfer at the contacting interface are considered to be: 1) solid conduction through the true contact area; 2) gaseous, molecular, or other conduction through the interstitial fluid or filler; and 3) thermal radiation.

The thermal contact conductance is defined as

$$h_c = \frac{q/A}{T_1 - T_2}$$

where T_1 and T_2 are the temperatures of the bounding surfaces of the contact gap, and q/A is the heat flux per unit area.

Thus, contact resistance would be defined as

$$R_c = \frac{1}{h_c} = \frac{T_1 - T_2}{q/A}$$

PREVIOUS INVESTIGATIONS

The existing experimental work on the thermal conductance of metallic contacts with interstitial fillers in various environments has been reviewed. Several of the investigators have presented thoughts concerning the effect of interstitial fillers (9, 12, 17, 19, 21, 25, 28), however, their ideas are generally applicable only to specific conditions. Data are presented over a wide range of contact pressures, surface roughnesses, metallic specimens, interstitial fillers, and environmental conditions. The interstitial media used in these investigations may be divided into three different categories: solid, liquid, and gas. Environment pressures ranged from atmospheric to 10^{-6} Torr. A representative sample of metallic specimens and solid or grease interstitial fillers used in these investigations is listed in Table I.

Centinkale and Fishendon (9) developed an expression for predicting the contact conductance, with interstitial fillers, for an environmental pressure of one atmosphere. This expression was suitable only for ground surfaces with contact pressures from 19-800 psi. Use of other surface finishes would require re-evaluation of the constants in the equation.

Laming (28) proposed a semi-empirical approach based on "Simple Conductance Theory" where the total conductance is made up of the solid and fluid conductance. The expression developed was suitable for predicting the thermal contact conductance in a vacuum environment, and compared well with the data presented. Contact pressures ranged from 20-700 psi for this investigation.

Only a very limited amount of data for the contact conductance of metallic joints with interstitial fillers is tabulated for ready use, and

TABLE I

PREVIOUS INVESTIGATIONS

Ref.	Author	Metallic Specimen	Interstitial Material
8	Brunot and Buckland	AISI M27 Steel	Steel Shim (22 mil) Aluminum Shim (31 mil) Aluminum Foil (3-14 mil)
36	Wells and Ryder	SAE 4140 Steel AMS 4846 Bronze Aluminum	Texaco AEO-120 Oil
28	Laming	Steel Brass Aluminum	Air Glycerol Water
14	Dailey and Kaspareck	6061-T6 Aluminum AZ91C Magnesium Almag 35 Aluminum 356	Silicone Vacuum Grease Indium Foil Aluminum Foil
12	Cunnington	6061-T4 Aluminum AZ-31 Magnesium	Indium Foil Silicone Vacuum Grease Dow Corning DC-340
25	Jansson	Aluminum Beryllium	Epoxy Cement Indium Foil Lead Foil Aluminum Leaf Gold Leaf
21	Fried and Costello	AZ-31 Magnesium 2024-T3 Aluminum	Lead Foil Aluminum Foil Copper Screen
17,19	Fried	2024-T4 Aluminum 304 Stainless Beryllium AZ-31 Magnesium	Silicone Vacuum Grease Silicone Rubber
9	Cetinkale and Fishenden	Steel Brass Aluminum	Air Spindle Oil Glycerol
5	Barzelay	2024-T6 Aluminum 2024-T3 Aluminum Inconel X	Aluminum Sheet Brass Shim Asbestos Sheet Teflon Sheet Zinc Chromate Primer
10	Clausing and Chao	Brass AZ-31B Magnesium 303 Stainless 2024-T4 Aluminum	Silicone Vacuum Grease

generally only trends are shown. Values presented are rarely defined in similar manners, and test conditions are not uniform; thus there is very little correlation. But even more important is the lack of design information on the use of low conductance interstitial materials to provide thermal isolation. Figure 1 indicates the variation of contact conductance as a function of some high conductance interstitial materials and apparent load pressures for Aluminum specimens.

INVESTIGATION OBJECTIVE

The primary objective of this investigation is to provide information to be used in predicting the thermal contact resistance for the case of thermal barriers (insulators) inserted between plane parallel metal surfaces. The investigation will be composed of three distinct parts:

Part I - Assembly and experimental verification of the NASA test apparatus

Part II - Selection of promising interstitial materials

Part III - Detailed study of selected materials

The test apparatus to be used in this investigation was designed and constructed at the Ames Research Center and is on loan for the purposes of this investigation.

After assembly of the test apparatus, the initial tests (Part I) were conducted with Armco Iron specimens in contact in a vacuum environment. The purpose of these tests was to check the validity of the measured data, the magnitude of the heat loss, and the deviation from one-dimensional heat flow. Aluminum specimens in direct contact were used next. The data obtained from the measurements with Aluminum contacts were compared with

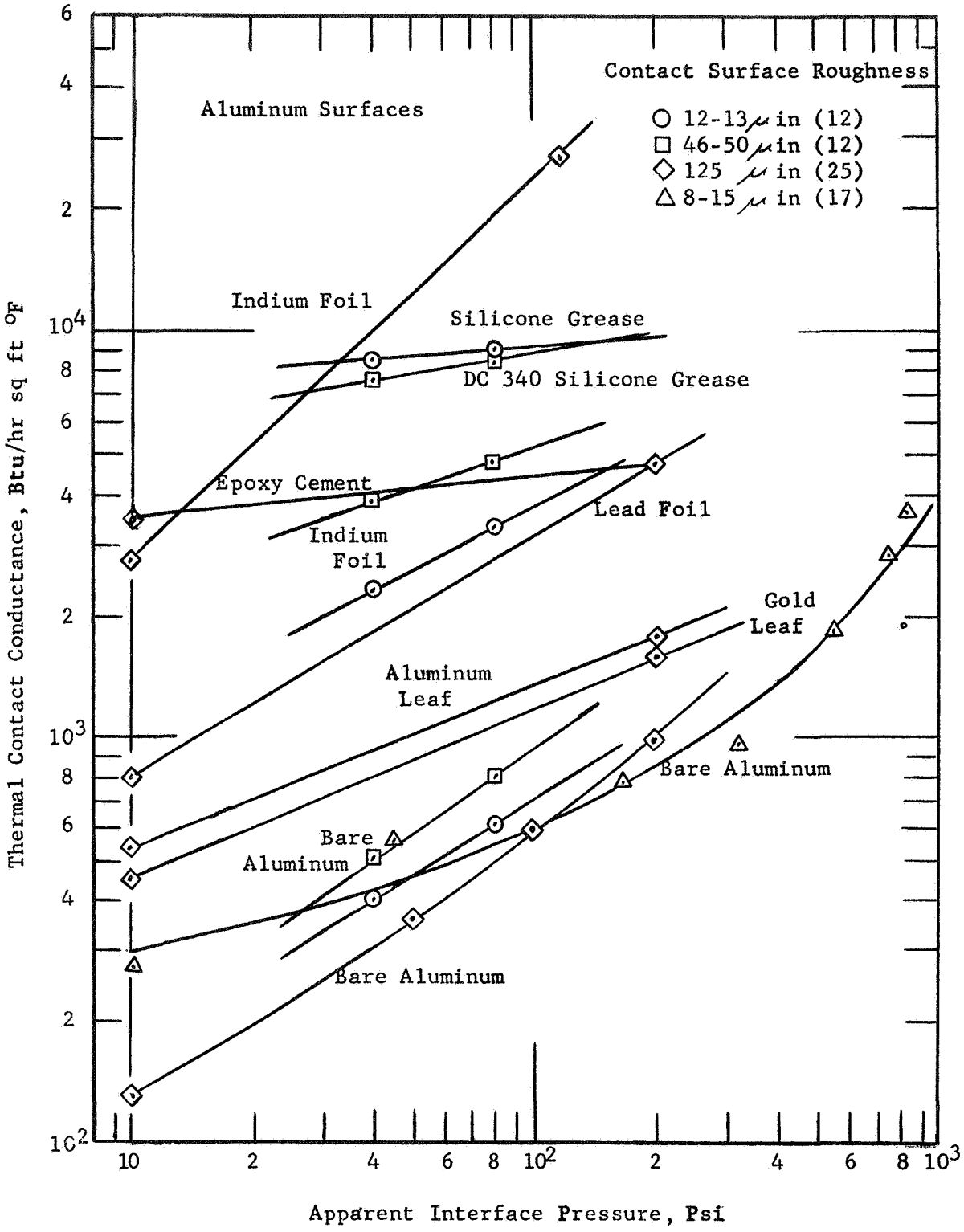

Figure 1. The Variation of Thermal Contact Conductance with Apparent Interface Pressure for Selected Interstitial Materials.

the results of other investigators (10, 19, 37) as a further check on the reliability of the experimental data. Techniques were developed (for specimen surface preparation, thermocouple installation, specimen alignment and loading, etc.) and the apparatus was modified (to include additional thermocouples, insulation, radiation shields, guard heaters, etc.) in order to assure satisfactory data. In this investigation, satisfactory data means that the overall experimental error in the values of contact resistance (or conductance) is less than 10 to 15 percent.

CHAPTER II

DESIGN OF THE NASA APPARATUS

The analysis and review of previous thermal contact conductance investigations indicates that in addition to experimental studies of interstitial filler materials, several areas warrant investigation. Of major importance would be first, an explanation of the directionality of the contact conductance according to the direction of heat flow across an interface between dissimilar metals, including supporting experimental results. Second, an analytical explanation of the basic heat transfer mechanisms at an interface, with substantiating experimental data. The experimental apparatus required to investigate thermal contact conductance should be flexible enough to subject the test samples to various environmental and physical conditions, and sophisticated enough to insure the accurate measurement of these conditions. An apparatus was designed to include as many of these criteria as possible. The general specifications for the experimental apparatus were based on the experience and recommendations of Blum (7), Clausing and Chao (10), Fried (18, 19, 20), Stubstad (34), and others.

A vacuum chamber was incorporated into the experimental apparatus for three primary reasons. First, the interstitial fluid present in an interface transfers heat across the junction by conduction. Thus, it was desirable to perform tests with and without an interstitial fluid to determine its relative effect on interface conductance. Second, contact conductance is of vital concern to the space industry because it has a

substantial effect on the heat transfer in, and the resultant heat dissipation from space vehicles. Hence, it was necessary to investigate interface conductance in a vacuum environment. Third, filler materials are often placed in an interface to improve or retard the transfer of heat across the junction. Therefore, it was desired to study the relative effects of various filler materials in the absence of an interstitial fluid and to ascertain the effect that a vacuum environment had on the various substances used.

Shlykov and Ganin (33) and Stubstad (34) have shown that the convection or conductivity effect of gas begins to decrease at approximately 70 Torr and measurably disappears at 10^{-1} Torr. Other investigators have stated that a vacuum in the range of 10^{-4} Torr is sufficient to negate the effect of interstitial fluids. Since a small pressure gradient exists in any vacuum facility (15, 27), a system capable of operating in the range of 10^{-5} Torr or lower was deemed desirable.

Design of the test specimens was a major consideration for several reasons. First, its size and shape dictated the design criteria for most of the other test section components. Second, the technique used to evaluate the thermal contact conductance required uniform heat flux above and below the interface. Finally, it was desirable to keep the geometry of the specimen as simple as possible to facilitate fabricating the relatively large number required.

A basic cylindrical configuration was specified and installed as a vertical column under axial load with the contacting surfaces located at the mid-point of the column. A uniform heat flux above and below the interface was achieved by minimizing the surface heat losses from the

specimen and by making the constant cross-sectional area of the specimen long enough to allow the temperature gradients to become uniform. Most spacecraft components and structures are fabricated from light weight metallic materials, such as aluminum, magnesium, and beryllium. Aluminum 2024-T4* was selected as a suitable test specimen material, since published data for bare metal junctions were available for comparison (10, 19, 38). Likewise, in keeping with other investigators (20, 28, 31), test samples one inch in diameter were specified.

It is well known that the thermal resistance of a metal-to-metal interface in a vacuum is a function of load pressure, junction temperature, material properties, and surface finish. Also, in some cases of dissimilar metals in contact there is an indication (4, 11, 30, 31) that the magnitude of the heat flux may have some influence on the thermal resistance. With an interstitial filler material at the junction, other variables should be considered. These are the interstitial material properties, dimensions, shape, porosity, etc. Depending on the type of interstitial filler, it

*The specimens used in this investigation were machined from 1 5/8 inch diameter aluminum rod. After consulting with representatives of Reynolds, Alcoa, and Kaiser Aluminum Companies, it was found that Aluminum 2024-T4 rod is not manufactured larger than 7/16 inch diameter, and that larger diameter rod is often called T4 but is in actuality T351. According to the Reynolds representative, the thermal properties are considered to be the same for Aluminum 2024-T4 and 2024-T351.

The ASTM Report on Physical Properties of Metals and Alloys (16) indicates thermal conductivity data for Aluminum 2024 with various heat treatments, and all data are combined to yield one curve for thermal conductivity as a function of temperature. The thermal conductivity data obtained in the present investigation compare favorably with results presented in ASTM-296. Thus, the aluminum material used may be considered 2024-T4. For purposes of convenience, it will be referred to as Aluminum 2024.

may be found that certain variables have very little, if any, effect on the thermal resistance. To demonstrate the influence of surface finish, three different finishes, typical of particular machining operations were chosen: ground (5 - 15 micro-inches, rms); mill cut (15 - 70 micro-inches, rms); and lathe cut (70 - 120 micro-inches, rms). However, for verification of the NASA test apparatus, machine lapped surfaces were used.

The finish of bare junction surfaces has a strong effect on the interface conductance (6, 37, 38). The surface finish is described by the rms roughness and the waviness or flatness deviation. These are two separate and distinct characteristics. Surface roughness is considered to be a measure of the small surface perturbations which result from the action of the finishing process. On the other hand, surface waviness is considered to be the variations in the overall surface configuration that result from such things as warping or periodic oscillations in the finishing process. The specimen surface measurements for this investigation were made using a Bendix Micrometrical Proficorder and profilometer. It should be noted that the results given by Proficorders and profilometers represent only one trace across the specimen and may or may not be representative of the complete test surface.

Rogers (31) and Clausing (11) reported a change in the interface conductance between dissimilar metals with the direction of heat flux across the junction. To make the test section suitable to the investigation of this phenomenon, it was decided to make the source and the sink flexible enough so that the specimens could be interchanged.

Possible aerospace applications of immediate interest dictated a temperature test range of $-100^{\circ}F$ to $600^{\circ}F$. Based on this requirement, a

review of the available literature was conducted to determine the most suitable method of temperature measurement for this particular situation. In view of the information obtained from Baker (3), and Dahl (13), electrical resistance thermometers and thermoelectric thermometry were considered. Thermoelectric thermometry was selected because of its relative flexibility, availability, and economy. The use of only one type of thermocouple in the system was considered desirable to simplify the instrumentation of the test section, and to simplify the installation of thermocouple vacuum feedthroughs. In view of the characteristics of the various types of thermocouples, copper-constantan was selected since it is easy to fabricate and dependable over the range of temperatures from -300°F to 750°F with an accuracy of $\pm$ 0.5°F when carefully calibrated.

Based on the recommendations of Clausing and Chao (10), number 30 gage, high accuracy thermocouple wire was decided upon. A heavier gage wire would have been more durable, but the smaller gage wire would minimize the conduction of heat along the wire away from the specimen. In addition, smaller wires tend to exhibit adverse EMF characteristics due to the wire-drawing process.

In light of the requirements established by the heat source location, the temperature criteria and the dimensions of the specimens, a 300 watt Acrawatt strap type circumferential heater was selected as the source. The heat source was insulated and surrounded by a guard heater to reduce radial heat losses. The heat sink was constructed from a cylindrical copper block, drilled and tapped to accept the threaded end of the metal test specimen. A copper cooling coil was soldered to the outside surface of the copper cylinder. Several different coolant fluids, such as water, air, and

liquid nitrogen, are used to provide a wide variation in the test temperatures.

The apparent mechanical pressure applied to an interface has a major influence on the resulting thermal contact conductance. Therefore, the experimental apparatus had to incorporate a means of applying a variable load to the test junction, and adequate instrumentation to measure the load accurately. In typical Saturn applications, contact pressures of approximately 1000 psi between dissimilar light metal surfaces are expected (14). The resistance to heat transfer created by a junction at this pressure, is usually small enough to be of little concern. In most applications where the effects of contact conductance are considered, apparent pressures of 1000 psi are rarely exceeded. Thus, it was decided that the loading mechanism should be suitable for variation of the apparent interface pressure over the range of approximately 0 to 1000 psi. The area of the interface formed by the specimens was 0.785 square inches. Hence, the loading mechanism should be capable of transmitting loads up to at least 780 pounds. It was also decided that the load mechanism should enable specimen contact to be made after the vacuum chamber is evacuated in order to facilitate outgassing of the junction.

For load application to the test specimens, a high pressure Nitrogen gas bellows chamber was selected as an integral part of the test apparatus. The Nitrogen bellows simplified specimen loading and permitted relatively accurate load monitoring. The effect of load pressure was determined by varying the nitrogen gas pressure in the bellows-chamber. In the present sense, load pressure is defined as the load force divided by the cross-sectional area of the cylindrical Aluminum test specimens. The load force

was determined from a compression load cell located in the specimen column.

The final test section configuration was relatively simple and flexible. The components were fabricated from materials particularly well suited for use in a vacuum environment. A schematic diagram of the resulting apparatus is presented in Figure 2. Specific details of thermocouple installation, specimen load column assembly, and other apparatus specifications are discussed in the following chapters. Drawings of selected components are presented in Appendix A.

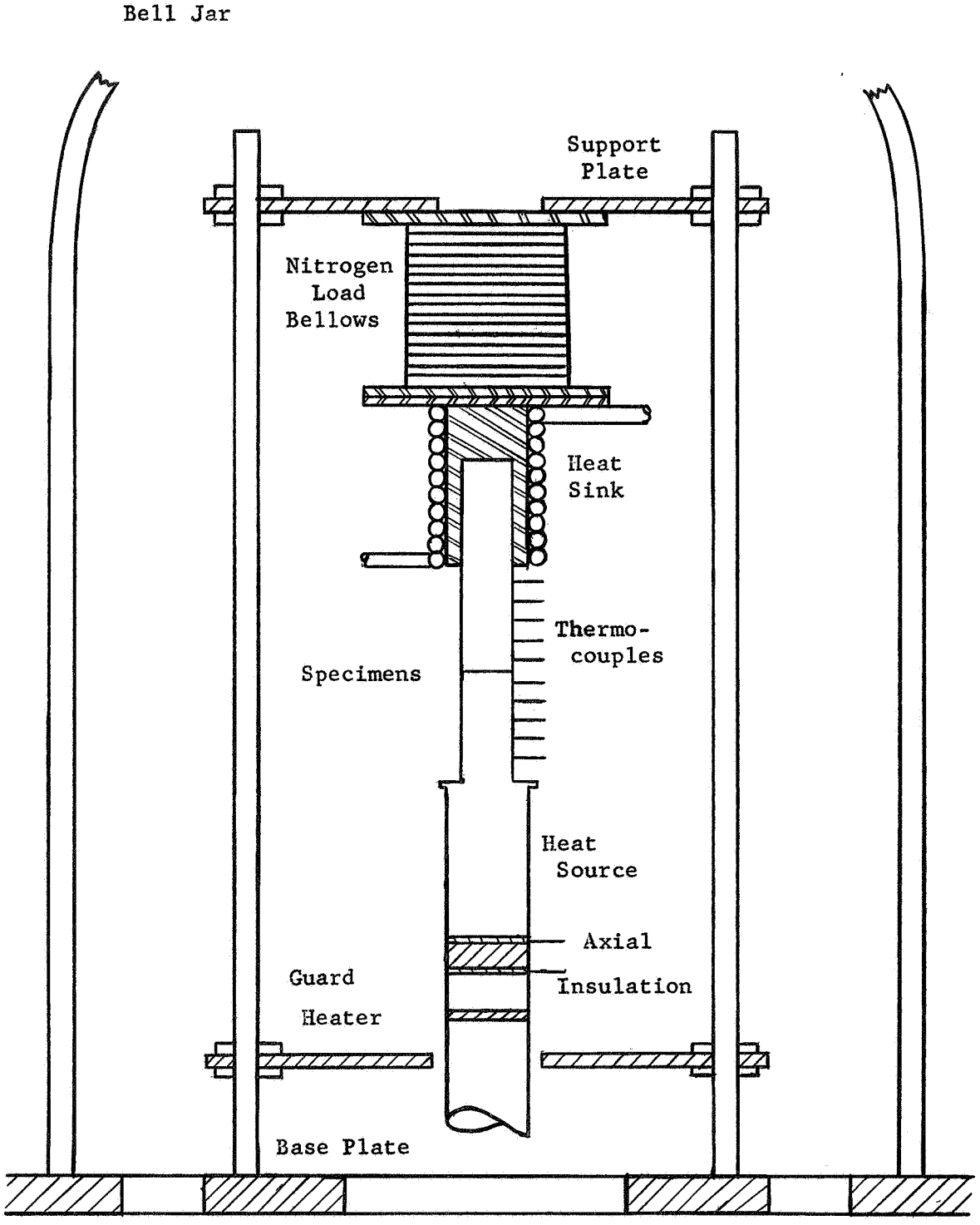

Figure 2. Schematic Diagram of the NASA Experimental Apparatus.

CHAPTER III

VACUUM FACILITY AND INSTRUMENTATION

The vacuum facility and associated instrumentation were designed and constructed specifically for the investigation of thermal contact conductance. The facility includes many flexible features offering a wide variation of environmental and physical test conditions. A photograph of the facility is shown in Figure 3. The following sections will be only a general description of the facility; a more detailed description has been given by Abbott (1).

THE VACUUM SYSTEM

The vacuum system is composed of a vacuum chamber, an oil diffusion pump, a mechanical forepump, a chevron cooling baffle, high vacuum valves, and the necessary vacuum measuring devices. The system was fabricated from commercially manufactured components combined with accessories constructed locally. A schematic of the system is illustrated in Figure 4. Dry nitrogen was introduced into the vacuum chamber for purposes of purging the air from the system, and for providing an oxygen free atmosphere.

The vacuum chamber was composed of a bell jar and a base plate with a vacuum port and ten vacuum feedthroughs. A pyrex bell jar was selected in the interest of economy and visibility. The bell jar is 18 inches in diameter and 30 inches high. Occasionally, glass bell jars will implode under the influence of a vacuum. To reduce the hazard associated with such an occurrence, a metal guard was fabricated to cover the bell jar. A small

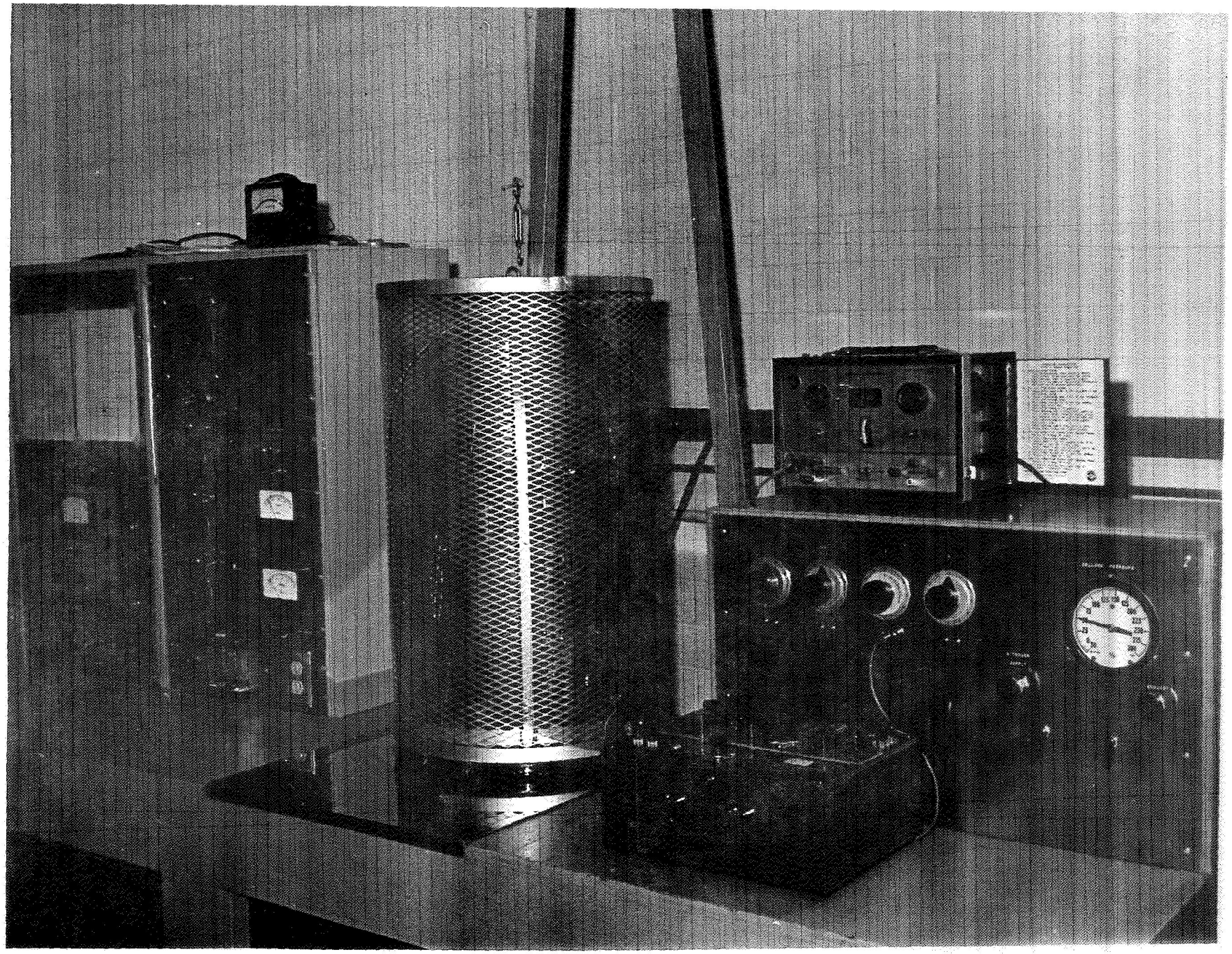

Figure 3. Photograph of the Thermal Contact Resistance Test Facility.

(1) Bell Jar
(2) Nitrogen Load Bellows Passthrough
(3) Passthrough Bellows
(4) Entry Gland
(5) High Vacuum Valve
(6) Water Cooling Baffle
(7) Oil Diffusion Pump
(8)(12)(14) Vacuum Thermocouple Gage
(9)(13) Vacuum Valves
(10) Ionization Gage
(11) Nitrogen Bleed Port
(15) Mechanical Pump

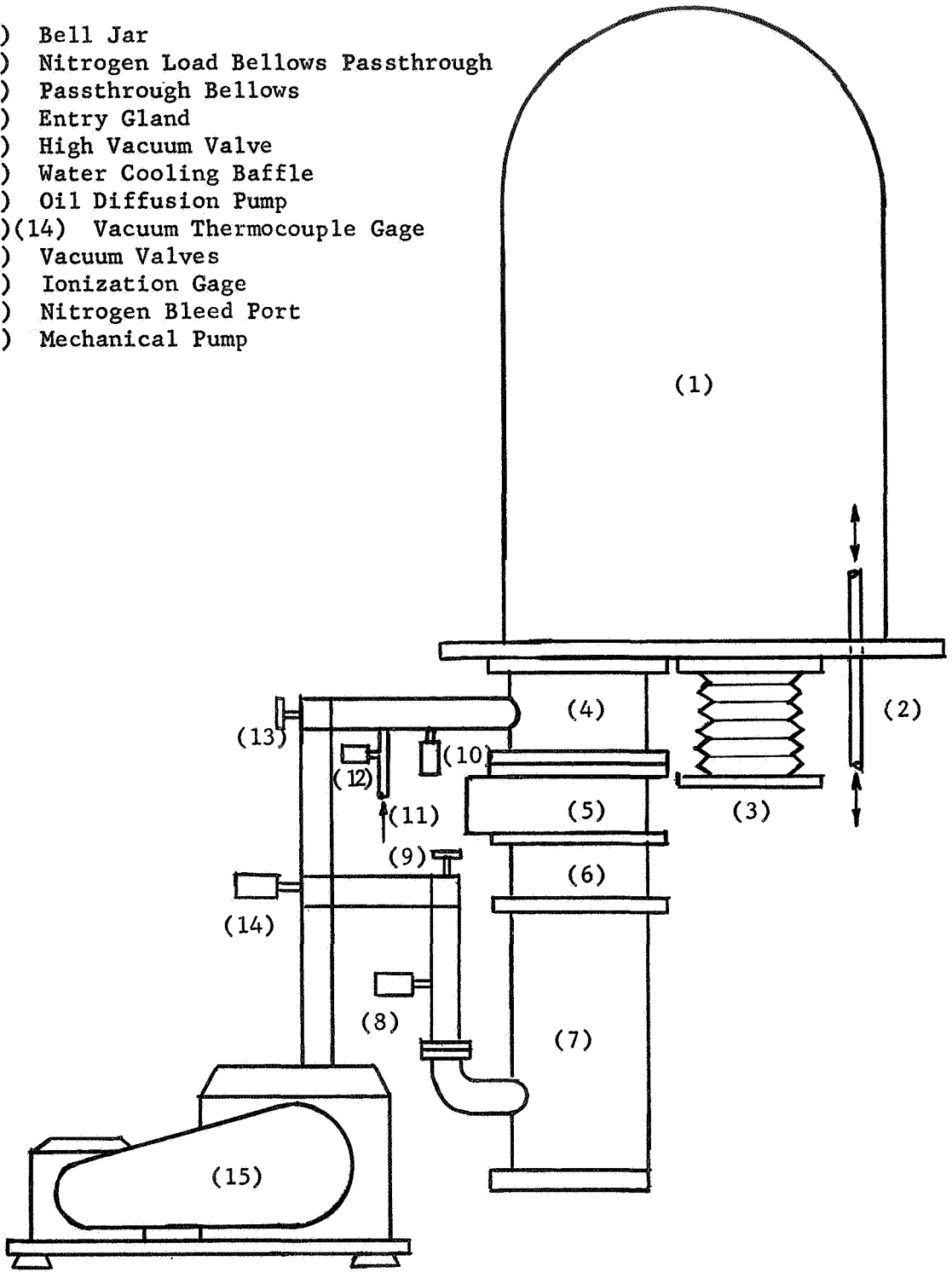

Figure 4. Schematic of the Vacuum System.

electric hoist was built into the system to lift the bell jar assembly in order to provide easy access to the test section. The bell jar was sealed to the base plate with a neoprene gasket. The numerous types of base plates available commercially all had the vacuum port located in the center. This feature was not compatible with the loading mechanism required. Therefore, a base plate was designed to fit the specifications of the test section. (Note drawing in Appendix A). It was manufactured locally from high carbon steel which was chrome plated, in order to eliminate oxidation and outgassing from the steel. All of the ten feedthroughs were made from stainless steel. To provide as much flexibility as possible, five universal feedthroughs manufactured by Cooke Vacuum, Inc., were used. Three of these were used to seal the passages for the test section support rods. The electrical heater input and the high pressure Nitrogen line to the load bellows were mounted in the remaining universal feedthroughs.

One Vacumen Corporation thermocouple feedthrough with a capacity of 24 Copper-Constantan thermocouples was used. A doublepass fluid feedthrough was used to circulate cooling fluid into the vacuum chamber. A stainless steel bellows was installed to transmit the loading force into the system. Another feedthrough was used as a vacuum release valve by seating an o-ring in the outer end of it and sealing the end with a threaded cap. The remaining feedthrough was a blank that is to be replaced with a doublepass liquid nitrogen feedthrough when needed. All the feedthroughs were sealed to the base plate with Buna-N O-rings.

Oil vapor diffusion pumps have no moving parts but instead depend upon the motion of the oil vapor for pumping. For a complete discussion of how a diffusion pump operates, the reader is directed to Dushman (15).

There are several working fluids available for diffusion pumps, but silicone oils are recommended. They have a vapor pressure in the range of 10^{-7} Torr or lower and are not subject to oxidation as are hydrocarbon oils. A Dresser Vacuum Model DPD 4-1000 diffusion pump was selected for the vacuum system. The pump was charged with Dow Corning 704 diffusion pump oil.

A Cenco Hyvac 45 mechanical pump was used as the roughing pump. It is a two-stage pump with a free air capacity of 16 cfm with an adjustable gas-ballast. The capacity of the pump was approximately twice that specified for the diffusion pump under normal operating conditions. The greater capacity was necessary to overcome the relatively high outgassing rate associated with some of the materials, such as insulation, used in the test section.

Cooling baffles or traps may be placed at the inlet to a diffusion pump to condense the oil vapor that comes in contact with them. This prevents the vapor from backstreaming into the vacuum chamber, which fulfills two basic purposes. First, it reduces the contamination of the system by the pump oil vapor. Second, condensing the oil vapor makes it possible to reduce the pressure in the vacuum chamber faster and lower by eliminating the increase in pressure that would result from the oil vapor. Cooling traps are available in a variety of types. The two most common ones are liquid nitrogen traps and cooling-water baffles. The liquid nitrogen traps are very useful when ultra-high vacuums are required, but these traps are relatively expensive and require the addition of special controls to monitor the liquid nitrogen. Cooling-water baffles

are suitable for use down to 10^{-8} Torr and are relatively inexpensive and easy to use. Thus, a Cenco Model 90011-4 water-cooled chevron baffle was installed in the vacuum system. A schematic of the cooling water system is shown in Figure 5.

Three vacuum valves were necessary in the vacuum system. Two Cenco Model 94605-6 angle valves with 1 5/8 inches inside diameters were used. One was placed between the mechanical pump and the vacuum chamber and the other was located between the mechanical pump and oil diffusion pump as shown in Figure 4. A Vacuum Research Company Model 4T4 gate valve supplied by Cenco was placed between the cooling baffle and the vacuum chamber to make it possible to isolate the diffusion pump from the system.

An NRC Model 710B thermocouple-ionization gage control was incorporated into the system, as shown in Figure 6. This controller will monitor two thermocouple gages and an ionization gage. An NRC Model 507 ionization gage, suitable for measuring pressures over the range from 1×10^{-7} to 5×10^{-3} Torr, was attached to the vacuum chamber. Three NRC Model 501 thermocouple gages were also included in the system. One was mounted beside the ion gage to record pressures in the vacuum chamber. The other two were mounted in the vacuum line between the diffusion pump and mechanical pump. One of these was mounted on each side of the valve separating the two pumps, as shown in Figure 4.

The major vacuum components were formed into a system by connecting them together with accessories fabricated locally. Some materials perform better in a vacuum environment than others. Of the relatively common metals, stainless steel has proven to be the best. Aluminum and brass are also quite good. Certain other materials such as latex rubber and

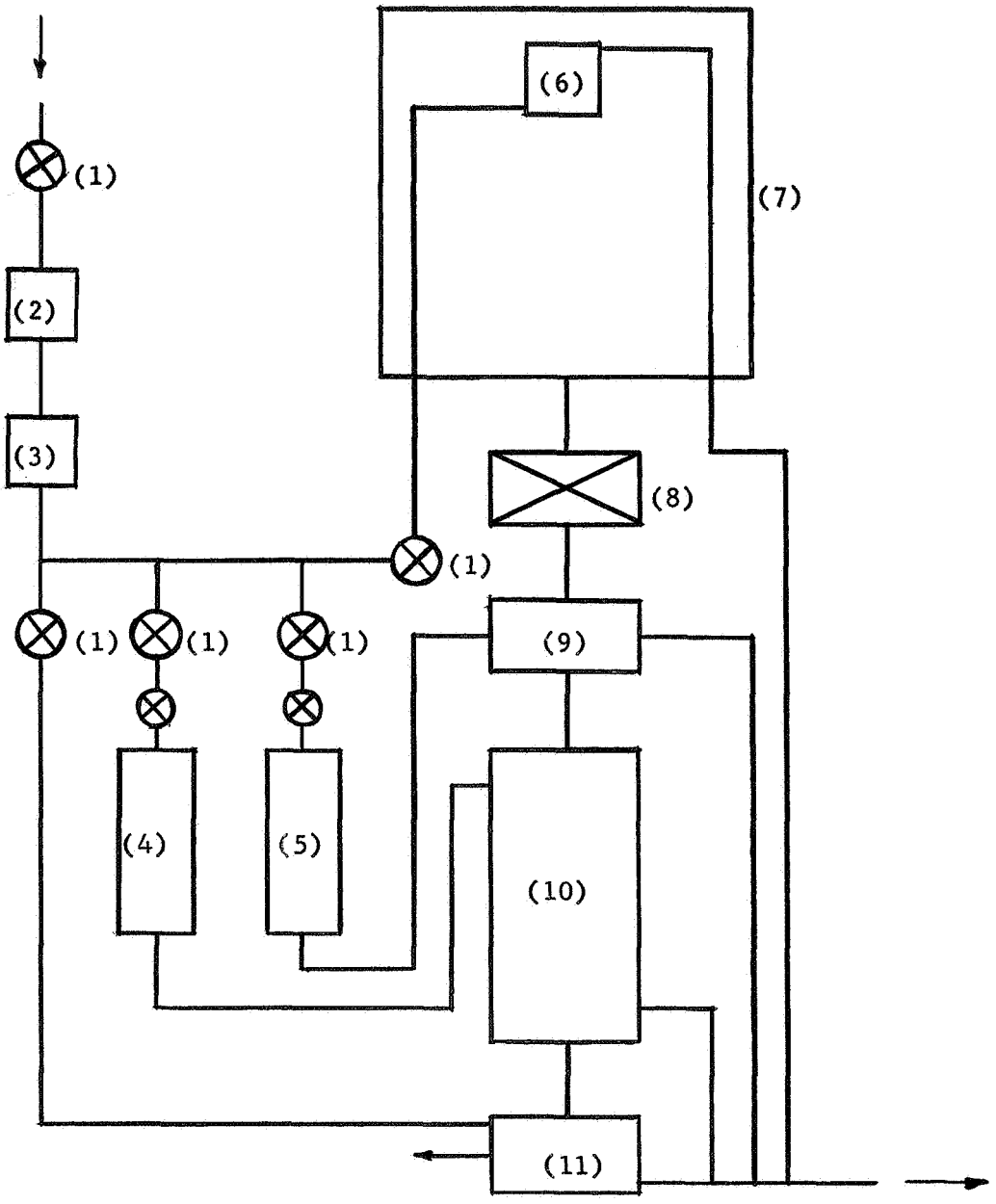

(1) Water Valve
(2) Water Filter
(3) Water Pressure-Power Interlock
(4)(5) Flowmeter
(6) Heat Sink
(7) Vacuum Chamber
(8) Vacuum Valve
(9) Chevron Baffle
(10) Diffusion Pump-Barrel
(11) Diffusion Pump-Forearm

Figure 5. Diagram of the Water Cooling System.

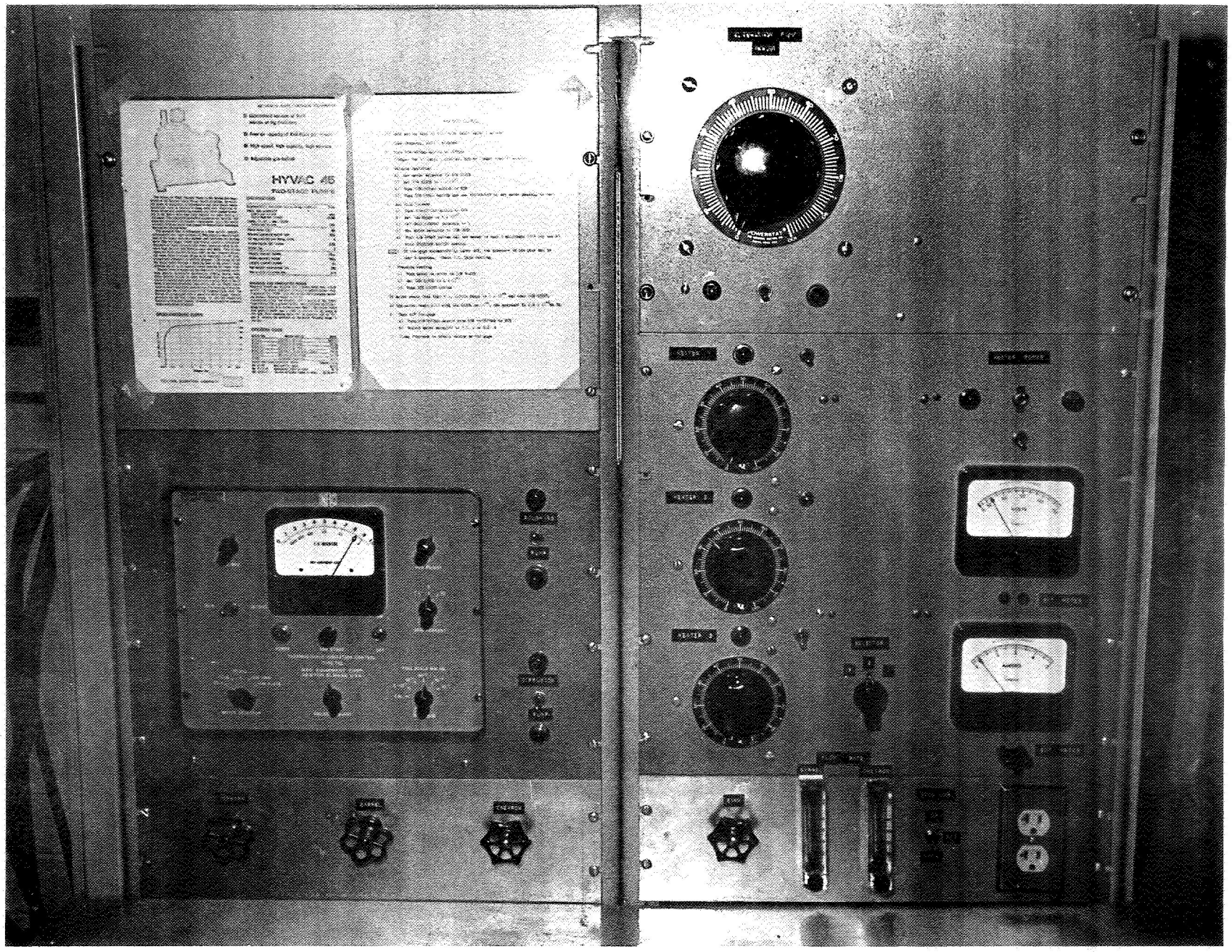

Figure 6. Photograph of the Instrumentation Console.

pure rubber are satisfactory for use in regions at a pressure above 1 micron. Hence, the connections on the high vacuum side of the diffusion pump were fabricated from stainless steel and those on the higher pressure side were made from red rubber and brass.

All the components of a vacuum system must be cleaned thoroughly before they are assembled. The metal and glass parts should be washed with a solvent such as trichloroethane and then rinsed with a high quality acetone to remove the film that trichloroethane deposits. The rubber parts such as the seals should be cleaned with isopropyl alcohol. The rubber parts should not be exposed to the other cleaning agents as they will remove the sealer applied to the gasket during manufacture. After the parts are cleaned, it is desirable to bake those items that will withstand high temperatures. The heat will vaporize the water and cleaning agents that have been absorbed. This will considerably reduce the time required to outgas the system.

Certain lubricants are very useful in sealing the joints between the components. Dow Corning 704 diffusion pump oil has been used for sealing joints with "O"-Rings and other rubber gaskets. Dow Corning high vacuum silicone grease is also quite flexible as a sealer, and is recommended for use over the temperature range of -40° to 200° C. Dow Corning 806A Aerospace sealer has been found an excellent sealant for all parts of the vacuum system, and essentially solves minor leakage problems.

Operation of the vacuum system generally yields a chamber pressure on the order of 1×10^{-5} Torr after two hours of operation, and as low as 1×10^{-6} Torr after 12 hours of operation.

INSTRUMENTATION

The validity of the results obtained by experimentation depends greatly upon the accuracy of the instrumentation used. Instrumentation is required for the measurement of the heat flux (i.e., the electrical power input), the force applied to the interface, and the temperature measurements.

Power to the heater system was controlled by three powerstats as shown in Figures 6 and 7. A 300 watt Acrawatt BLOEF band heater, 1 1/2-inch diameter by 3 inches long was wrapped around the source end of the specimen to serve as the main heater. The second powerstat was used for regulating power to the guard heater, and the remaining powerstat provided an additional power supply to the vacuum chamber, for use with radiation shield heating, for baking the system for outgassing, or other purposes.

The source end of the specimen with bank heater was insulated axially and radially to minimize the heat losses. The radial insulation was PFW glass insulation loosely packed around the heater and held in place by a small sheet of aluminum foil. To shield other components and further reduce the losses, an aluminum radiation shield was located about 1 inch away from the insulated heater. An aluminum cap was placed on top of the cylinder formed by this outer shield to prevent radiation to the instrumented section of the specimen. The axial insulator was made from 1/16-inch aluminum sheeting and asbestos board insulating material. Thermocouples were located in the insulation separated aluminum disks for monitoring the axial heat loss.

For better control of the heat losses from the source, an axial guard heater was installed below the insulator. The guard heater provided a

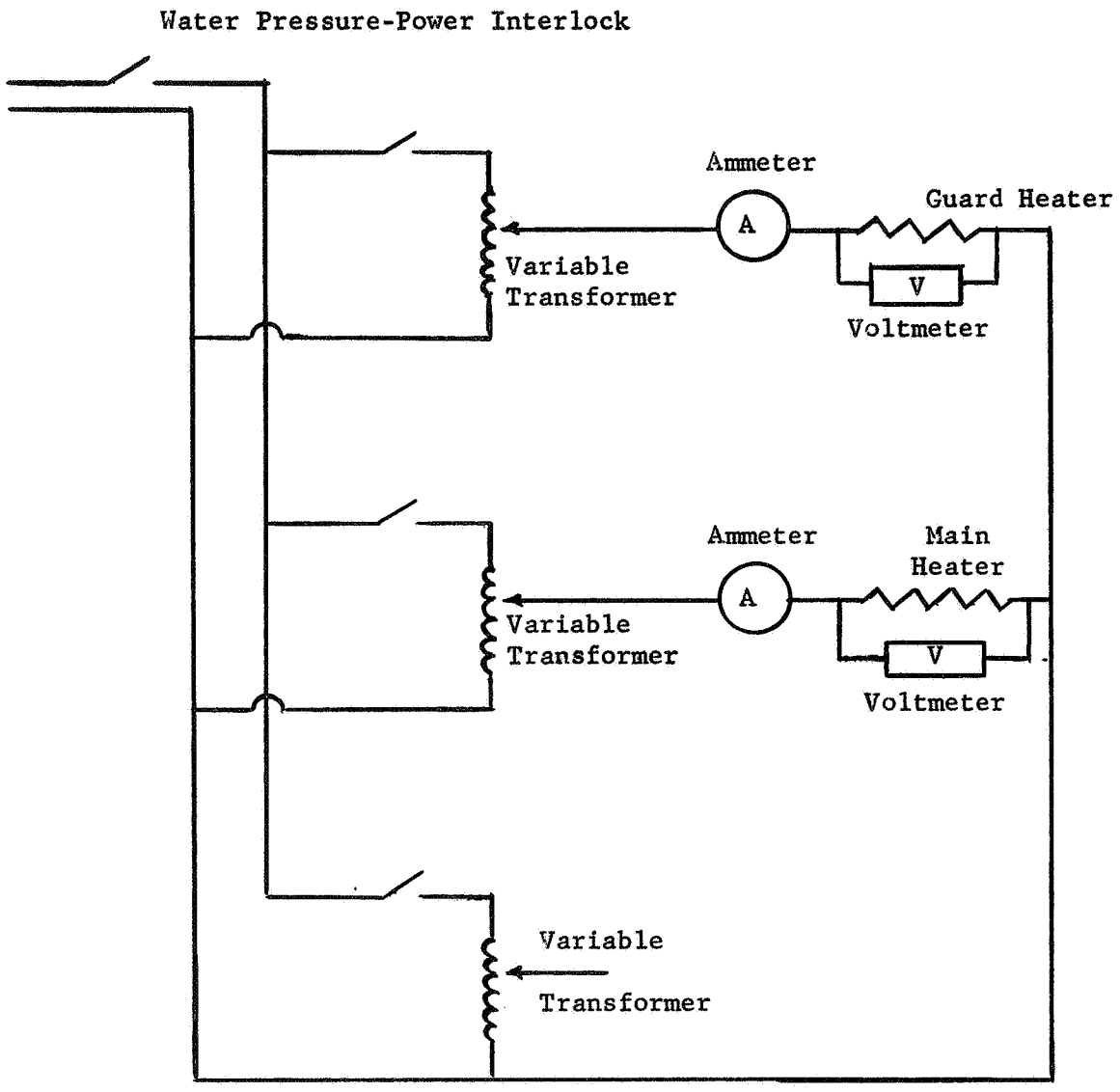

Figure 7. Schematic of the Power Supply and Heater Controls.

positive means of controlling the conduction heat losses along the specimen by enabling accurate control of the temperatures on each side of the axial insulator, and reduced the time necessary to reach steady state. The heating element, a coil of 24 gage nichrome resistance wire 3/16-inch in diameter and 5 inches long, was embedded in unfired lava stone. This heating element was then encased in a stainless steel cylinder 2 inches in diameter and 1.25 inches long, to withstand the compressive loads applied to the interface. The resulting guard heater responded rapidly to changes in power input and withstood the relatively high temperatures well.

It was necessary to measure the power input into the specimen and guard heaters to insure their operating limits were not exceeded and permit a check on the heat losses. Heat losses are based upon the power input supplied to the heat source. Thus, to calculate the electrical power input, it was necessary to measure the current through the heating element, and the drop in potential across the heater. The voltage and current were measured with a Weston Model 904 voltmeter and a Weston Model 904 ammeter, respectively. Both instruments had an accuracy of $\pm$ 0.5 percent of the full scale reading. They had multiple ranges which made it possible to use the upper half of a scale to record a reading. The power input could also have been measured directly with a wattmeter, if losses in the leads were considered. A wiring diagram of the heater power system with instruments is shown in Figure 7.

The sink for cooling the end of the specimen was made from 1 1/2-inch diameter copper rod with copper tubing cooling coils attached with silver solder, as shown in Appendix A. The specimen is then screwed into this sink with 8 threads/inch. The system is set up such that the cooling fluid

may be water, steam, air, or liquid nitrogen. The water coolant system is shown in Figure 5. The steam, air or liquid N_2 systems are similar to the water coolant system.

The apparent pressure on an interface is normally determined by dividing the force applied to the specimens by the cross sectional area of the interface. Thus, it was necessary to determine accurately the magnitude of the force applied to the interface. Since the interface was located in a vacuum environment, measuring the applied force presented a problem.

It was decided to measure the applied force external to the vacuum system. The force was recorded with a BLH Model C3P1 load cell coupled to a BLH Model 120C strain indicator. The load cell was calibrated and the results and calibration technique are given in Appendix B. To obtain the force actually applied to the interface, the measured load had to be corrected for the effect of the passthrough bellows and the weight of the test column between the interface and the load cell. The correction to the applied force for the effect of the passthrough bellows was determined by measuring the resisting force as a function of the bellows deflection. Results of this calibration are also given in Appendix B. Loading of the specimen was provided by the dry Nitrogen bellows located in the vacuum chamber. The high pressure Nitrogen system is shown in Figure 8.

A Simplex Model J2 worm-gear screw jack was used to facilitate specimen alignment and permit separation of the contacting surfaces. This screw jack, located below the passthrough bellows, has a two ton capacity and a 15:1 gear ratio. The passthrough manufactured by Stepco, was designed as an expansion joint for high pressure applications, but its suitability

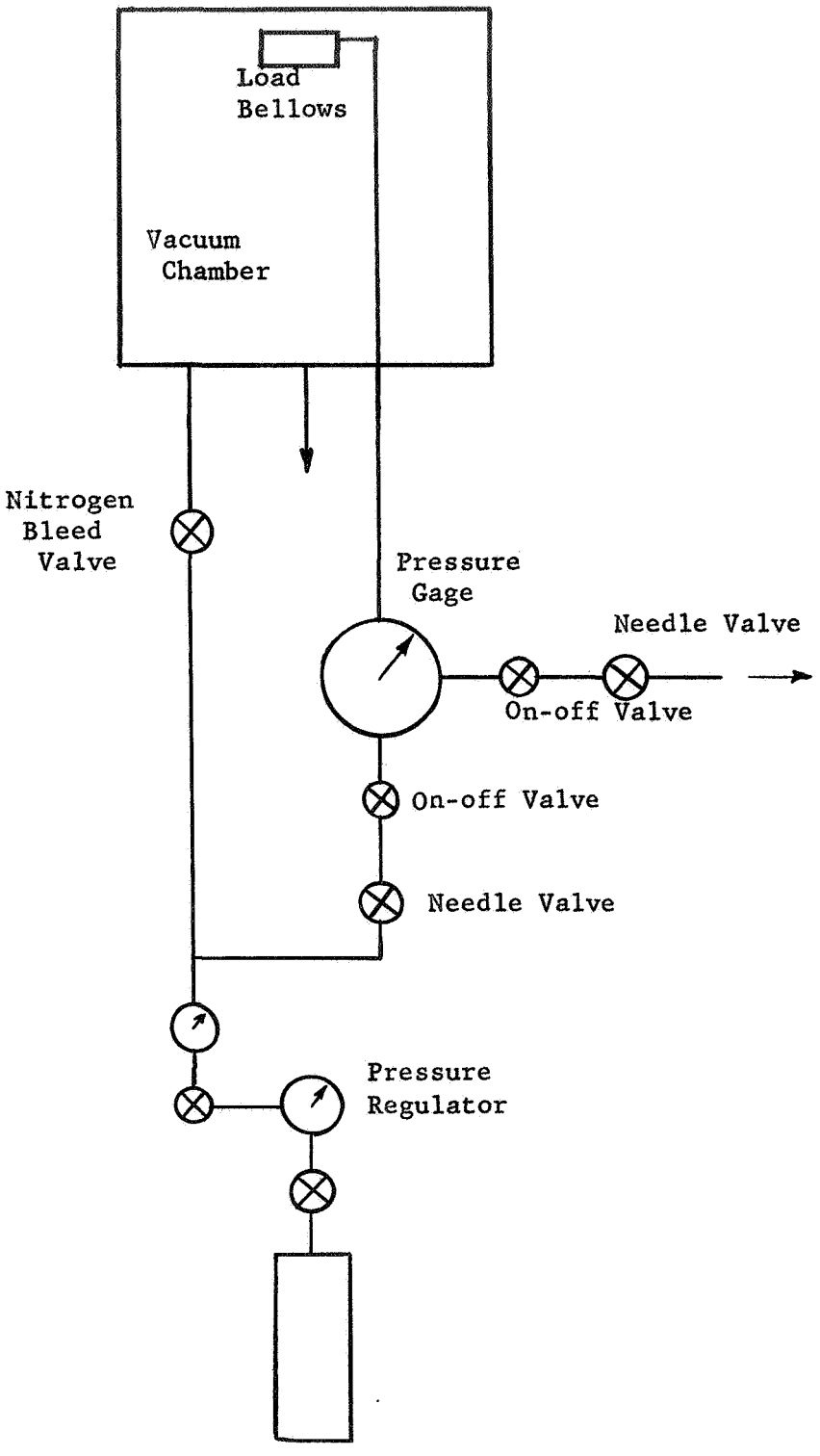

Figure 8. Diagram of the High Pressure Nitrogen System.

for vacuum work was verified by a factory representative. The load cell used to measure the force was mounted between the screw jack and the passthrough bellows. Two centering devices were incorporated into the load mechanism to keep the bellows and the interface in alignment.

The test section was mounted in a stainless steel framework as shown in Figure 9. The vertical supports of the framework were three 5/8-inch diameter stainless steel rods. These were extended through the base plate by universal feedthroughs that provided compression seals to make them vacuum-tight. These rods were in turn attached to the bottom support plate of the NASA apparatus to permit rigid support. This type of framework construction prevented the force applied to the interface from being transmitted to the base plate. Thus, it was only necessary for the base plate to support the weight of the test section.

The accuracy of the determination of the interface contact resistance is greatly dependent on the accuracy of the temperature measurements. Hence, the precision of the thermocouples and thermocouple readout system is of major importance in the experimental program. The system consists of Leeds and Northrup Model 8248 twelve-point thermocouple switches; Vacumen Corporation potted thermocouple passthroughs with either 24 copper-constantan or 24 iron-constantan thermocouple leads; teflon terminal strips in the vacuum chamber; ice junctions; and associated wiring.

After the instrumented test specimens are placed in the test apparatus, the thermocouple leads are attached to two teflon terminal strips with brass bolts and stainless steel nuts. These materials were selected on the basis of their thermal, electrical, and vacuum environment properties. Each terminal strip supports 12 thermocouples and is fixed

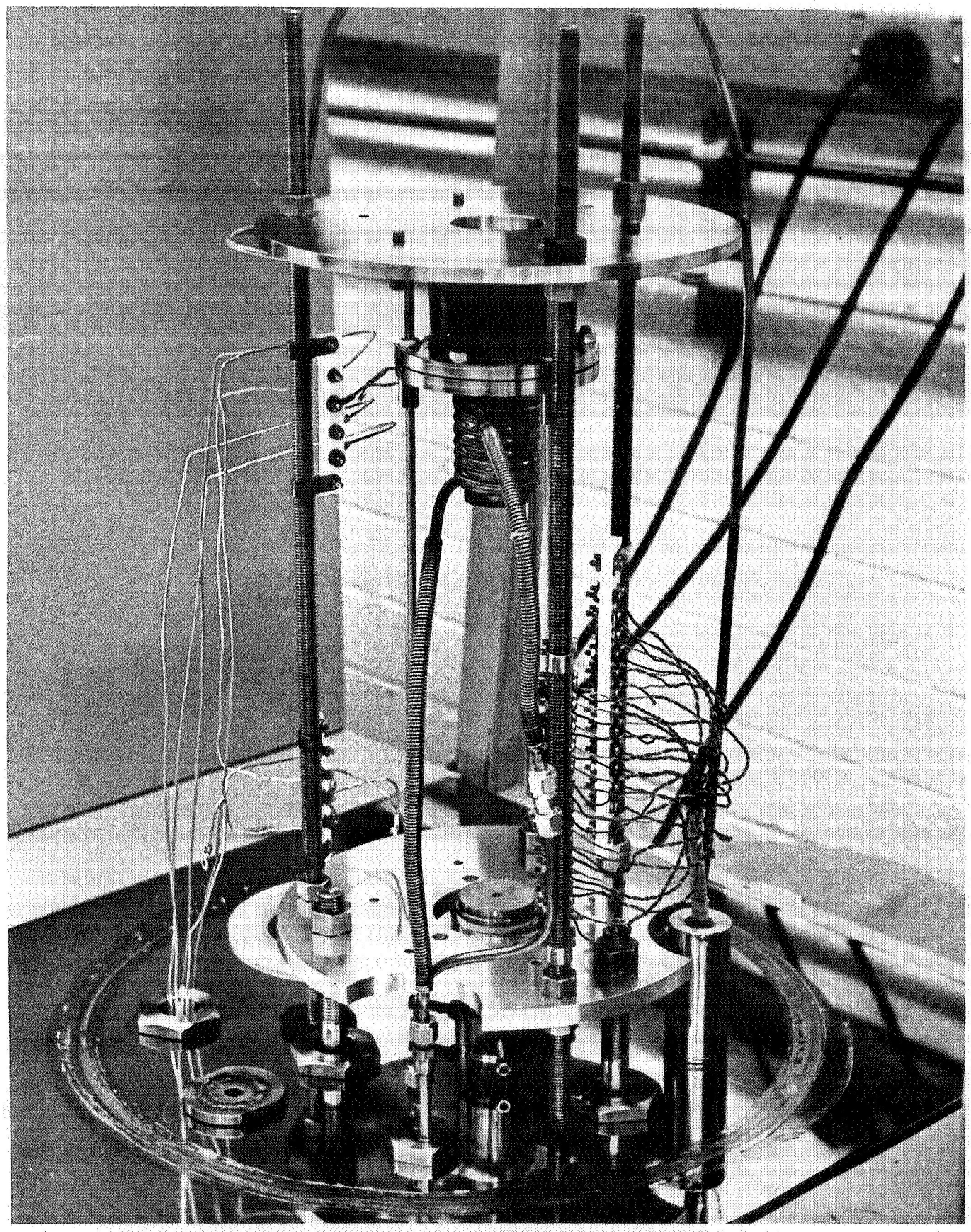

Figure 9. Photograph of the NASA Experimental Apparatus Installed in the Vacuum Facility

to the vertical support rods of the apparatus. The thermocouple leads from the passthrough are likewise attached to the terminal strip and the complete strip is shielded from the heated specimen, to maintain isothermal conditions at the strip junction. The thermocouple leads from the vacuum chamber are attached to bakelite terminal strips in a shielded region free from air currents with leads from the respective thermocouple switches as shown in Figure 10.

Special high-quality copper lead wires, insulated with teflon, were utilized to extend the thermocouple wires to the thermocouple switches and the potentiometer. The lead wires were all shielded with conduit that was grounded. The shielding prevented induced EMF from affecting the thermocouple outputs. A reference junction was included in the circuit for each selector switch which in essence provided an individual cold junction for each thermocouple. The cold junction thermocouples were each placed in small, oil-filled, glass tubes that were immersed in a water and ice bath to provide an accurate 32° F reference temperature. Distilled water and ice were used to eliminate any errors from impurities in the water. The thermocouple outputs were recorded with a Leeds and Northrup Model 8686 millivolt potentiometer. The smallest scale division on the potentiometer was 5 microvolts which represented 0.2° F for copper-constantan thermocouples for the range of temperatures considered. Thus, the uncertainty associated with the potentiometer was 0.2° F.

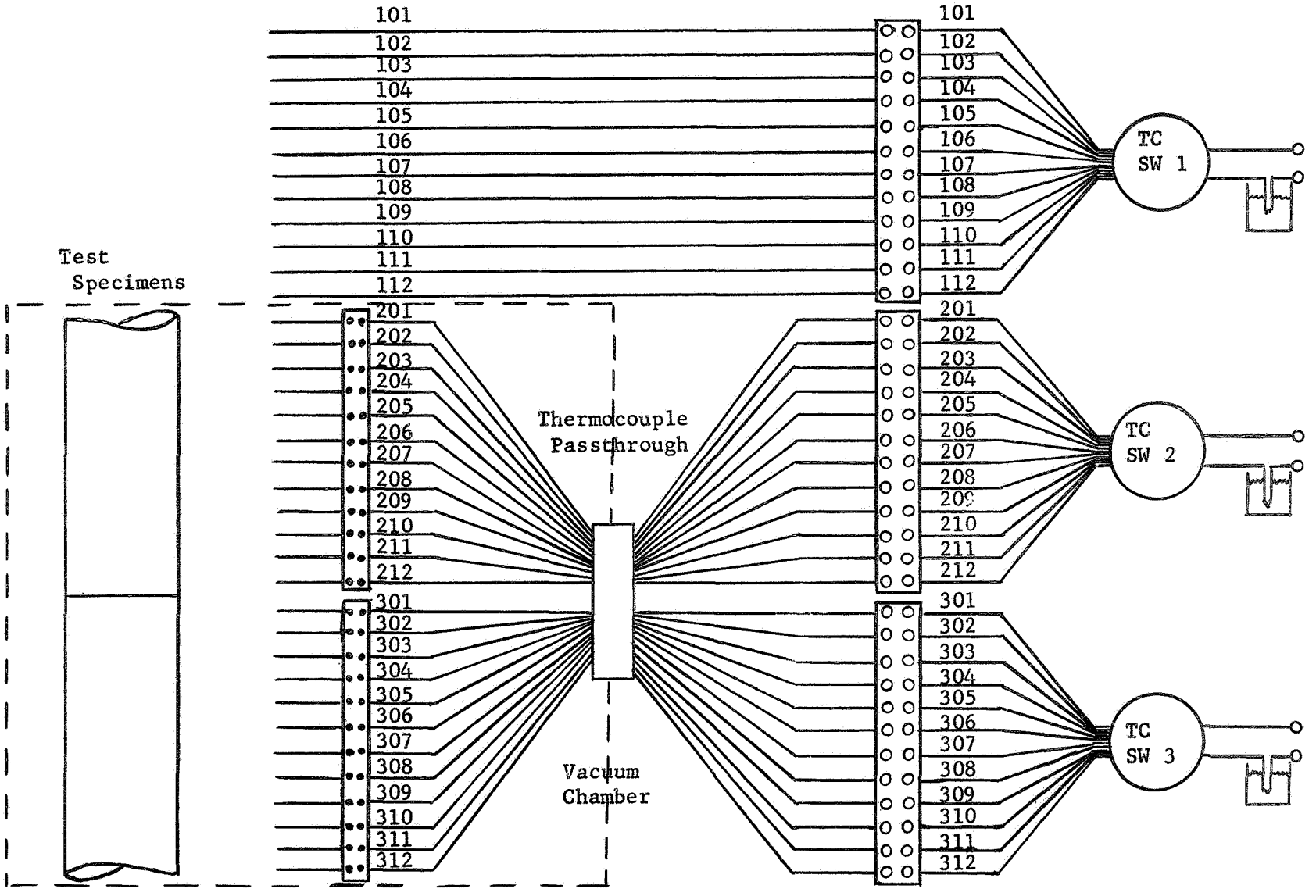

Figure 10. Schematic of the Thermocouple System.

CHAPTER IV

EXPERIMENTAL PROGRAM

Incorporation of the NASA apparatus in the present vacuum facility required a few modifications of the existing equipment. A few changes were made in the original NASA equipment to facilitate installation and operation. Since experimental verification of the design and operation of the NASA thermal contact conductance apparatus required knowledge of the thermal conductivity and surface condition of the test specimens, separate tests were made to determine these characteristics. Acceptance tests were then conducted using specimens of Armco Iron and Aluminum 2024 to finalize the test section configuration.

APPARATUS AND VACUUM FACILITY MODIFICATIONS

Before the NASA apparatus could be placed in the vacuum chamber, the lower support plate was modified to allow for existing vacuum feed-throughs and holes for the support rods and load shaft. In addition, slight changes were made in the test specimens, the dry nitrogen bellows system, sink assembly and axial load assembly. A drawing of the installed NASA apparatus is shown in Figure A-1.

The specimens were lengthened from two to two and one-half inches, and five centerline thermocouple holes were drilled at one-half inch increments starting at one-fourth of an inch from the interface edge. In addition, three holes one-sixteenth of an inch deep were drilled, diametrically opposed to the five holes, for measurement of surface

temperatures. Detailed drawings of the sink and source specimens are shown in Figures A-4 and A-5.

The dry nitrogen bellows system and sink assembly were installed using Swagelock fittings, to facilitate assembly and disassembly of the apparatus.

The original NASA apparatus design called for installation of the load cell within the vacuum chamber, however, the load cell provided was not modified for vacuum use. Although a representative of the BLH Company stated that the load cell could be installed in a vacuum, it was deemed desirable to place the load cell outside of the vacuum chamber. The resulting axial load system is shown in Figure 11.

Modifications of the vacuum facility included the addition of a cryogenic passthrough for the liquid nitrogen coolant, and a passthrough for the dry nitrogen line to the load bellows. Shorter support rods were machined for purposes of securing the test apparatus firmly to the base plate. The control panel was modified to include the pressure regulation for the dry nitrogen load bellows. The dry nitrogen system is shown in Figure 9. This system included two high pressure needle valves and two positive action on-off valves in conjunction with a pressure regulator and a gage for monitoring the bellows pressure.

THERMAL CONDUCTIVITY MEASUREMENT

An apparatus to measure the steady state thermal conductivity of test specimen materials was constructed. It consists of a central heater sandwiched between two four inch by one and one half inch diameter cylinders of the test materials, with guard heaters at each end to maintain a

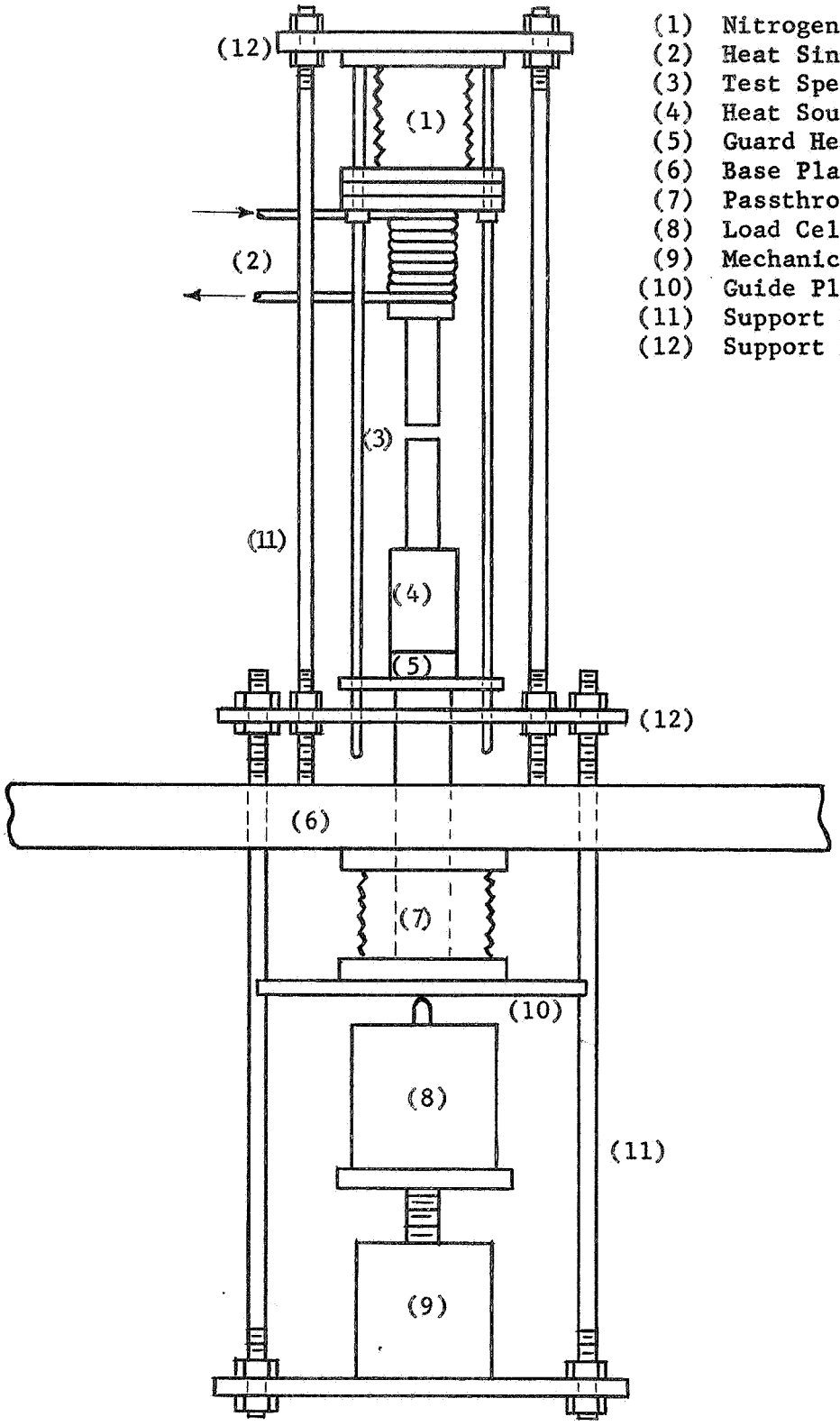

Figure 11. Diagram of the Axial Loading System.

temperature gradient of approximate 20°F in the test samples. Thermocouples are located at one-half-inch intervals along the specimens to monitor the linearity of the temperature gradient. The test samples and central heater are inserted into a ten-inch-diameter cylinder filled with vermiculite to minimize heat losses. The ends of the specimens are attached to water cooled plates to insure proper temperature control. A more detailed description and discussion of the thermal conductivity measurement may be found in Appendix D.

Tests with Armco Iron were used to determine the heat loss from the apparatus as a function of temperature. The thermal conductivity of "as received" and "annealed" Aluminum 2024 was then calculated. The results and uncertainty intervals are presented in Figure 12. The data are extremely sensitive to variations in the heat loss coefficient. The uncertainty for the "as received" aluminum is approximately 5 percent, however, an uncertainty of approximately 10 percent is shown for the "annealed" aluminum as a result of the lower temperature gradient for the same heat flux.

SPECIMEN PREPARATION

Since surface condition is a major factor affecting thermal contact resistance, extreme care must be taken in finishing the contact surface. With the lathe equipment available, it is possible to acquire a waviness or flatness deviation of 2/10,000 of an inch. The surface roughness ranges between 10 and 12 microinches, rms. Thus, the initial finishing of the specimen yields a surface which is adequate for experimental use.

However, to improve the surfaces, the specimens are lapped on a Lapmaster 12, a product of the Crane Packing Company. They are placed

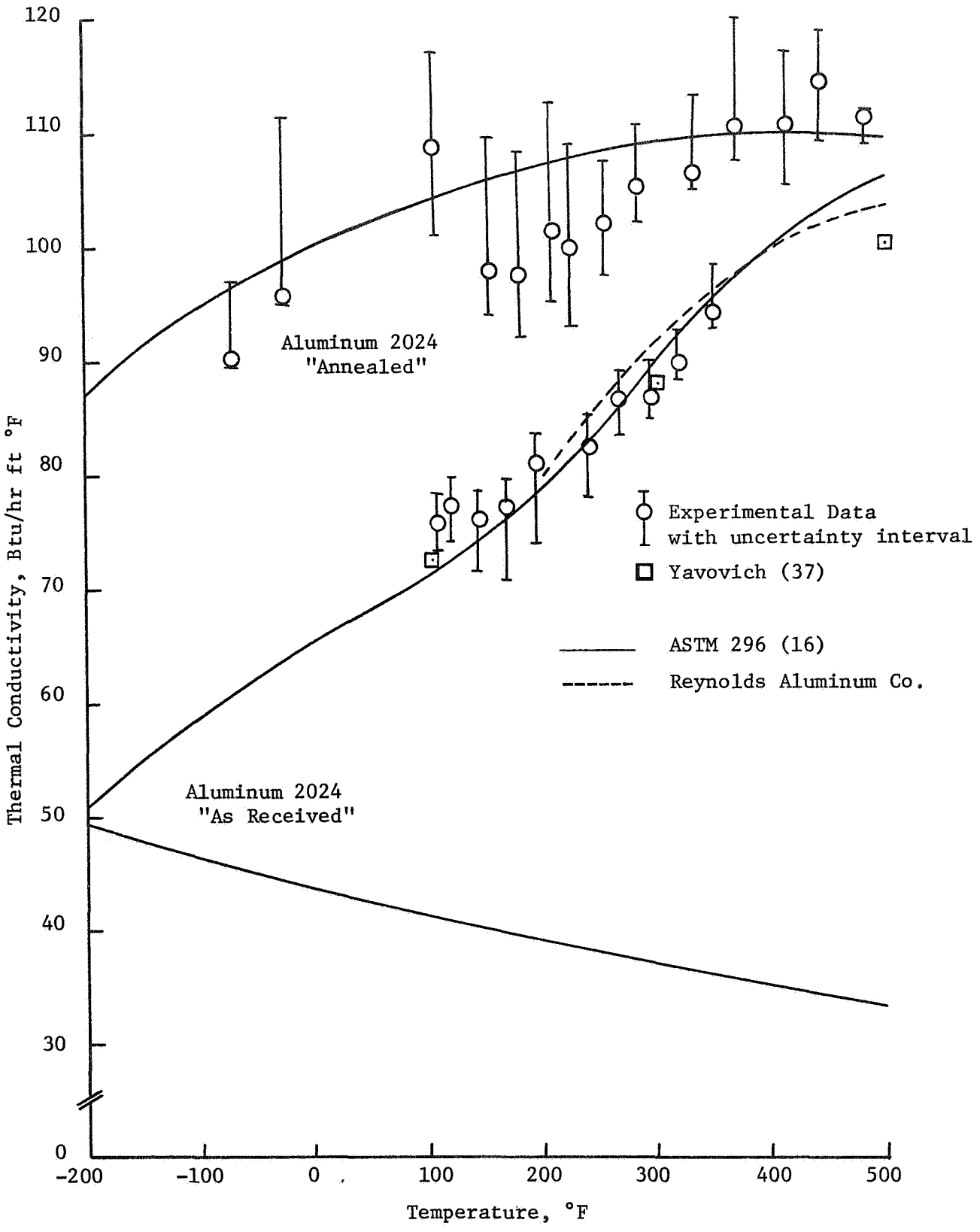

Figure 12. The Variation of Thermal Conductivity with Temperature for Armco Iron and Aluminum 2024.

in a brass jig which keeps the specimen perpendicular to the lapping plane. The finishing process is done with a fine lapping compound. On completion, the specimen is removed and polished on a polishing cloth. The resultant flatness deviation is within 2/1,000,000.

The flatness of the surface is measured by interference refraction. This process consists of refracting a light beam of helium through an optical flat (quartz glass), on to the surface to be measured. The irregularities in the specimen surface will cause interference bands or fringes to appear on the surface of the optical flat. These bands are shadows one-half the wavelength of the illuminating light.

Teflon caps were made, to place over the end of the specimens for protection of the finished surface. These covers are tapered inside, so that they do not touch the test surfaces. Use of these caps minimized damage and oxidation of the polished surface.

The thermocouples used in this investigation must be small in order to permit point temperature measurement, reduce conduction losses, and must be tough enough to withstand the rigors of assembly and testing. In an attempt to determine the best method of fabricating the thermocouples, several different techniques were tried. The best results were obtained when the bare parts of the wires were twisted together tightly for about one-fourth of an inch, the joint silver soldered, and the excess wire cut off to the point where the wires first made contact. This procedure is used for all thermocouple construction in this investigation. The thermocouples are then checked for continuity.

To measure the center line temperatures of the specimen, thermocouples are mounted in holes 0.046 inches in diameter, and 0.531 inches

deep. The leads are wrapped once around the specimen to minimize heat losses through the wire. The thermocouples are held in position by packing them in the holes with aluminum powder. A considerable amount of care is taken to insure that the thermocouple and insulation are not damaged during this operation. The resistance of each thermocouple is checked before and after installation. If the resistance varies between the reading, it is assumed that damage has occurred and the thermocouple is then replaced.

The surface temperatures are measured by placing thermocouples in holes 0.046 inches in diameter and 0.062 inches deep, diametrically opposed to the centerline holes. The leads are wrapped twice around the specimen for the purpose of minimizing heat losses and for convenience in installation.

An X-ray of the specimens is taken for the purpose of determining the exact location of the thermocouples. It also shows if there are any flaws in the metal or thermocouple installation which would affect the accuracy of the temperature measurement. Figure 13 is a representative X-ray of an Aluminum 2024 specimen set.

DEVELOPMENT TESTS

The effects produced by the installation of radiation shields, guard heaters, and insulation; by polishing the surface of the specimen and by various heater installation techniques were evaluated experimentally in a series of tests conducted by Abbott (1). The tests were selected so that the results could be directly compared to indicate the relative effectiveness of each test section configuration. Clausing (11)

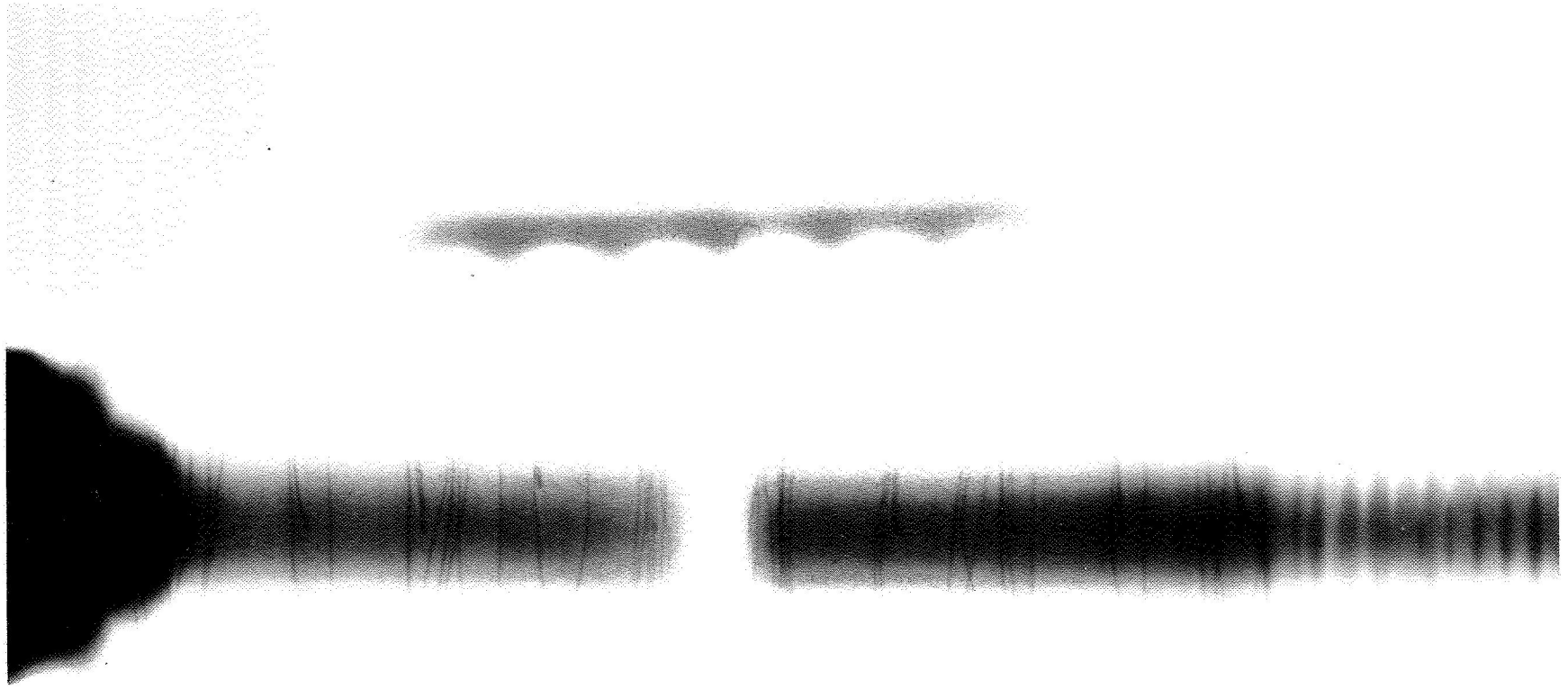

Figure 13. A representative X-ray of an Aluminum 2024 Specimen Set.

indicated that heat losses from the test specimens were a major source of concern because such losses created a non-uniform heat flow. Hence, the reduction of heat losses was the principle factor considered in deciding which of the test section configurations was the most desirable.

A series of tests were performed using the NASA apparatus to determine a suitable test section configuration. Tests were conducted using test specimens machined from Armco Iron and Aluminum 2024. In addition to the test section configuration described previously, several different radiation shields were tested to determine which type of shield would minimize the surface heat losses and permit a more uniform temperature gradient in the test specimens. The resulting shield was constructed from stainless steel screen formed into a cylinder 1 7/8 inches in diameter and 2 1/2 inches in length. Layers of aluminum foil and dexiglass insulation were secured to the inside surface of the screen cylinder. This radiation shield was placed around the heated specimen and a split aluminum disk placed across the top to completely enclose the heated specimen without touching it. A photograph of the assembled test section with radiation shield is shown in Figure 14. Use of this test section yielded relatively uniform temperature gradients with minimum heat losses.

The performance of these tests provided an opportunity to check and refine the test section configuration, as well as establish a procedure for operating the apparatus.

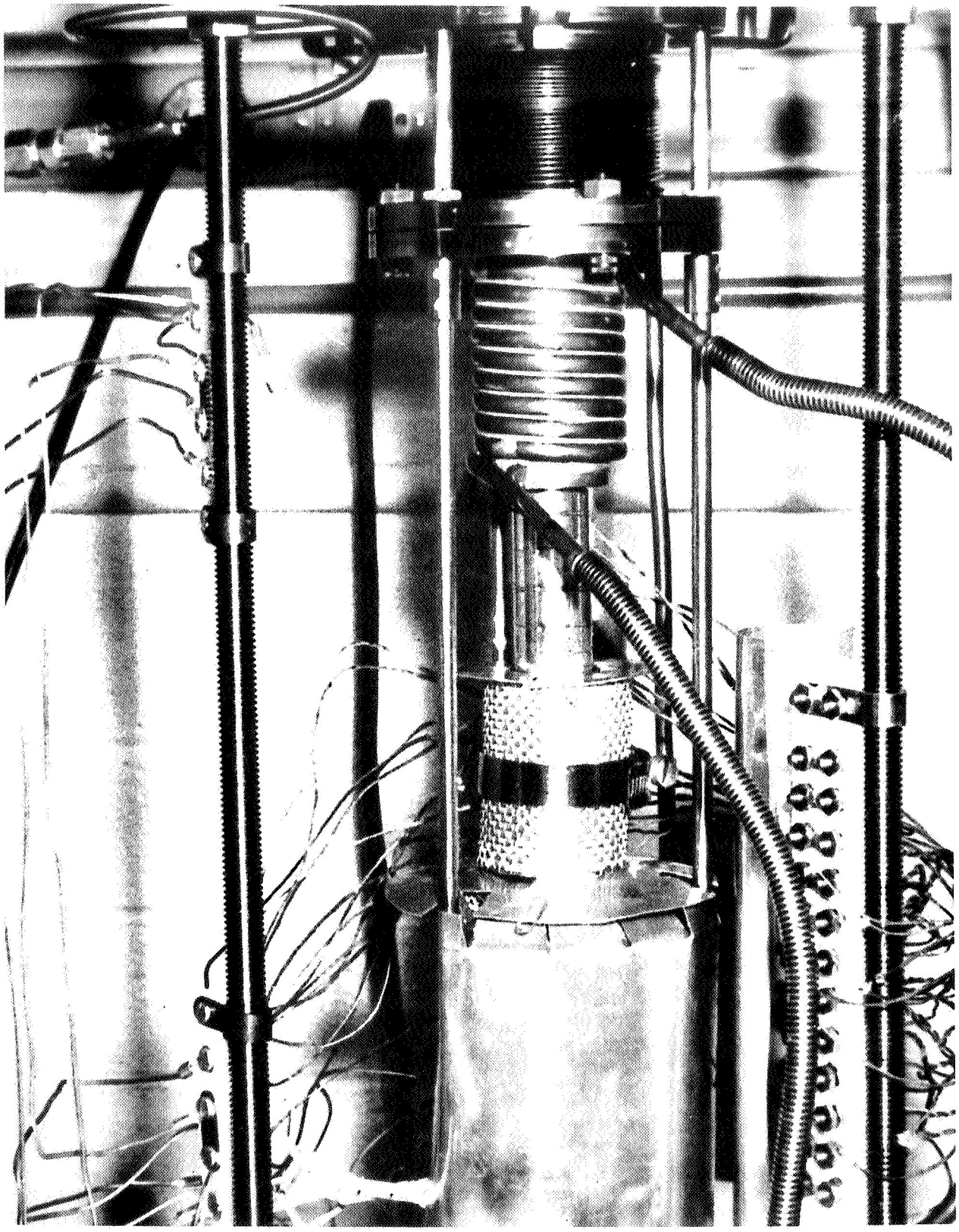

Figure 14. Photograph of the Assembled Test Section with Radiation Shield.

CHAPTER V

TEST RESULTS AND DISCUSSION

The final test section configuration and method of installation were selected as a result of a series of preliminary tests conducted with Armco Iron and Aluminum 2024 test specimens. Additional tests were performed with Armco Iron specimens to ascertain the magnitude of the heat losses from the assembled test apparatus and for final verification of the test section configuration. Aluminum 2024 was then used to obtain thermal conductance data for bare junction tests. The results of these tests were compared with Clausing and Chao (10), Fried (19), and Yavonovich (37), to further demonstrate the validity of the data determined with this experimental apparatus.

The final test section configuration consisted of the instrumented test specimens, the fluid cooled sink, the band heater source, an axial insulator, an axial guard heater, and the associated radiation shields. The band heater was insulated with glass wool and covered with Aluminum foil. This insulation improved the axial heat transfer by permitting a lower power input to maintain the same interface temperature. The heat radiation to surrounding components of the apparatus was further reduced by shielding the heater section (Figure 14). Additional radiation shields were installed to guard the thermocouple terminal strips from extraneous heat radiation, and to reduce surface heat loss from the test specimens.

The experimental measurement of thermal contact conductance is dependent on the assumption of an established uniform heat flux through the test specimen. Thus radial heat loss from the specimen should be reduced to a minimum. The axial temperature gradient, the difference

between the specimen surface and centerline temperatures, and the magnitude of the heat loss from the specimen surface indicate the degree of uniformity of the heat flux. The cylindrical radiation shield surrounding the test specimen reduced the surface heat loss so that specimen surface and internal temperatures were maintained in all tests within 1.5° F at the interface and within 0.5 percent or less at other thermocouple locations. The uncertainty in temperature measurement estimated from the thermocouple calibration was also 0.5 percent (Appendix C). The surface and centerline temperatures were plotted against distance along the specimen, as shown in Figure 15. The trend toward an increasing temperature gradient was caused by a decrease in the thermal conductivity of the specimens with decreasing temperature. The heat fluxes calculated from the measured temperatures are also shown in Figure 15.

The experimental measurements and apparatus were checked by investigating the heat losses from a set of Armco Iron specimens. Since calculation of the thermal contact conductance requires that the magnitude of the heat flux be known at the interface, the heat losses from the heated half of the specimen were investigated. The heat flux was calculated by assuming one-dimensional heat conduction through the specimens. The temperature gradient was estimated between each of the centerline thermocouples by subtracting each succeeding temperature from the one adjacent to it and dividing by the distance between the thermocouples. The thermal conductivity of the specimen was read from Figure 12 at the mean temperature corresponding to the particular location. To evaluate the heat losses, the calculated values of the heat flux were plotted versus the corresponding station along the specimen. The slope of the curve drawn through these points reflects the rate of heat loss per unit length along

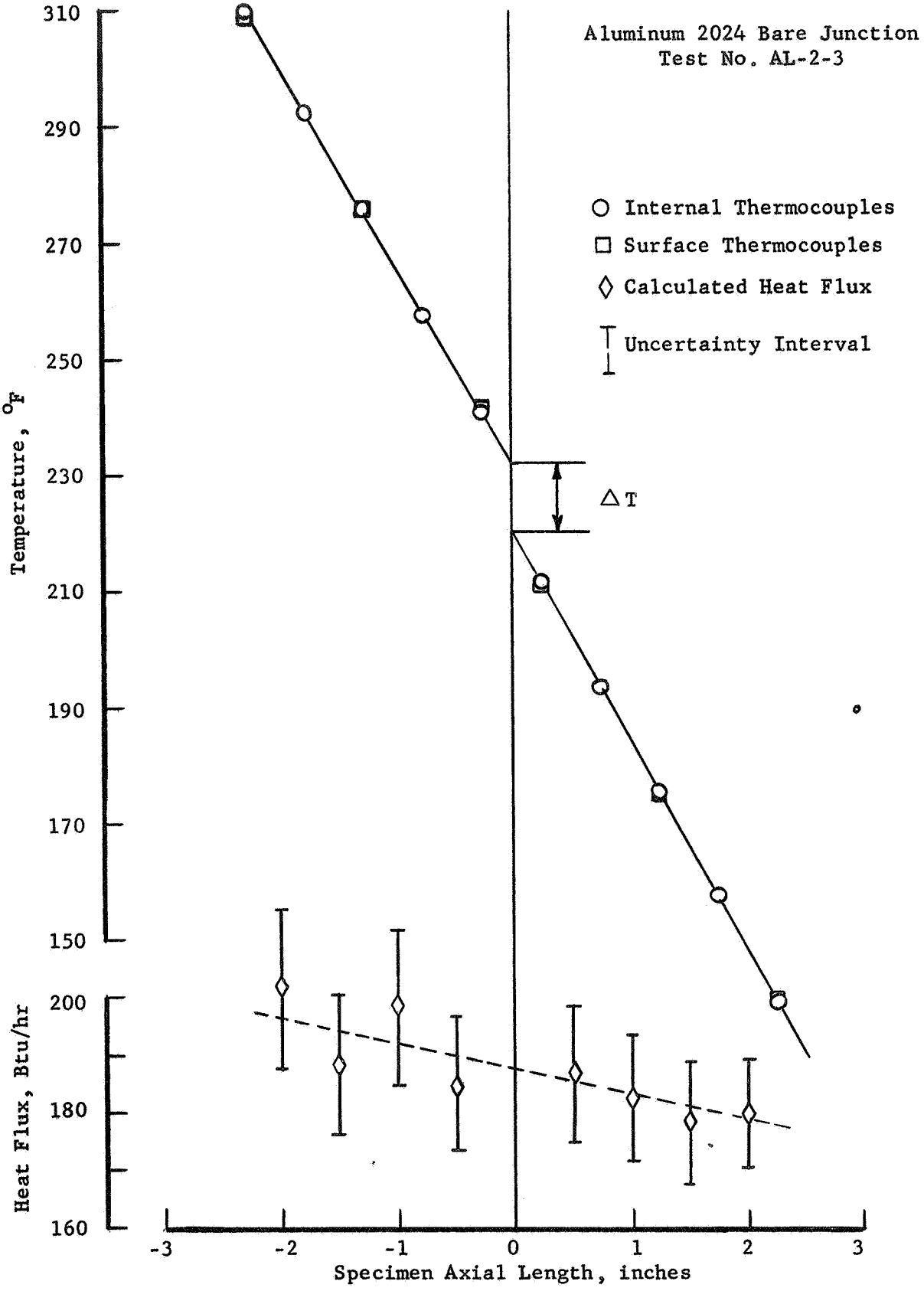

Figure 15. The Variation of Temperature and Heat Flux with Axial Length.

the test portion of the specimen.

There was a definite increase in the heat loss from the test section of the Armco Iron specimens with increased temperature. However, these losses never exceeded more than 4.5 percent of the initial heat flux in the heated specimen, as shown in Appendix E. Heat losses from Aluminum 2024 test specimens with polished surfaces were less than 3 percent of the initial heat flux. The low surface losses and the comparatively linear temperature gradients depicted in Figure 15 indicate that the heat flux established by the final test section configuration was relatively uniform.

The Armco Iron specimen tests were performed at an environmental pressure of approximately 5×10^{-6} Torr at which the effect of surface convection is insignificant. Thus, heat losses had to occur by conduction and radiation. The thermocouples provided the only paths for conduction losses from the test section of the specimen. For thermocouple lead wires not wrapped around the specimen and surface temperatures of 300° F, calculated losses of 0.6 percent of the axial heat flux may be expected for 30 gage wire (3). Since the thermocouple leads in this investigation were wrapped around the specimen, conduction losses were considerably less. By assuming the test portion of the specimen and the radiation shield to be gray surfaces, it was possible to further analyze the radiation characteristics of the final test section configuration. Results of this analysis indicate that the heat losses may be accurately predicted, as shown in Appendix E.

After the heat loss analysis was completed, a series of tests were performed using Aluminum 2024 specimens. These tests were conducted to verify the experimental apparatus and procedure for investigating thermal contact conductance. The contacting surfaces of the Aluminum specimens

were finished on a lathe and then lapped as described in Chapter 4. The resulting surfaces had a 3 to 5 microinch roughness and approximately a 20 to 25 microinch flatness deviation, as shown in Figure 16. The tests were performed at an environmental pressure of 5×10^{-6} Torr for a range of interface pressures and two heat fluxes.

Thermal contact conductance was defined in Chapter I by the relationship

$$h_c = \frac{q/A}{\Delta T}$$

where ΔT is the temperature difference at the interface. The axial temperatures were plotted versus the distance from the interface, and extrapolated to the interface by a least squares fit of the data for each test run to find the respective temperature differences (Figure 15). Since the thermal conductivity of the test specimen material was known (Figure 12), the heat flux, q/A, in the specimen was found from the calculated temperature gradients in the specimen nearest room temperature and thermal conductivity, both of which were determined from the temperatures measured along the specimen. The heat flux determined by subtracting the estimated losses from the measured heater input was compared with the heat flux calculated by use of the thermal conductivity and temperature gradient. The average difference between the heat fluxes was 7 percent for Series 2 and 1.5 percent for Series 3 and 4. The large change in the difference between Series 2 and Series 3 and 4 may be attributed to the fact that the heated aluminum specimen properties were changing due to a slow annealing process during Series 2. In later runs (Series 3 and 4), the aluminum specimen had become fully annealed and in addition, the specimen

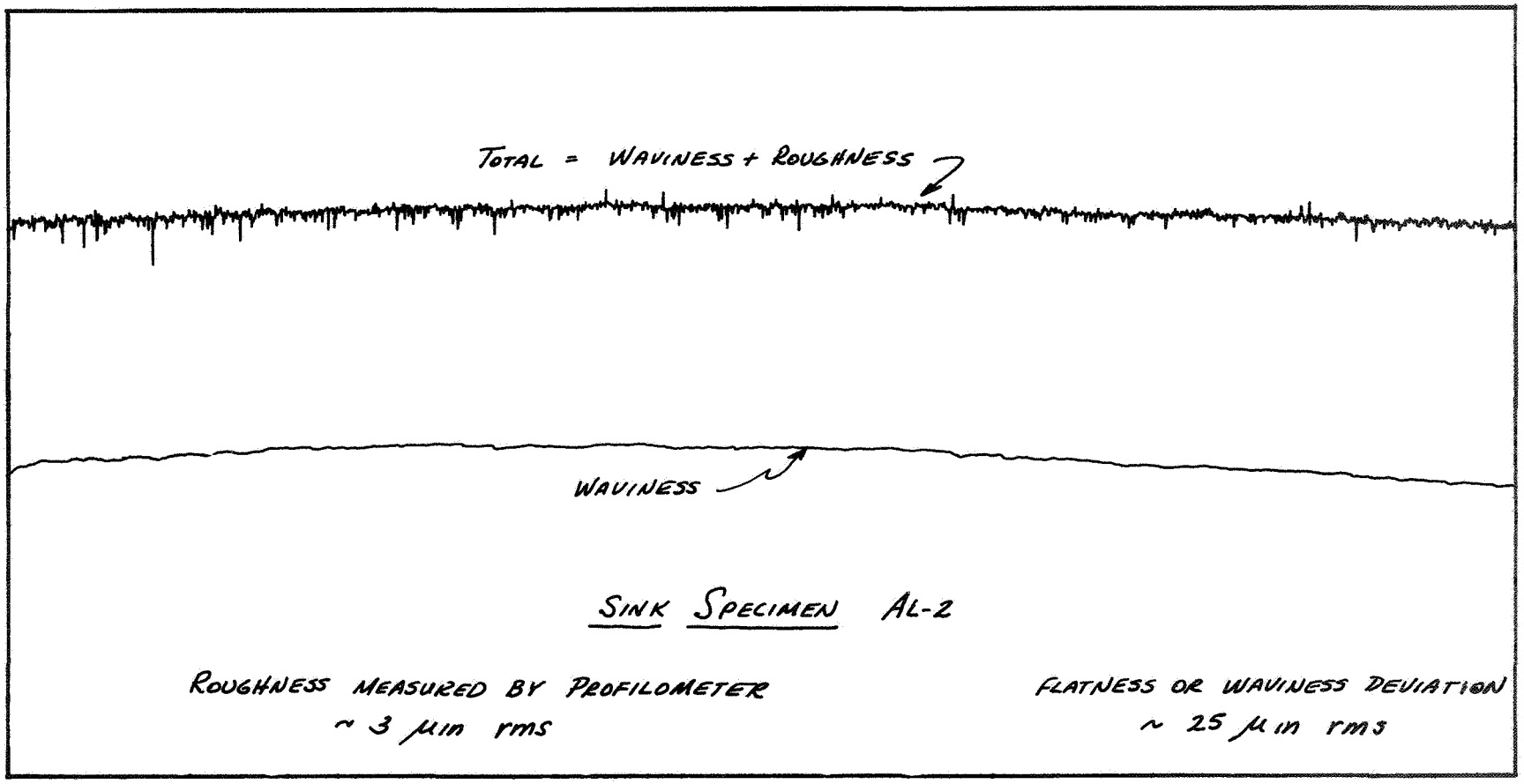

Figure 16. A Proficorder Trace of a Typical Specimen Surface.

TABLE II

TABULATED EXPERIMENTAL RESULTS

Series 2

P_a psi	h_c Btu/hr sq ft °F	ΔT_j °F	q/A Btu/hr sq ft	T_m °F
Loading:				
118	792	35.9	28,420	215
251	2720	13.3	36,170	232
384	4710	7.9	37,210	233
539	7900	5.0	39,510	240
702	9440	4.1	38,690	232
834	12,120	3.2	38,780	236
1009	14,200	2.6	36,910	229
Unloading:				
737	12,660	3.0	37,980	233
415	7080	5.3	37,530	233

TABLE II (Continued)

Series 3

P_a psi	h_c Btu/hr sq ft °F	ΔT_j °F	q/A Btu/hr sq ft	T_m °F
114	1270	34.5	43,780	280
268	2190	22.3	48,830	289
418	3550	14.3	50,730	291
567	5240	10.0	52,430	293
732	6190	8.6	53,240	294
881	7190	7.5	53,930	295
1038	8680	6.3	54,650	296

Series 4 (Repeatability Check for Series 3)

P_a psi	h_c Btu/hr sq ft °F	ΔT_j °F	q/A Btu/hr sq ft	T_m °F
260	2340	20.0	48,560	285
406	3400	13.8	49,350	281
554	4370	11.1	52,420	292
722	5400	9.1	53,490	293
860	7520	6.5	53,410	293

surfaces were refinished. Therefore the results of Series 3 and 4 compare well (Figure 19), but Series 2 shows a different trend. The experimental results of thermal contact conductance obtained for this investigation are listed in Table II.

An uncertainty analysis (Appendix F), was performed to estimate the range of error in the heat flux and thermal contact conductance. Uncertainty for the heat flux was 8.9 percent or less as shown in Figure 15. Uncertainty for the thermal contact conductance was on the order of 11.6 percent. The repeatability of the data obtained using this test apparatus was checked by conducting a second series of tests at comparable test conditions. To insure that the initial conditions were similar, the test specimens were separated and the system was shut down for several hours. The experimental procedure was the same as that used for the initial tests. The energy input to the source heater and the contact pressure in Series 4 were reproduced as closely as possible to those of Series 3. The data for these repeatability tests are also presented in Table II.

Fried (19) and Clausing and Chao (10) conducted some of their tests at a constant interface mean temperature. However, some question exists as to the necessity for maintaining this condition. Rogers (31) reported that in a vacuum environment the thermal contact conductance increased only slightly with increasing mean temperature. Clausing and Chao, on the other hand, showed that at a constant load the interface conductance increased appreciably and rather uniformly with the interface mean temperature. Hence, in this investigation an effort was made to maintain the interface mean temperature at a constant

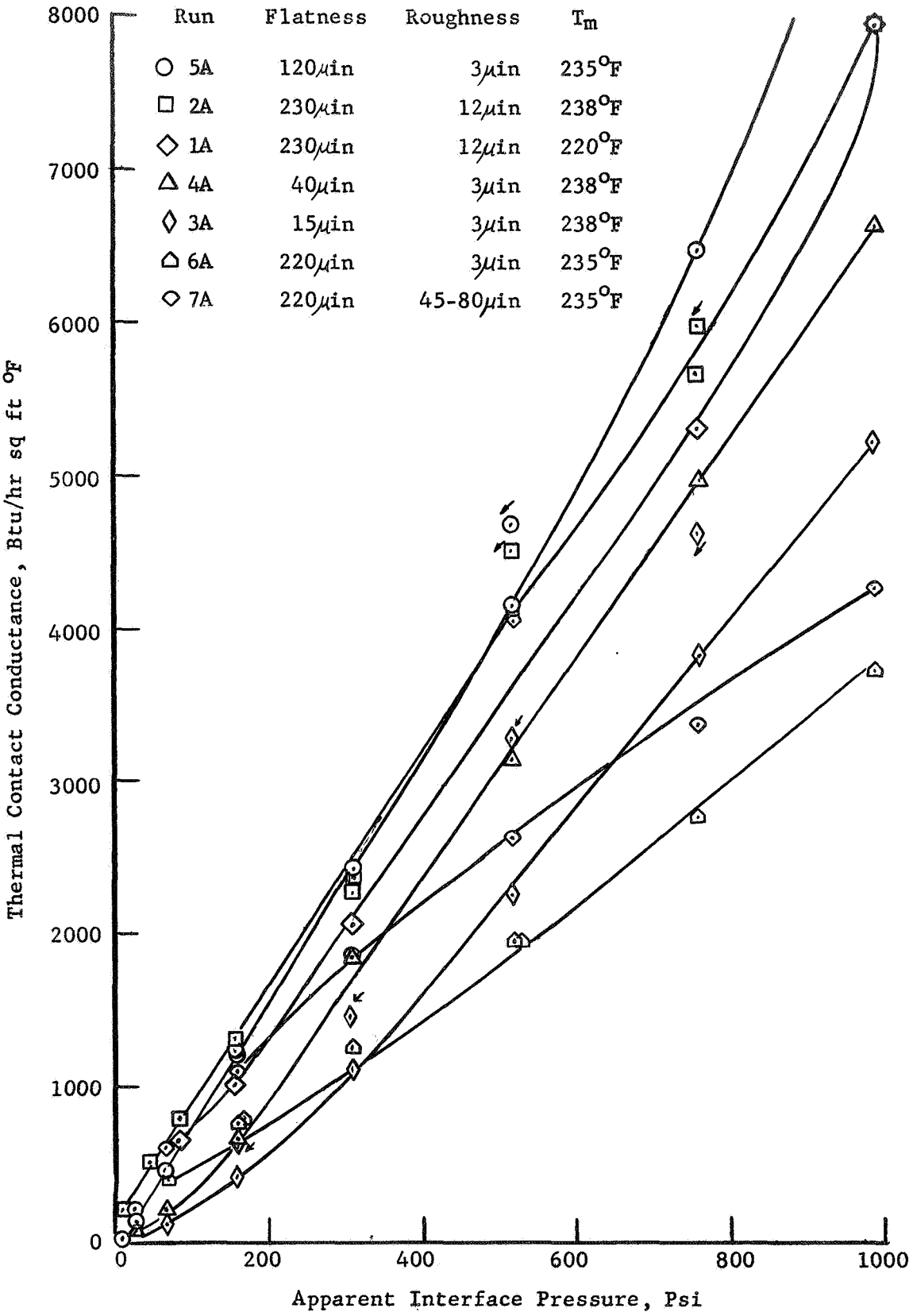

Figure 17. The Variation of Thermal Contact Conductance with Apparent Interface Pressure - Experimental Results of Clausing and Chao (10).

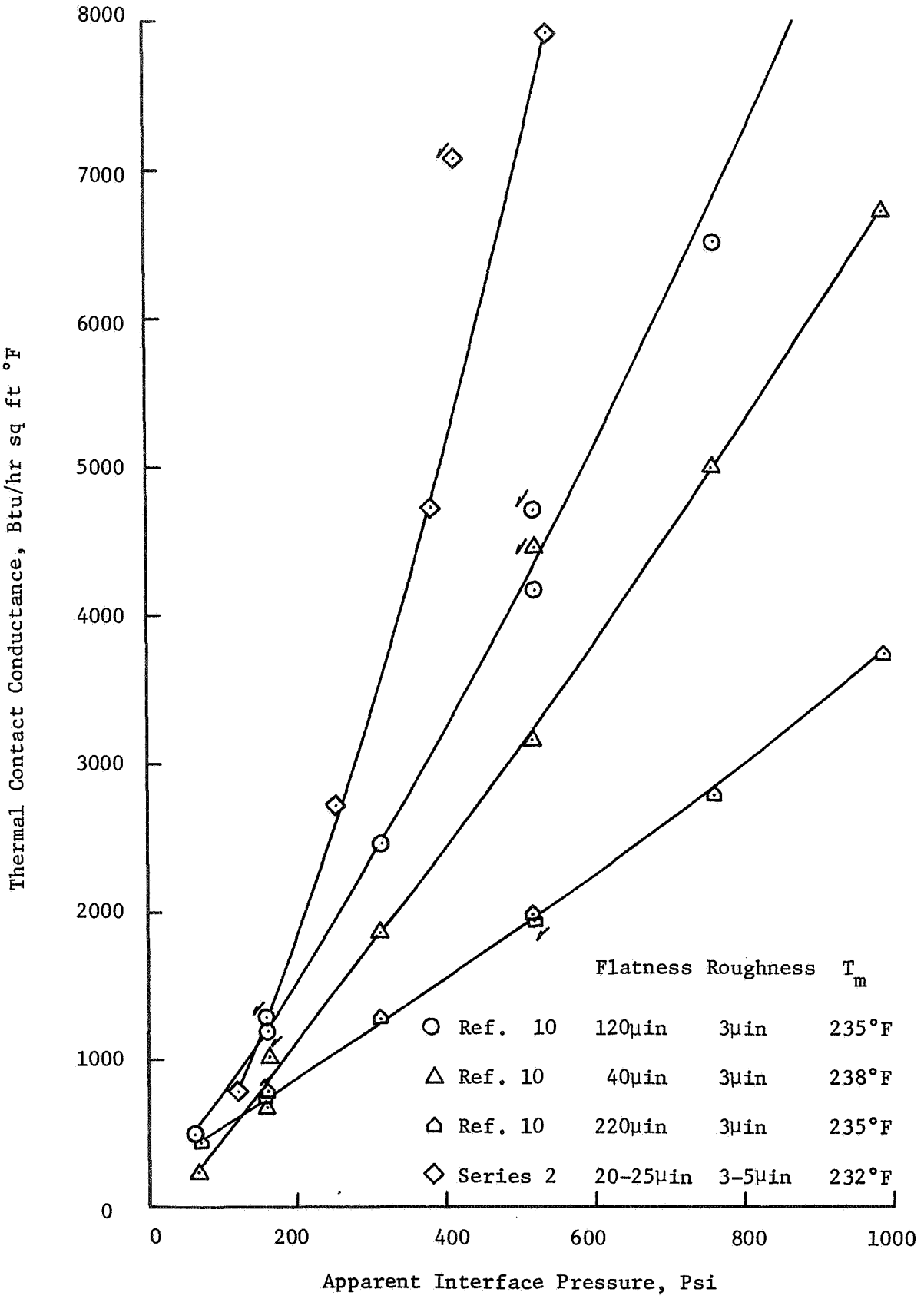

Figure 18. The Variation of Thermal Contact Conductance with Apparent Interface Pressure - Comparison with Clausing and Chao (10).

value, plus or minus 5 percent for each series of runs, as listed in Table II.

Thermal contact conductance values for Aluminum 2024 bare metal spherical faces obtained by Clausing and Chao (10) are shown in Figure 17. As may be seen, their investigation does not show a clear trend between contact conductance and surface finish. Several test runs shown in Figure 17 were plotted for comparison with Series 2 data of this investigation, as shown in Figure 18. In order to permit similar testing conditions, junction temperatures were maintained within a few percent of those given by Clausing and Chao. Although the data clearly are not identical, it should be noted that the curves do show the trend of increased conductance with decreased flatness deviation.

Experimental results presented by Bloom (6) and Fried (19) show that thermal contact conductance increases as surface roughness and flatness deviation decrease. In the work of Clausing and Chao (10), however, results of several tests show that contact conductance increases with increased surface roughness and flatness deviation, while results of the remainder of their tests exhibit the opposite trend (Figure 17). Thus, actual comparison with specific test runs can only be approximate, since such a wide variation of thermal contact conductance with surface finish exists.

Thermal contact conductance values determined as a result of unloading the junction are approximately 25 percent higher than loading values, as shown in Figures 17 and 18. This phenomena has also been noted by Clausing and Chao (10), Fried (19), and Yavonovich (37). Although there has been no interpretation presented in the literature,

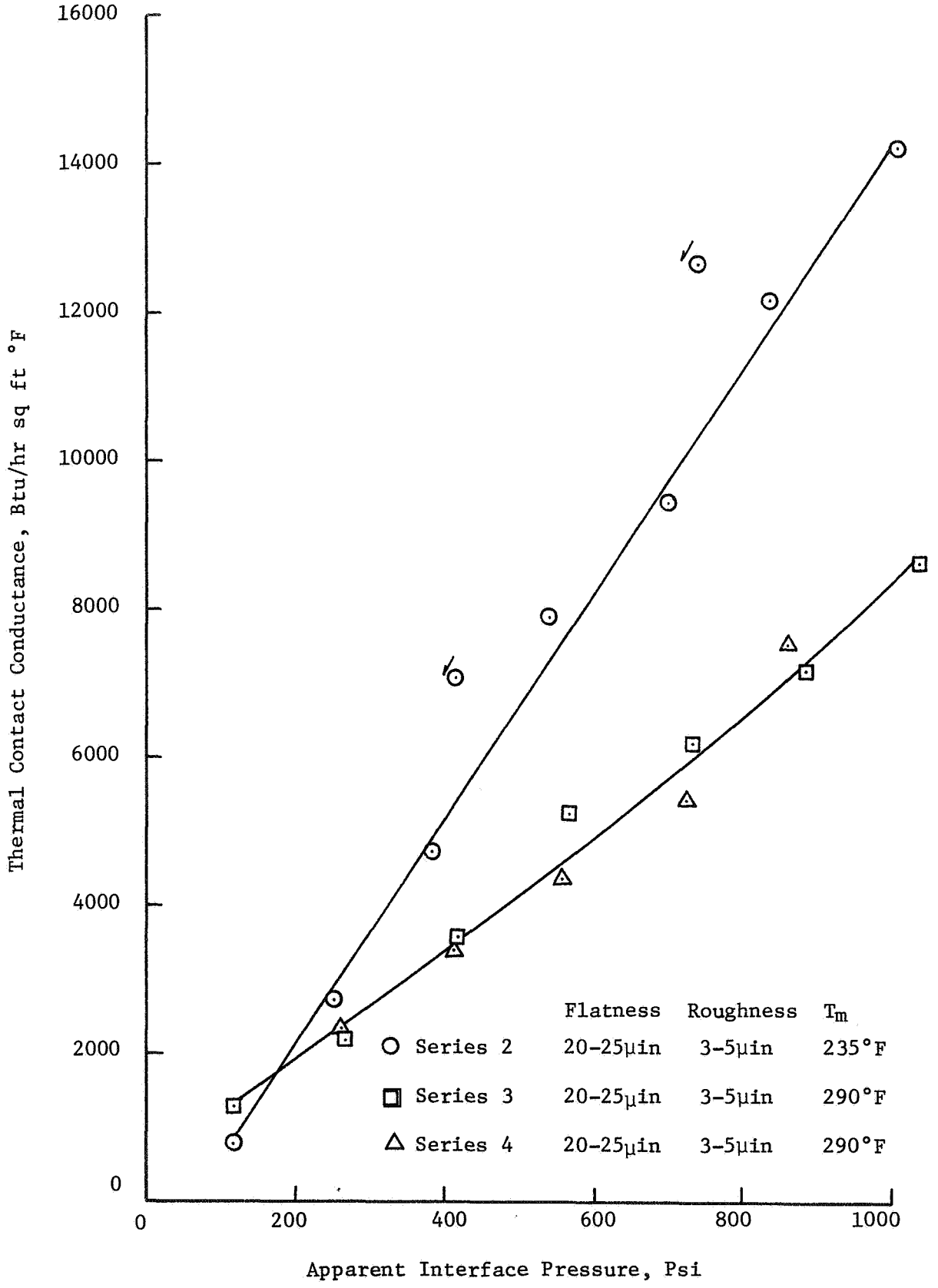

Figure 19. The Variation of Thermal Contact Conductance with Apparent Interface Pressure for Mean Junction Temperatures of 230-240°F and 290-300°F.

the increased value of thermal contact conductance for unloading conditions may be explained by considering the action at the interface. As the surfaces are loaded, there is a tendency for any microscopic protuberance to be flattened, resulting in a smoother surface. Thus, as would be expected, unloading the interface to some lower value will result in a higher value of contact conductance due to the smoother surface. During a subsequent test in Part II of this investigation, it was noticed that specimens tested enough times to assure repeatable data do not exhibit this phenomena, since after several cycles of loading and unloading the surface conditions tend to become uniform. Fried (19) has also shown that specimens tested several times exhibit little deviation between loading and unloading values of contact conductance.

Figure 19 shows a comparison of Series 2 data with that obtained in Series 3 and 4. It should be pointed out that although the same specimens were used for all tests, the surfaces were repolished between Series 2 and 3. The thermal contact conductance values for both average junction temperatures (235°F and 295°F) are similar functions of pressure. The variation in surface finish due to the polishing may account for the difference between the two curves, since a temperature increase of 50 to 60°F at the junction does not substantially effect the contact conductance (6,31). Series 4 was run as a repeatability check for Series 3, and as illustrated compares very favorably.

The experimental results obtained by Fried (19) for Aluminum 2024 are shown in Figure 20 for comparison with this investigation. The curves do show the same general trend, and as expected, the thermal contact conductance does increase with decreased surface roughness and flatness deviation. The increased contact conductance occurs not only

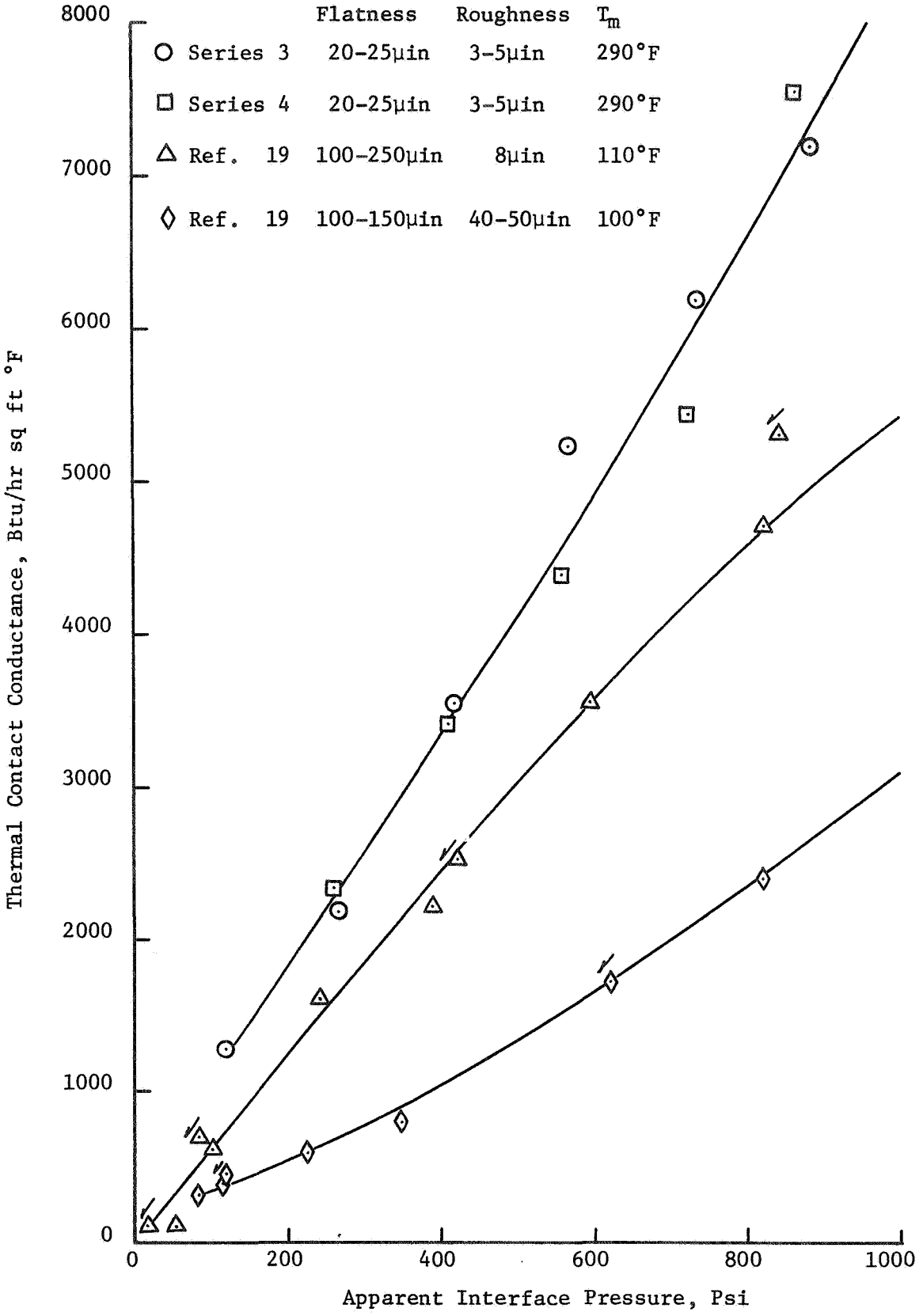

Figure 20. The Variation of Thermal Contact Conductance with Apparent Interface Pressure - Comparison with Fried (19).

because of a smoother surface finish, but also because of a higher mean temperature at the interface.

Comparison with the Aluminum 2024 experimental data of Yavonovich (37) is uninstructive due to his extremely large flatness deviation (1250 microinches). Similarly, the range of interface pressures (5,900 psi) far exceeds those normally expected in spacecraft applications. However, thermal conductance data of the present investigation are considerably higher than those of Yavonovich for load pressure of up to 1000 psi. This difference in thermal contact conductance is to be expected because of the large variation in flatness deviation.

Coarse finished surfaces appear to permit more reliable contact heat transfer prediction and provide more reproducible test data. Conversely, very fine finish surfaces (such as optically polished surfaces) result in the least reproducibility and predictability (19). This is evidenced by comparing the experimental results of Clausing and Chao (10), Fried (19), and Yavonovich (37). Enough surfaces with large flatness deviations (220 microinches or greater) compare favorably, whereas for smoother surfaces with relatively small flatness (50 microinches or less) deviations of more than 100 percent are exhibited (Figure 17).

The experimental values of thermal contact resistance determined with this apparatus are repeatable and comparable to the data of other investigators. These results indicate that the apparatus and techniques used are satisfactory for the investigation of thermal contact conductance with interstitial materials.

CHAPTER VI

CONCLUSIONS AND RECOMMENDATIONS

The experimental apparatus described in this report was designed and constructed for the purpose of investigating thermal contact conductance. It has the capability of subjecting the test interface to a wide range of physical and environmental conditions. A series of acceptance tests were conducted and the results were shown to compare favorably with those of other investigators. Thus, the major objective of this part of the overall investigation -- the verification of the thermal contact conductance values obtained with this apparatus -- has been accomplished. Experimental calculation techniques and procedures have also been established. The second phase of this investigation, a comparative study of interstitial materials, is now being undertaken.

The use of surface thermocouples (p. 40) in addition to the internal thermocouples permits a more detailed analysis of the axial heat flux and allows a continuous check of the effectiveness of the radiation shield. The location and installation of the thermocouples is extremely important (p. 40). Distances should be accurately measured to deduce the uncertainty in the calculated temperature gradients. After trying various methods of installation, it was found that the use of Aluminum powder packed around the thermocouple bead provides the most repeatable data (p. 39).

Controlling the temperature gradients in the specimen should permit a more accurate evaluation of the temperature difference (ΔT_j) at the interface. Such control can be accomplished by the use of heated fluids circulated through the sink assembly.

For the temperature range considered in this investigation, it was found that a radiation shield for the heated specimen was adequate. A split radiation shield was tested, however, results were not as satisfactory as the single heated specimen shield (p. 42). Materials for shields can be varied, but Aluminum foil provides the most versatility, with minimum heat loss by conduction.

As shown in Chapter 5, the experimental results of this investigation compare generally with those of Clausing and Chao (10) and Fried (19). Although specific comparisons are difficult due to the variation of surface finish and mean junction temperature, similar trends are evident (p. 55). Results of a repeatability check have shown a deviation of less than 5 percent in the thermal contact conductance (p. 55). Uncertainties for this investigation ranged from 5.0 to 8.9 percent for the heat fluxes, 7.2 to 11.6 percent for the thermal contact conductance, and 0.7 to 5.6 percent for the apparent load pressure (Appendix F). These results and uncertainties indicate that the apparatus and techniques used are satisfactory for the investigation of thermal contact conductance with interstitial materials.

RECOMMENDATIONS FOR INSTALLATION

One of the most important aspects of the test apparatus is the flexibility of the movements of the test specimens. The installation permits the initial alignment of the specimens as well as their separation and recontact in a vacuum environment. The following describes the test method of installating the test apparatus to achieve this flexibility.

The nitrogen load bellows and sink should be secured to the upper plate of the test apparatus (Figure 11). The addition of stops on the bellows guide rods will keep the loading chamber from expanding when placed in a vacuum environment. The source and specimen are attached to a loading rod which passes through both the base plate and the apparatus lower plate. This loading rod is connected to a bellows pass-through arrangement which is attached to the base plate (Figure 11). A mechanical screw-jack or equivalent, which will raise and lower the test specimen, should be placed directly below the bellows pass-through. The support rods for the screw-jack support should pass through the base plate and be attached to the test apparatus for the purpose of firmly securing the equipment to the main support. The load cell and associated leads should be electrically insulated to eliminate extraneous signals which might lead to inaccurate readings.

All components, which are located in the vacuum chamber, should be completely cleaned to remove all contaminents which might hinder high vacuum conditions. Also, specimens should be handled with care to avoid damage to the contact surfaces and thermocouples.

RECOMMENDATIONS FOR OPERATION

Once the test apparatus has been installed and secured to the vacuum facility the following operation procedure should be used:

1. An initial reading for zero load conditions should be made for both the load cell and the dial indicator on the pass-through bellows (Figure 11).
2. The specimens should then be aligned and brought together. They should be cycled several times between a 50 psi loading and separation to insure alignment and complete interface contact. If this repeatability requirement is met, the specimens are separated a few mils to permit any interstitial gases to be evacuated.
3. Next, the apparatus should be cleaned again to remove any contaminents which have been left on the equipment during the aligning procedure. The bell jar is then lowered into position.
4. The roughing pump should then be started and a small current applied to the heaters. This permits out-gassing of the apparatus components.
5. After a sufficiently low pressure has been attained (50-100 microns), the diffusion pump should be turned on and out-gassing continued for several more hours.
6. Next, the test specimens should be brought together and tests initiated.

7. Tests are conducted by first heating the specimens to some preselected junction temperature value to permit out-gassing of the materials and heater. Data are then obtained in an increasing load order, allowing time for each set of conditions to come to steady-state.
8. When the runs are completed, the power to the heaters should be turned off and the test cell sealed off from the rest of the vacuum facility. Dry nitrogen is introduced to the chamber and the specimens are allowed to cool, reducing the possibility of oxidation of interfaces.
9. The apparatus is then ready for removal or any required changes.

BIBLIOGRAPHY

1. Abbott, Rudolph E., "Experimental Facilities for Investigating Thermal Contact Conductance in a Vacuum Environment". Engineering Report, Arizona State University, 1967.

2. Atkins, Harry, "Bibliography on Thermal Metallic Contact Conductance", NASA TM X-53227, 1965.

3. Baker, D.H., E.A. Ryder and N.H. Baker, Temperature Measurement in Engineering, Volume 1. New York: John Wiley and Sons, Inc., 1953.

4. Barzelay, Martin E., Kin Nee Tong, and George F. Holloway, "Effect of Pressure on Thermal Conductance of Contact Joints", Syracuse University, NACA TN 3295, May 1955.

5. Barzelay, Martin E., "Range of Interface Thermal Conductance for Aircraft Joints", Syracuse University, NASA TN D-426, May 1960.

6. Bloom, M.F., "Thermal Contact Conductance in a Vacuum Environment", Douglas Aircraft Co. Report SM-47700, December 13, 1964.

7. Blum, H.A., "Heat Transfer Across Surfaces in Contact: Practical Effects of Transient Temperature and Pressure Environments", NASA Semi-Annual Report, October 1965.

8. Brunot, A.W. and F.F. Buckland, "Thermal Contact Resistance of Laminated and Machined Joints", Transactions of ASME, Volume 71, April 1949, pp. 253-257.

9. Cetinkale, T.N. and Margaret Fishenden, "Thermal Conductance of Metal Surfaces in Contact", General Discussions on Heat Transfer, Conference of the Institution of Mechanical Engineers and ASME, September 1951, pp. 271-275.

10. Clausing, A.M., and Chao, B.T., "Thermal Contact Resistance in a Vacuum Environment", University of Illinois Experimental Station Report ME-TN-242-1, August 1963.

11. Clausing, A.M., "Some Influences of Macroscopic Constrictions on the Thermal Contact Resistance", Engineering Experiment Station, Department of Mechanical and Industrial Engineering Report ME-TN-242-2, April 1965, NASA Grant NsG-242-62, University of Illinois, Urbana, Illinois.

12. Cunnington, G.R., Jr., "Thermal Conductance of Filled Aluminum and Magnesium Joints in a Vacuum Environment", ASME Paper No. 64-WA/HT-40, Presented at the Winter Annual Meeting, New York, N.Y., November 29-December 4, 1964.

13. Dahl, A.I., Temperature Its Measurement and Control in Science and Industry, Volume 3. New York: John Wiley & Sons, Inc. 1963.

14. Dailey, R.M., and Kaspareck, W.E., "Thermal Contact Conductance in a Vacuum", NASA TM X-53044, pages 108-116, May 1964.

15. Dushman, Saul, Scientific Foundations of Vacuum Technique (Second Edition). New York: John Wiley & Sons, Inc., 1962.

16. Eldridge, E.A. and H.W. Deem (eds.), "Report on Physical Properties of Metals and Alloys from Cryogenic to Elevated Temperatures", ASTM Special Technical Publication No. 296, Philadelphia: American Society for Testing Materials, April 1961.

17. Fried, Erwin, "Thermal Joint Conductance in a Vacuum", ASME Paper 63-AHGT-18 March 1963.

18. Fried, Erwin, "Study of Interface Thermal Contact Conductance", Summary Report, Document No. 64SD652, General Electric Company, 1964.

19. Fried, Erwin, "Study of Interface Thermal Contact Conductance, Summary Report, 27 March 1964 - 27 March 1965", Document No. 65SD4395, G.E. Spacecraft Department, Valley Forge Space Technology Center, Philadelphia.

20. Fried, Erwin, "Study of Interface Thermal Contact Conductance, Summary Report, 27 March 1965 - 31 July 1966", Document No. 66SD4471, G.E. Spacecraft Department, Valley Forge Space Technology Center, Philadelphia.

21. Fried, E., and Costello, F.A., "Interface Thermal Contact Resistance Problem in Space Vehicles", ARS Journal, Volume 32, pp. 237-243, February 1962.

22. Gex, Robert C., "Thermal Resistance of Metal-to-Metal Contacts: An Annotated Bibliography", Lockheed Missiles & Space Division, Special Bibliography SB-61-39, July 1961.

23. Goldsmith, A., T.E. Waterman and H.G. Hirschlorn, Handbook of Thermophysical Properties of Solid Materials, Volume 2. New York: Pergamon Press, 1961.

24. Hudack, Larry J., "An Engineering Analysis of Heat Transfer Through Metallic Surfaces in Contact", M.S. Thesis, Arizona State University, 1965.

25. Jansson, R.M., "The Heat Transfer Properties of Structural Elements for Space Instruments", M.I.T. Instrumentation Lab Report No. 1173, June 1962.

26. Kreith, Frank, Principles of Heat Transfer, Second Edition. Scranton, Pennsylvania: International Textbook Company, 1965.

27. Lafferty, J.M., "Techniques of High Vacuum", General Electric Report No. 64-R1-3791 G, November 1964.

28. Laming, L.C., "Thermal Conductance of Machined Metal Contacts", 1961 International Heat Transfer Conference, Part 1, No. 8, pp. 65-76, Boulder, Colorado, September 1961.

29. Minges, Merrill L., "Thermal Contact Resistance - A Review of the Literature", Air Force Systems Command, Air Force Materials Laboratory, TR-65-375, April 1966.

30. Powell, R.W., R.P. Tye and B.W. Jolliffe, "Heat Transfer at the Interface of Dissimilar Materials: Evidence of Thermal-Comparator Experiments", International Journal Heat Mass Transfer, Volume 5, pp. 897-902.

31. Rogers, G.F., "Heat Transfer at the Interface of Dissimilar Metals", International Journal of Heat Mass Transfer, Volume 2, 1961, pp. 150-154.

32. Schenck, Hilbert, Jr., Theories of Engineering Experimentation. New York: McGraw-Hill Book Company, Inc., 1961.

33. Shlykov, Yu P. and E.A. Ganin, "Experimental Study of Contact Heat Exchange", Teploenergetika, Volume 8, No. 7, 1961, pp. 73-76, (Urusky, W. (Translator), Translation Branch, Redstone Scientific Information Center, U.S. Army Missile Command, Redstone Arsenal, Alabama, January 1964).

34. Stubstad, W.R., "Measurements of Thermal Contact Conductance in Vacuum", ASME Paper NO. 63-WA-150, August 1963.

35. Vidoni, Carlotta, M., "Thermal Resistance of Contacting Surfaces: Heat Transfer Bibliography", Lawrence Radiation Laboratory, Livermore, California, UCRL-14264, 1965.

36. Weills, N.D. and Ryder, E.A., "Thermal Resistance Measurements of Joints Formed Between Stationary Metal Surfaces", Transactions ASME, Volume 71, pp. 259-267, 1949.

37. Yovanovich, M. Michael, "Thermal Contact Conductance in a Vacuum", Engineering Projects Laboratory, Massachusetts Institute of Technology, DSR Project No. 4542, November 1965.

38. Yovanovich, M. Michael, "Thermal Contact Resistance Between Smooth Rigid Isothermal Planes Separated by Elastically Deformed Smooth Spheres", AIAA Paper No. 66-461, 4th Aerospace Sciences Meeting, Los Angeles, California, June 27-29, 1966.

APPENDIX A

SELECTED TEST APPARATUS DRAWINGS

The following are selected detailed drawings of the NASA apparatus. Figure A-1 is an assembly drawing and Figures A-2 through A-6 are drawings of specific components.

Figure A-1: NASA Apparatus Assembly Drawing

Figure A-2: Base Plate Layout

Figure A-3: Sink Assembly

Figure A-4: Sink Specimen

Figure A-5: Source Specimen

Figure A-6: Load Bellows Assembly

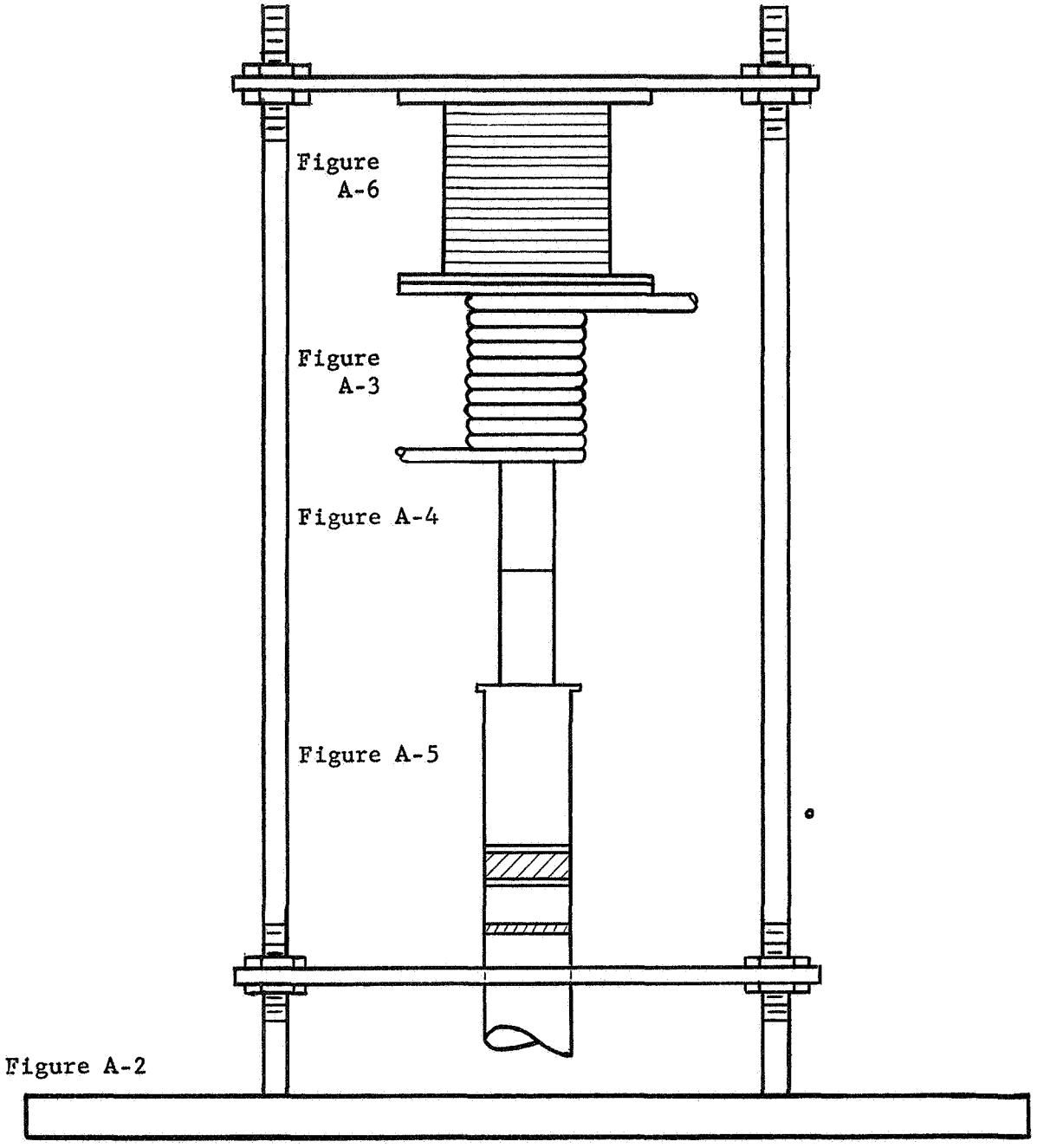

Figure A-1. NASA Apparatus Assembly Drawing.

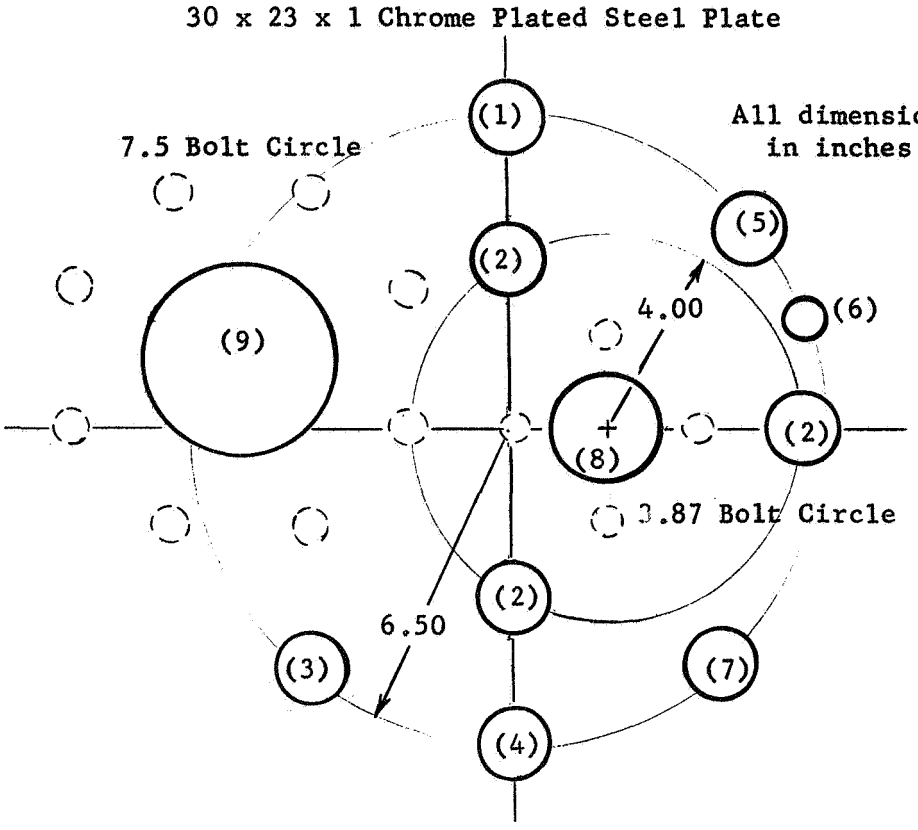

Diameters

(1) 1.006 - Blank
(2) 1.383 - Support Rod Passthrough
(3) 1.383 - Power input
(4) 1.383 - Cryogenic Passthrough
(5) 1.383 - Dry Nitrogen Passthrough
(6) 0.757 - Thermocouple Passthrough
(7) 1.008 - Sink Coolant Passthrough
(8) 2.000 - Load Passthrough Bellows
(9) 4.000 - Vacuum Port

Figure A-2. Details of the Baseplate Layout.

Note A: Bore and Tap for 1.00-8 Threads, Class 2 Fit.

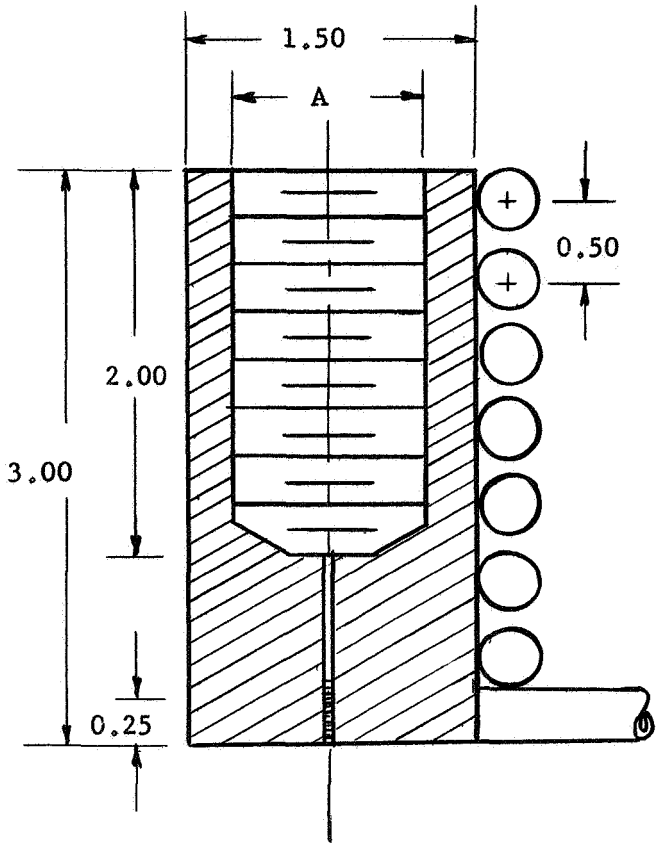

All dimensions in inches.

Figure A-3. Details of the Sink Assembly.

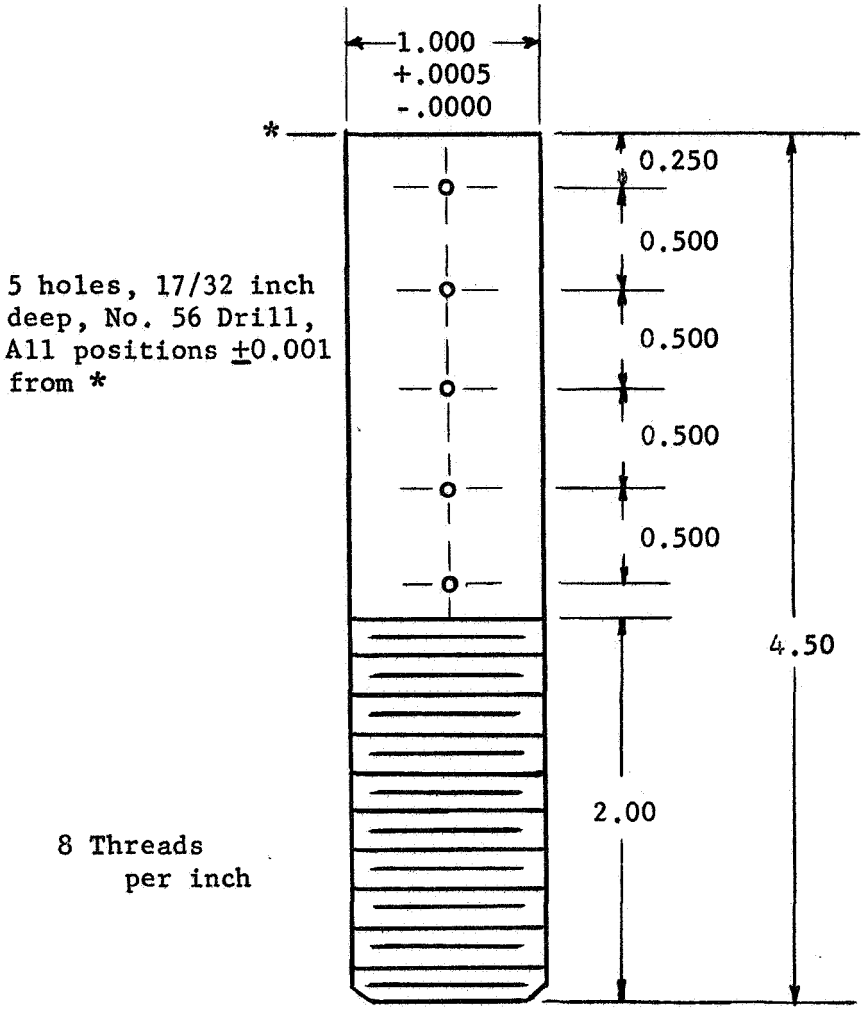

All dimensions in inches.

Figure A-4. Details of the Sink Specimen.

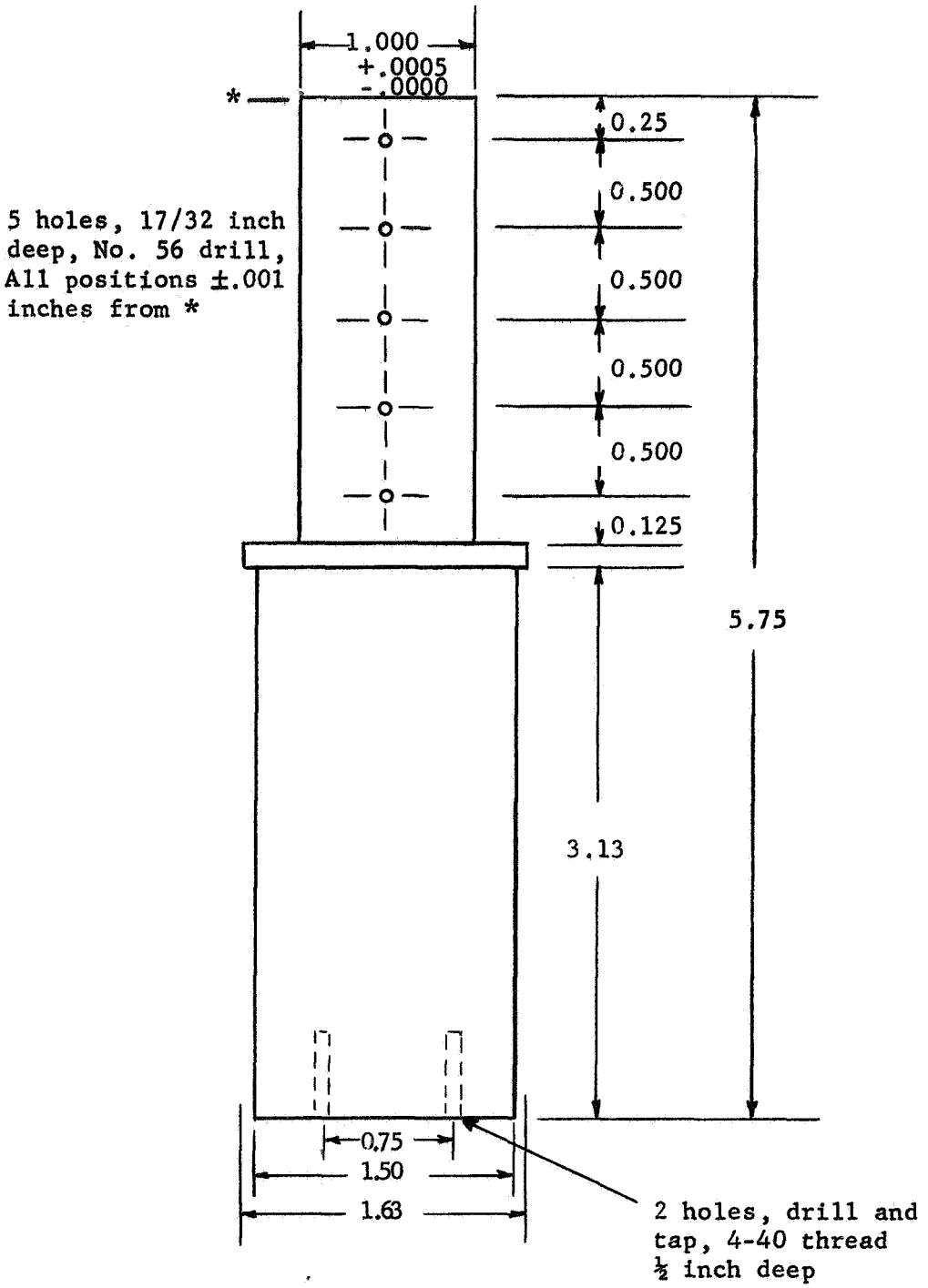

All dimensions in inches.

Figure A-5. Details of the Source Specimen.

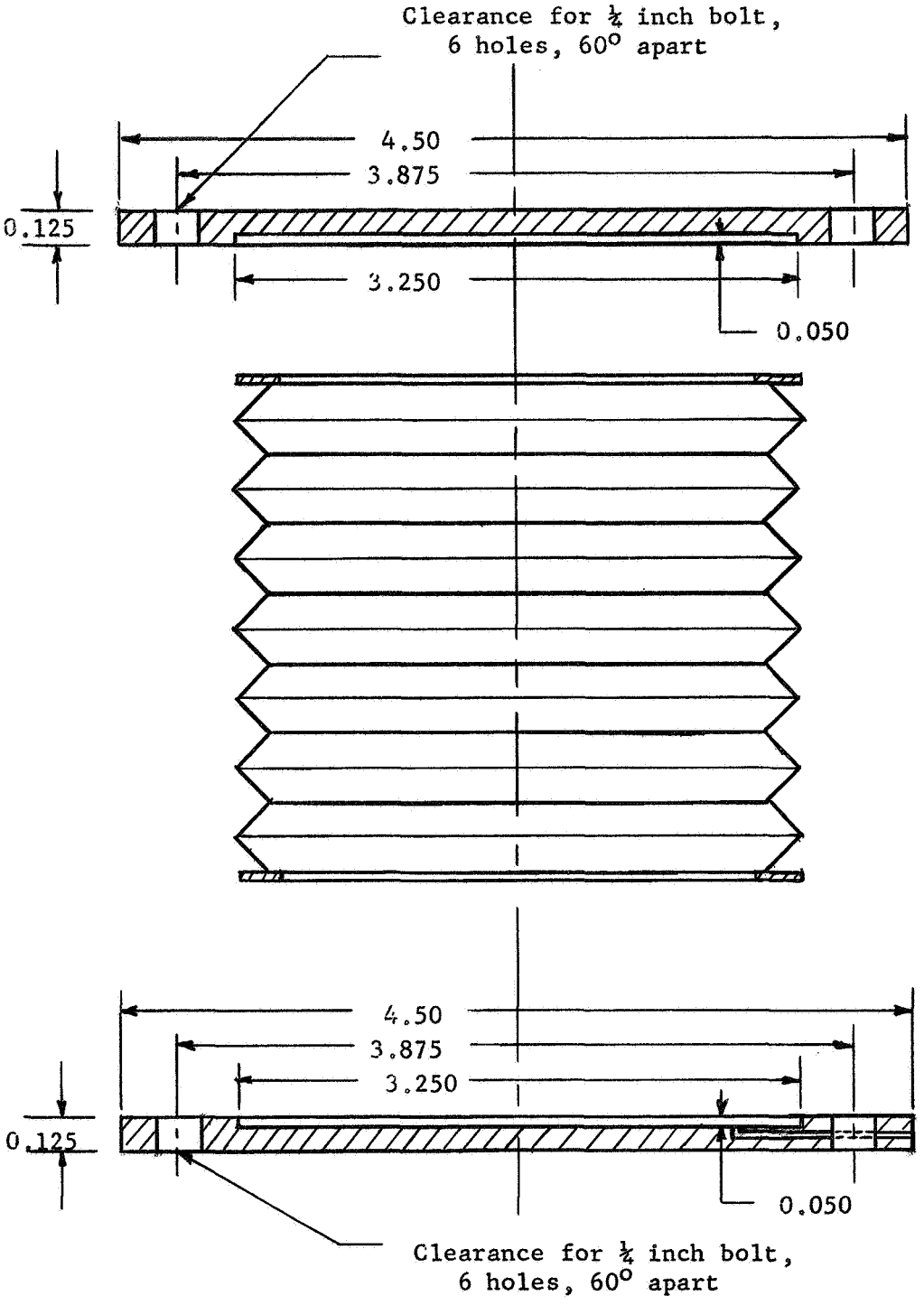

All dimensions in inches.

Figure A-6. Details of the Load Bellows Assembly.

APPENDIX B

CALIBRATION OF THE COMPRESSION LOAD CELL AND LOAD PASSTHROUGH BELLOWS

A BLH Model C3P1 compression only load cell with a range of 0 to 1000 pounds was supplied by Ames Research Center to measure the force applied to the test column. Before the load cell could be calibrated, it was necessary to establish a suitable gage factor for it. To determine the gage factor, the load cell was coupled to the four arm side of a BLH Model 120 strain indicator. Various gage factors were set on the strain indicator, until one was found that gave a near zero deflection reading with the null indicator centered. The gage factor of 2.00 yielded a centered null indicator with a deflection reading of 4 microinches and an add-on reading of 30,000 set on the strain indicator. (See BLH TM No. 100-465, Instruction Manual for Model 120C Strain Indicator, for a description of the factors associated with the strain indicator.)

To calibrate the load cell, a force of known magnitude that was continuously increased from 0 to 1000 pounds was applied to the load cell. The resulting output of the load cell in microinches of deflection was recorded at each 10 pound increment of force applied. The force was applied by a Tinius-Olsen Universal Testing Machine (See Table B-1, for a description of the machine) with its automatic load control adjusted to increase the force on the load cell at a rate of approximately 10 pounds per minute. The Universal Testing Machine was accurate to within 0.1 percent or less. As the force indicating dial on the Universal Testing Machine passed through

each 10 pound increment, the resulting deflection of the load cell was recorded from the same BLH strain indicator used to obtain the gage factor.

The calibration results are plotted for easier use in Figure B-1. It should be noted that the load cell was quite linear over the entire range from 0 to 1000 pounds and had a "calibration factor" of 6 microinches deflection per pound of force applied. A check calibration of the load cell was made for the present investigation and results are shown on Figure B-1.

The stainless steel passthrough bellows chamber was located between the test apparatus and the load cell. Thus, the deflection of the bellows that resulted from the load created an additional force on the load cell. A correction for this effect was obtained by calibrating the load bellows to determine the force that resulted from a given deflection.

The force required for load bellows deflections of 0.5, 0.4, 0.3, 0.25 and 0.2 inches were found in the following manner. First, the bellows was allowed to attain a neutral position with no force applied. This was taken as the zero deflection point and the dial indicator was adjusted to zero at this location. The load cell was brought into contact with the bellows by extending the screw jack. Then, the bellows was deflected at .025 inch increments as recorded on the dial indicator until the desired deflection was reached. At each increment, the total deflection and the force on the load cell were recorded. Readings were taken while both loading and unloading the bellows. In some cases, the bellows was allowed to sit at a certain deflection for several minutes to see if the resulting force changed. To determine the repeatability of the results, two runs were made

for deflections of 0.5 and 0.2 inches which were the two extremes. These data are graphically illustrated in Figure B-2.

The results proved several points. First, the force applied by the bellows for a given deflection was repeatable. Second, when increasing the load, the force of the bellows was the same for a given deflection. Third, the force obtained while decreasing the load was a function of the total deflection. Finally, the load was not a function of time. That is, the force applied by the bellows did not change when the deflection was held at some point for a period of time.

The effect of the pressure differential on the bellows created by the vacuum was investigated in two ways. First, the pressure in the vacuum chamber was assumed to be zero and the force on the bellows was assumed to be that created by one atmosphere acting on the inside area of the bellows. An upward force of 54.1 pounds was found by this method. Second, a vacuum was formed in the chamber and the deflection it caused in the bellows was read from the dial indicator. The resulting force on the bellows was taken from Figure B-2 at the deflection caused by the vacuum. This was done three times and the forces obtained were 54.1, 54.0, and 54.3 pounds. Thus, the force caused on the bellows by the pressure differential was taken to be 54.1 pounds.

To obtain the force on the interface, the load indicated on the load cell must be corrected for the deflection of the bellows and the effect of the pressure differential.

Specimen loading was accomplished by pressurizing the Nitrogen load bellows to the desired gage pressure. The force on the interface was then determined by adding 54.1 pounds to the load cell reading (Figure B-1) and

subtracting the resisting force due to the passthrough bellows deflection (Figure B-2).

The approximate force at the interface was easily determined by multiplying the absolute Nitrogen pressure by the area of the load bellows normal to the specimen column. This approximate method yielded results within 3 percent of actual force determined by the load cell.

TABLE B-1

CALIBRATION INFORMATION OF THE
BLH MODEL C3P1 COMPRESSION AND LOAD CELL

Load Cell	
Manufacturer	BLH Electronics, Division of Baldwin-Lima-Hamilton, Inc. Walham, Mass.
Model	C3P1
Capacity	0.1000 pounds
Type	Compression only
Gage factor	2.00
Strain Indicator	
Manufacturer	BLH Electronics
Model	120C
Capacity	0-60,000 micro inches
Scales used	30,000-35,000 micro inches
	35,000-40,000 micro inches
Universal Testing Machine	
Manufacturer	Tinius Olsen Testing Machine Co.
Model	Super L
Capacity	0-60,000 pounds (3 scales)
Scales used	0-1200 pounds
Calibration data:	
Date	11 August 1965
Result	Accurate to 0.1 percent or less
Load Cell	
Calibration Performed	24 January 1967
Check Calibration	14 June 1967

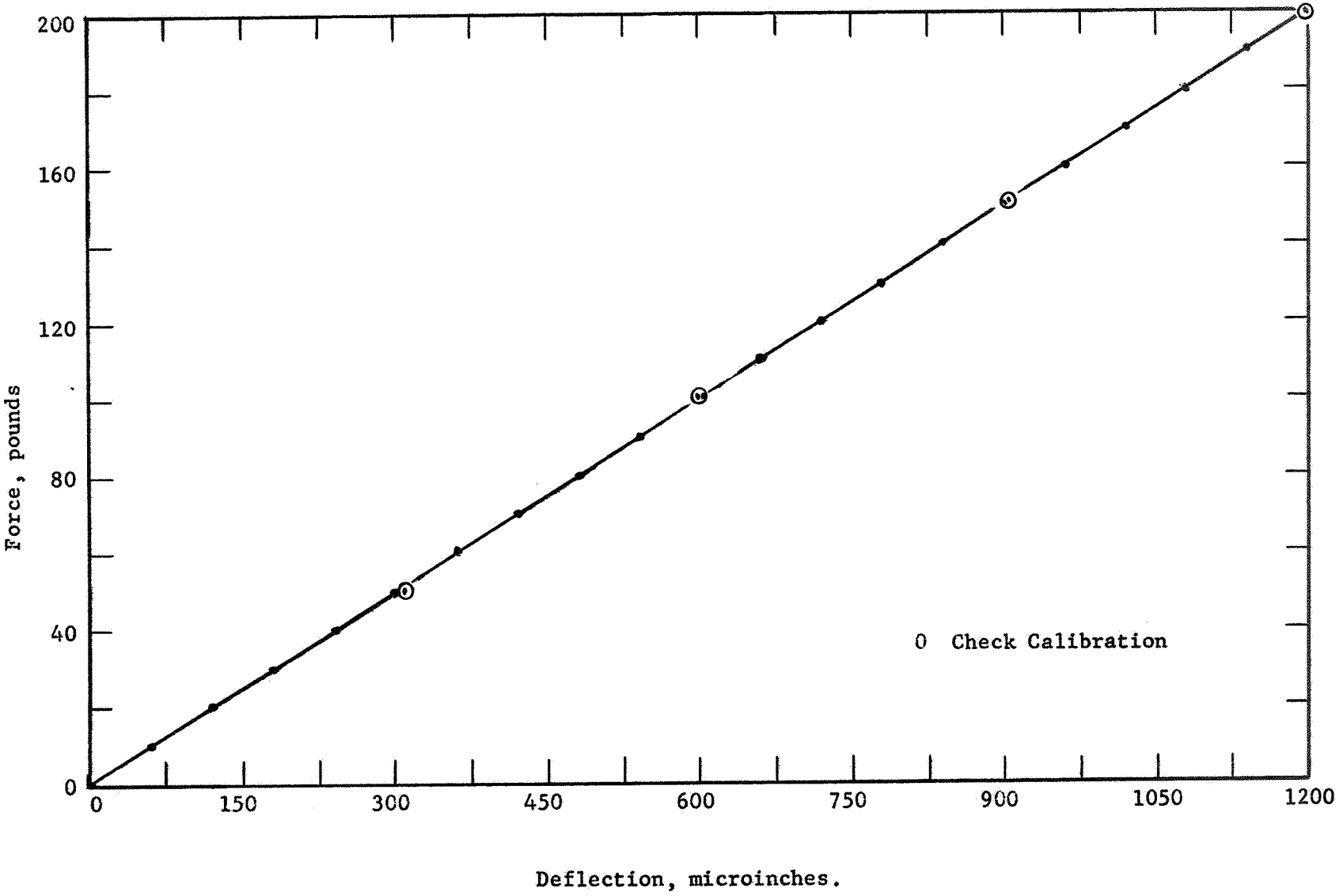

Figure B-1. Calibration Curve for the BLH-C3P1 Load Cell.

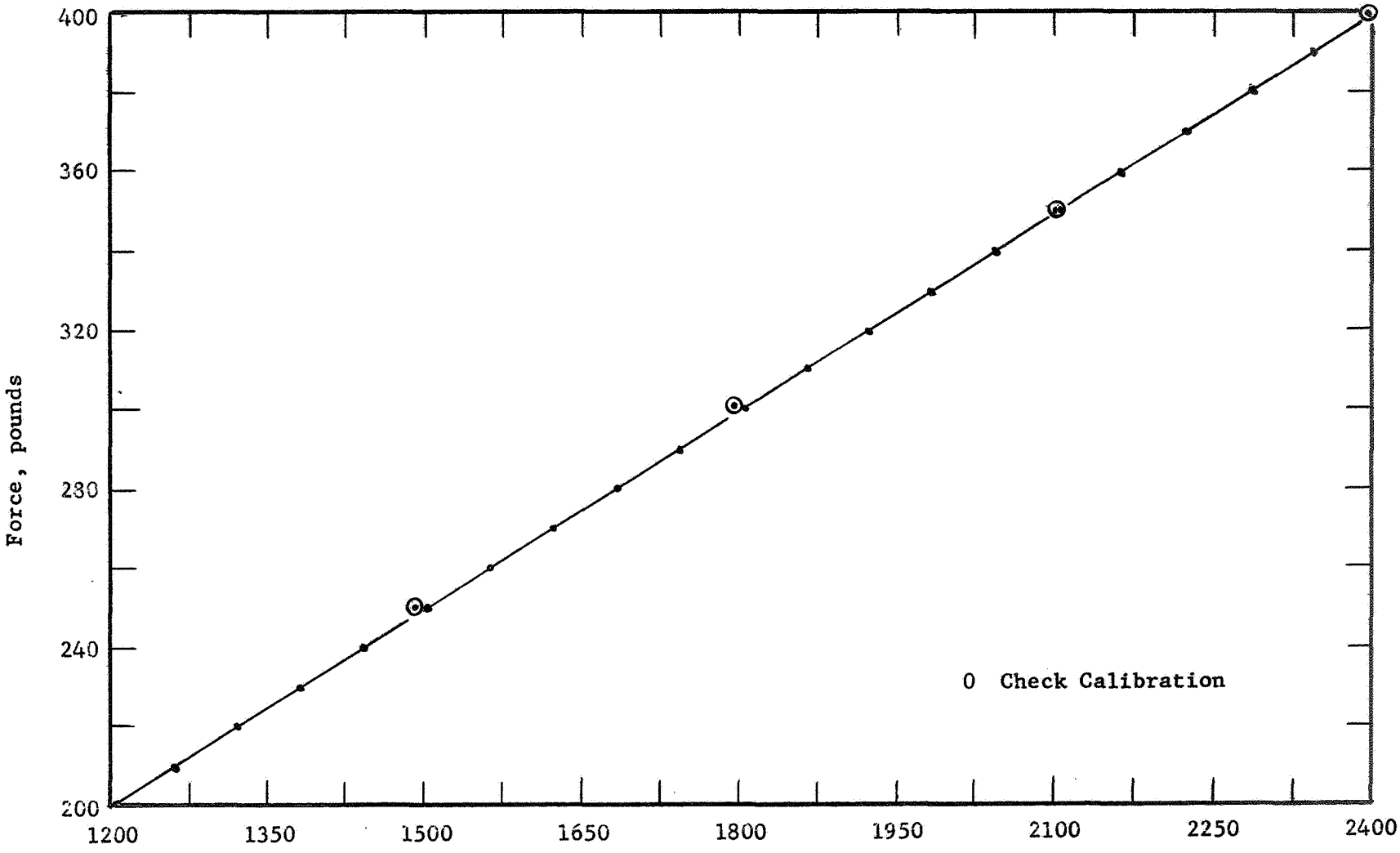

Figure B-1. continued

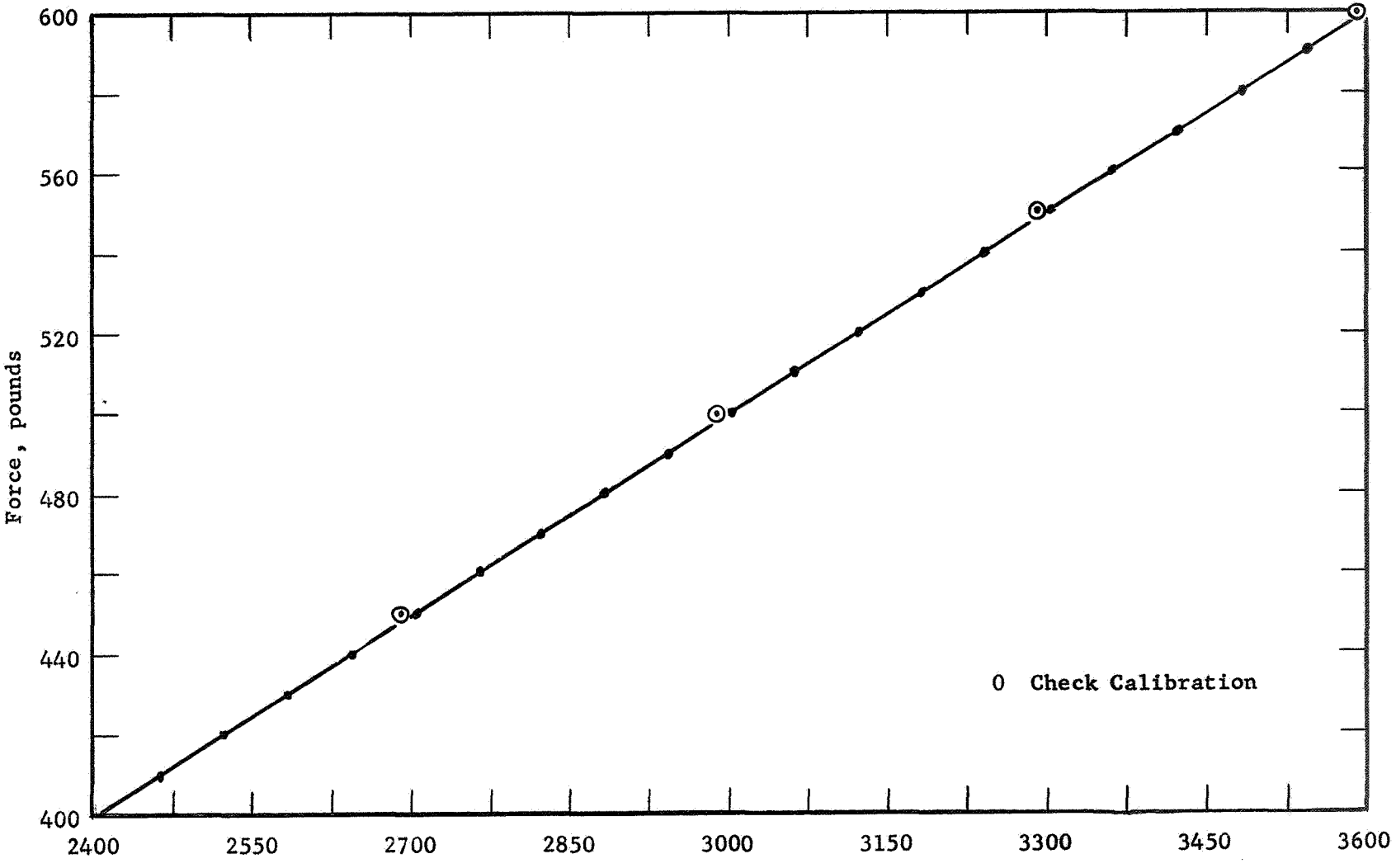

Figure B-1. continued

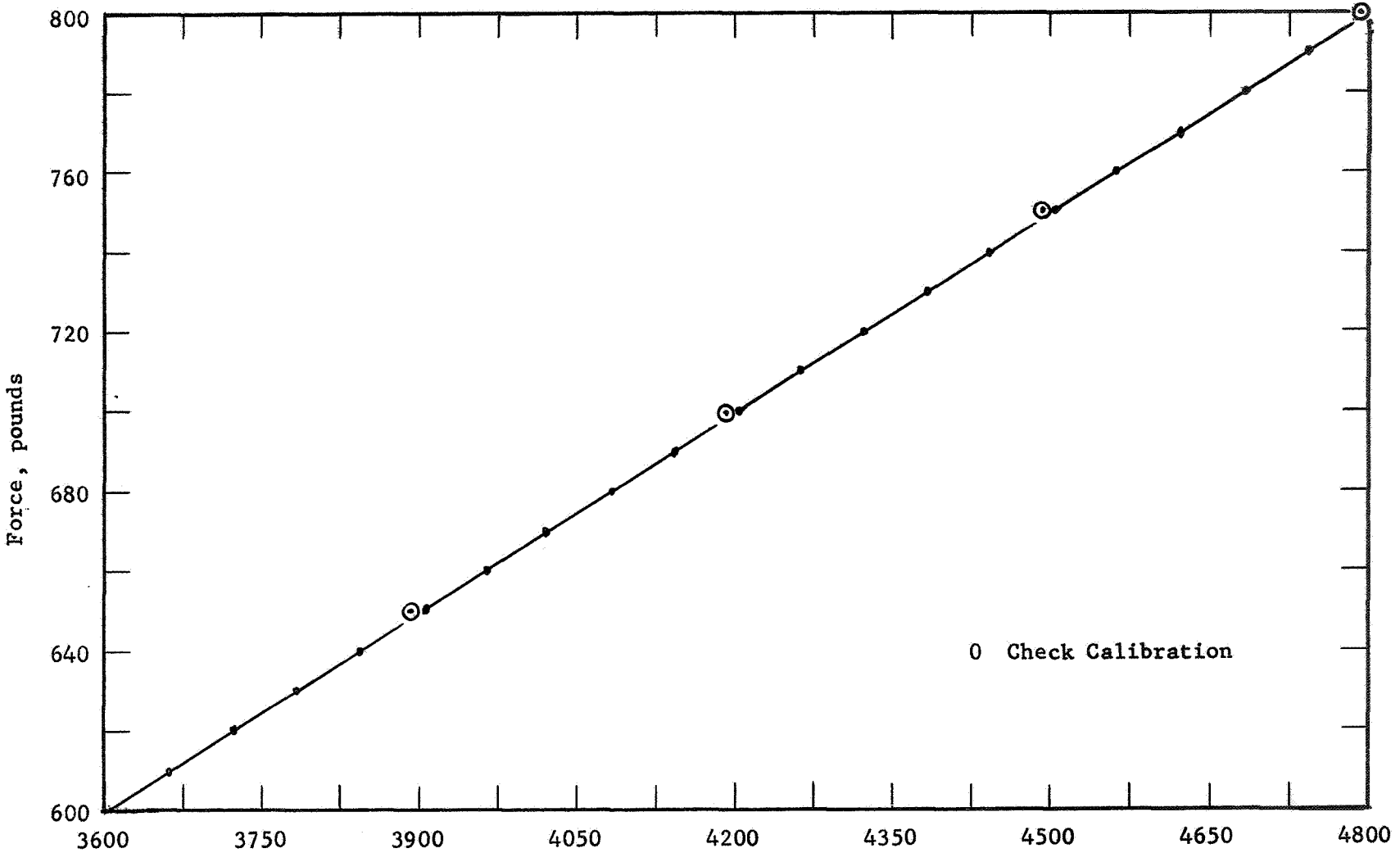

Figure B-1. continued

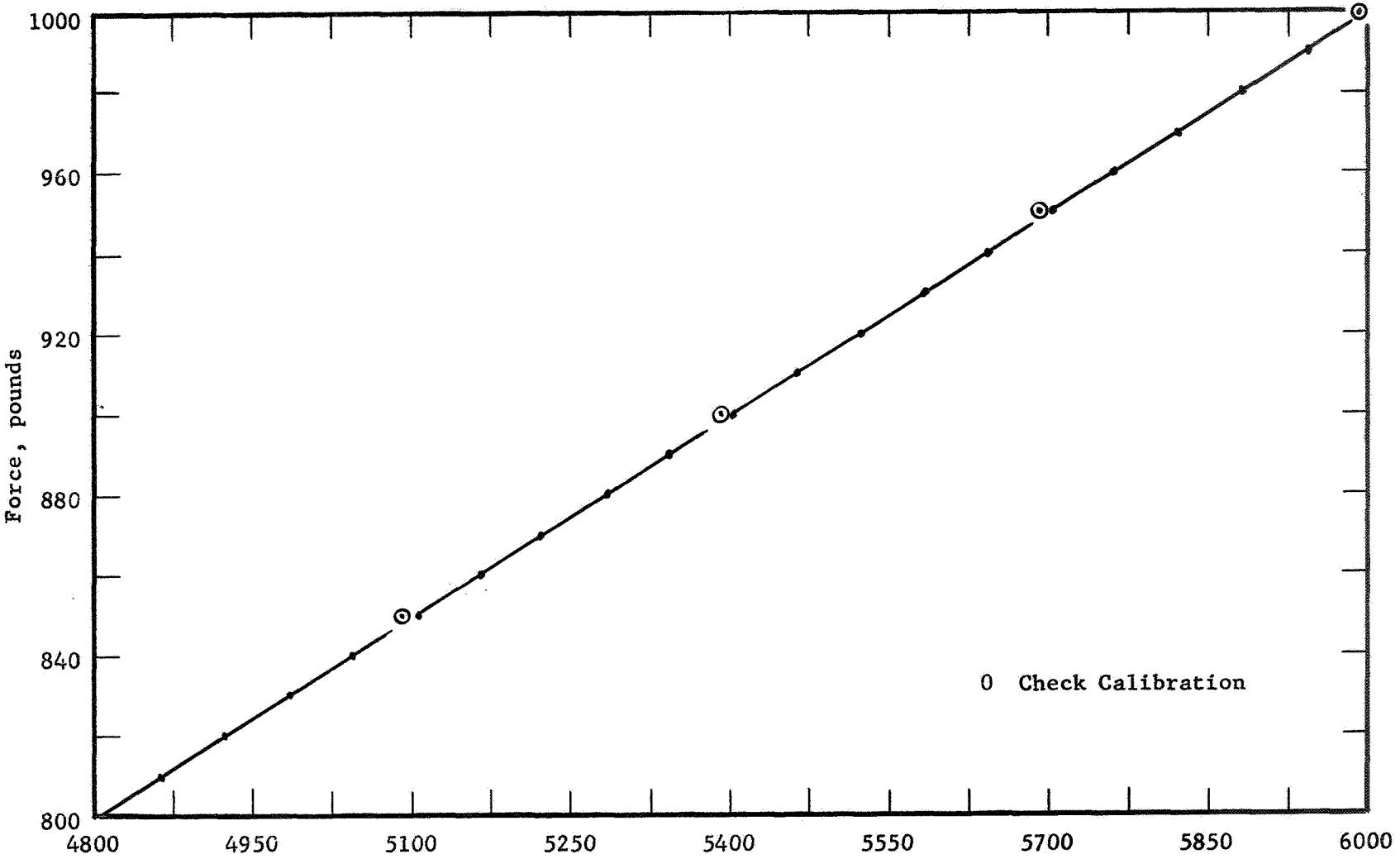

Figure B-1. concluded

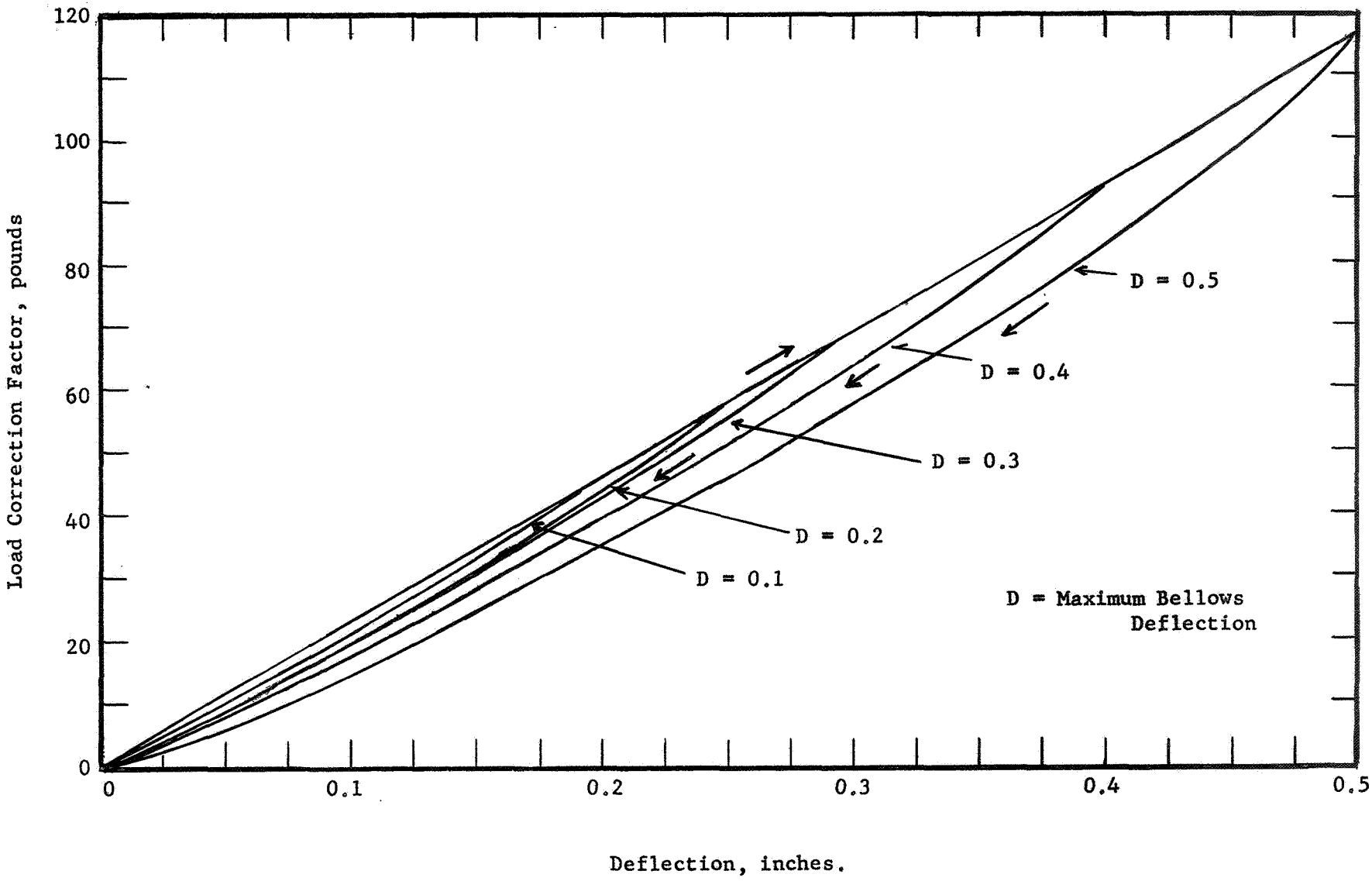

Figure B-2. Load Correction Factors for the Passthrough Bellows.

APPENDIX C

CALIBRATION OF THERMOCOUPLES AND THERMOCOUPLE READOUT SYSTEM

There are many ways to determine the accuracy of thermocouples and thermocouple systems. The calibration of the thermocouples and the associated wiring must be checked for contribution to error. The temperature measurement system was described in Chapter 3. The method used to check the accuracy of the system is described below.

Twenty-four 17 inch lengths of ThermoElectric Copper-Constantan (NN-28-DT) teflon-glass insulated thermocouple wire were made into thermocouples following the procedure specified in Chapter 4. These thermocouples were installed in a one and one-half inch diameter, one inch long slug of Aluminum 2024. The installation procedure was similar to that used for attaching thermocouples to the test specimens. In addition, a hole was drilled in the center of the slug for a certificated "Standard" Platinum-Platinum 10% Rhodium thermocouple manufactured by Leeds and Northrup Company. (Control Standard 784-24-S, Test No. 177706-M-19).

In order to calibrate the thermocouple system, the copper-constantan thermocouples were attached to the teflon terminal strips in the vacuum chamber. All twenty-four thermocouples in the passthrough, as well as two thermocouple switches and ice junctions, were included. The calibration was conducted using an 8686 Leeds and Northrup millivolt potentiometer. The Platinum-Platinum 10% Rhodium thermocouple was attached directly to a second Leeds and Northrup 8686 millivolt potentiometer with

an internal reference junction. A Schaar high accuracy mercury thermometer was used for reference junction temperatures.

The Aluminum slug was placed in an oil bath and room temperature was measured. Oil temperatures of approximately 330° F and 500° F were set and calibration data obtained. At each temperature condition the emf of the Platinum thermocouple was recorded twelve times, while the 24 copper-constantan thermocouples were read.

Thermocouples used in the test specimens were made from ThermoElectric NN-30-DT high accuracy wire and constructed in the manner described in Chapter 4. Several thermocouples made at different times were compared with the Platinum "Standard" in a laboratory furnace over the range of temperatures used in this investigation. Results of this check calibration indicated a deviation of 0.5 percent increasing linearly with temperature from 150° F to 600° F.

The accuracy of the Leeds and Northrup 8686 millivolt potentiometer was on the order of 5 microvolts for the range of interest, corresponding to a maximum error of 0.2° F. Thus the results of the thermocouple check calibration and the accuracy of the equipment employed in the system indicate that the relative accuracy of any particular thermocouple was within 0.5 percent of the temperature.

A standard conversion table for copper-constantan thermocouples (extracted by Leeds and Northrup from National Bureau of Standards Circular 561) was used. The appropriate section of the same table was used for the certificated "Standard" Platinum-Platinum 10% Rhodium thermocouple.

APPENDIX D

THERMAL CONDUCTIVITY MEASUREMENT

Knowledge of the thermal conductivity as a function of temperature is essential for determination of thermal contact conductance. An experimental apparatus was constructed to check the steady-state thermal conductivity for metallic materials used in this investigation. To verify the accuracy of this experimental apparatus and determine the heat loss, a series of tests were conducted using Armco Iron as a standard for comparison.

The apparatus consisted of two metallic specimens instrumented with iron constantan thermocouples, a central heater and two guard heaters, water cooled end plates and associated instrumentation. A schematic of the test apparatus is shown in Figure D-1.

The specimens were cylindrical, four and one-half inches long and one and five-eighths inches in diameter. Seven thermocouples were attached to each specimen in holes drilled at one-half inch intervals and thirteen sixteenths of an inch deep. Recessed holes in each end of the specimens accommodated the central heater and guard heaters.

The specimens were then placed together with the heat source in the center. Aluminum cooling plates, drilled for circulation of a cooling fluid, were clamped on as a heat sink. Before the top cooling plate was put into position, a 10-inch diameter, 9-inch high aluminum cylinder was placed around the test specimens. The space between the specimens and cylinder was filled with an insulation material, vermiculite, to reduce radial heat losses. A heat flux was then established through the

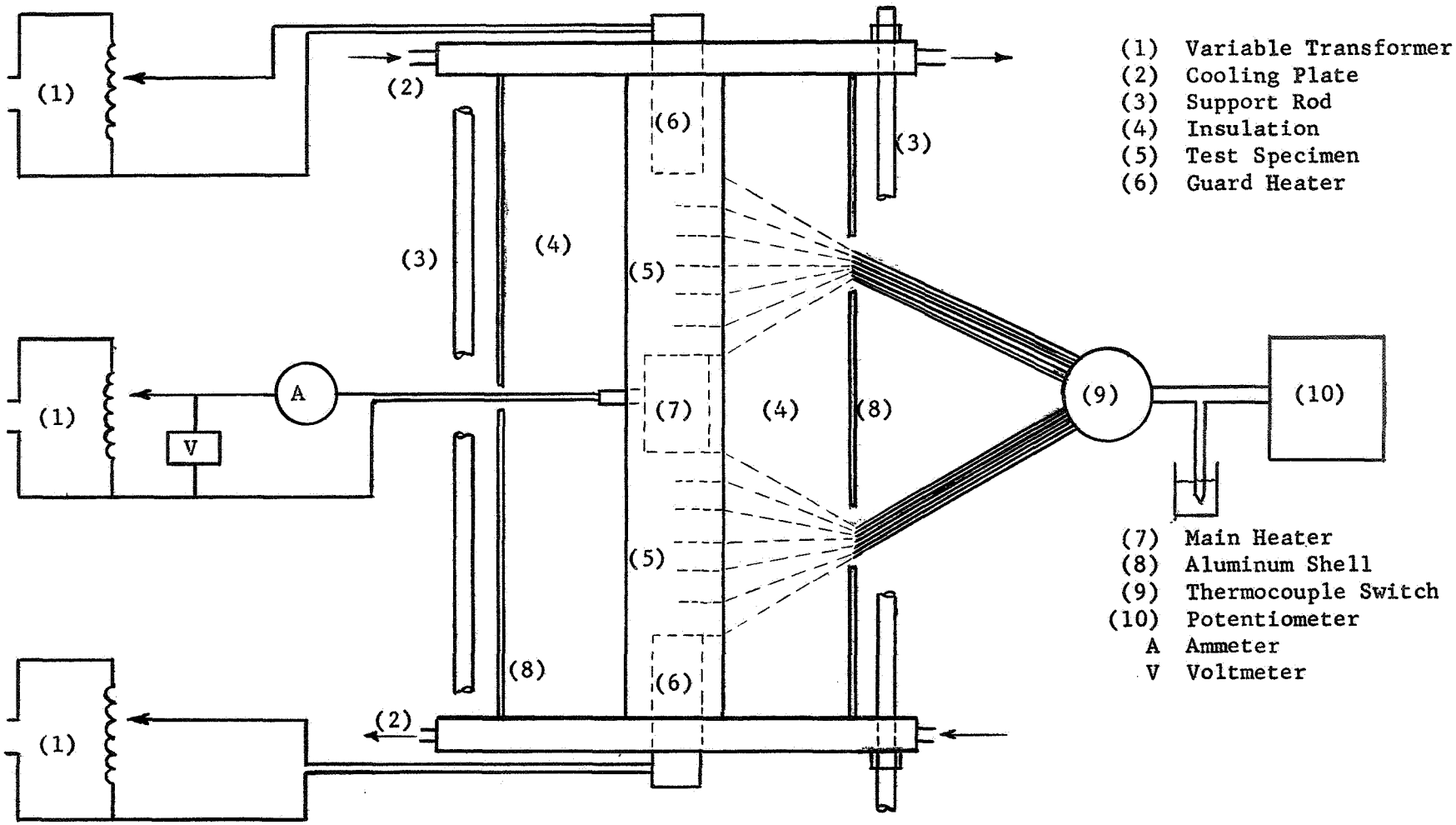

Figure D-1. Schematic of the Thermal Conductivity Test Apparatus.

test specimens by passing current through the heaters and by circulating water through the cooling plates. The energy input into the center heater was recorded by the voltmeter and ammeter, both of which were accurate to within $\pm$ 0.5 percent.

The arrangement of the heaters and surrounding insulation permitted the assumption of a one-dimensional heat flow, i.e., the heat was generated at the center heater and flowed in opposite directions through the specimens. The temperature gradient in each of the specimens was controlled by the use of a guard heater, as shown in Figure D-1. Knowledge of the heat flux and the temperature gradient permitted calculation of the thermal conductivity using Fourier's law for one-dimensional heat conduction (26) which states that

$$q = - k A \frac{\Delta T}{\Delta x}$$

The net heat flux, q, for determination of the thermal conductivity, is equal to the power supplied minus energy losses. The power supplied was determined from the relation

$$q_i = (3.413) E I, \quad \text{Btu/hr}$$

where E is the voltage drop across the heater, and I is the current through the heater. The energy loss is a combined function of the radial heat loss from the center heater through the insulation and the loss in the nichrome wire between the heating element and the point at which the voltage was measured. After careful analysis of the apparatus and measurement technique, the equation for the net axial heat flux was determined as

$$q_{net} = 3.413 E I - 1.365 I^2 - \frac{T - T_o}{HLC}$$

where T is the average specimen temperature, T_o is the ambient room temperature, I is the current, and E is the voltage, and HLC is

the heat loss coefficient. The thermal conductivity of the specimen

$$k = - \frac{2.89\ q_{net}}{\left(\frac{\Delta T}{\Delta x}\right)_{average}}, \quad \text{Btu/hr sq ft } ^\circ\text{F}$$

where q_{net} is determined from the preceding equation and $\frac{\Delta T}{\Delta x}$ is the average slope of the temperature gradients for each of the two specimens.

Experimental results for Aluminum 2024 ("as received" and "annealed") are presented in Table D-1 and shown graphically in Figure 12. Thermal conductivity values for Aluminum 2024 used by Yavonovich (37) in his analysis compare favorably with those determined for this investigation.

An uncertainty analysis following the procedure presented by Schenck (32), was performed to establish the validity of the data. The resulting equations for the uncertainty are

$$\frac{\delta q_{net}}{q_{net}} = \left[\frac{11.65\ I^2(\delta E)^2 + (3.41E - 2.73I)^2(\delta I)^2 + HLC^{-2}(\delta \Delta T)^2}{(q_{net})^2} \right]^{1/2}$$

and

$$\frac{\delta k}{k} = \left[\left(\frac{\delta q_{net}}{q_{net}}\right)^2 + \left(\frac{\delta \Delta T}{\Delta T}\right)^2 + \left(\frac{\delta \Delta x}{\Delta x}\right)^2 \right]^{1/2}$$

Thermocouple calibration (Appendix C) produced an uncertainty of $\pm$ 0.5 percent, current and voltage measurement were accurate within $\pm$ 0.5 percent, and the thermocouple locations were within 0.01 inch. Results of the uncertainty analysis for the thermal conductivity, using several representative sets of test data, indicated a maximum deviation of 3.2 percent for Aluminum 2024.

TABLE D-1

THERMAL CONDUCTIVITY FOR

ARMCO IRON AND ALUMINUM 2024

TABULATED RESULTS

	T avg, (°F)	k (Btu/hr ft °F)
ALUMINUM 2024 "As Received"	106.2	75.9
	118.1	77.3
	143.7	76.2
	166.4	77.1
	193.4	81.1
	238.6	82.5
	266.2	86.5
	293.9	86.9
	319.6	89.7
	349.4	94.2
ALUMINUM 2024 "Annealed"	104.7	108.9
	152.0	97.8
	179.0	97.5
	206.2	101.4
	222.2	99.9
	254.7	102.0
	283.7	105.1
	333.2	106.5
	369.0	110.4
	413.0	110.2
	443.5	114.4
	482.4	111.2
	-27.2	95.8
	-71.9	90.4

APPENDIX E

HEAT LOSS CALIBRATION

A heat loss calibration was performed with Armco Iron specimens since accurate values of the thermal conductivity were known (Figure 12). The experimental technique and calculation procedure are described in Chapter 5. Experimental results of the test are shown in Figures E-1 and E-2.

Figure E-1 shows the calculated heat flux plotted against the corresponding station along the specimen for three different initial heat fluxes. A greater heat loss from the higher temperature test was evident. The heat losses from the heated specimen (the specimen enclosed by the radiation shield) were never more than 4.5 percent of the initial heat flux. Figure E-2 shows the initial heat loss from the heater section plotted against the temperature of the thermocouple nearest the heater.

The net rate of heat exchange, q_n, between radiating gray surfaces is given by

$$q_n = \sigma A(\varepsilon F) (T_\alpha^4 - T_\beta^4)$$

where σ represents the Stephan-Boltzmann constant and is equal to 0.1714×10^{-8} Btu/hr sq ft $^oR^4$. The area, A, may be considered a unit length of the test specimen (1 inch in diameter, 1 inch long), radiating to the shield. The shape-factor is denoted as F, and the emissivity as ε. The temperature T_α is the average specimen temperature of the unit length, and T_β is the radiation shield temperature.

The term εF is known as the gray-body shape factor and allows for the departure of the radiating surfaces from black-body conditions. Solving for εF gives

$$\varepsilon F = \frac{q_n}{\sigma A (T_\alpha^4 - T_\beta^4)}$$

For the test specimen, q_n represented the radiation heat loss per unit length, determined from Figure E-1. T_α was taken as the mean temperature of a unit length of specimen, and T_β was the approximate temperature of the radiation shield. Since the emissivities of Armco Iron and Aluminum 2024 change only slightly between 200° F ahd 700° F (16), an average value of the gray body shape factor was estimated to be 0.19. Calculation of the heat exchange by radiation for subsequent test data using this gray body shape-factor resulted in radiation losses of no more than 3 percent of the initial heat flux.

The heat losses by conduction through the thermocouple wires were calculated in the manner described by Baker (3). Considering the five internal thermocouples in the heated specimen, the resulting heat loss was less than 0.6 percent of the initial heat flux. Thus, the net heat loss determined from analytical methods was on the order of 3.6 percent of the initial heat flux.

In summary, the initial heat losses for the heater region are 16.7, 21.3, and 27.3 percent for temperatures of 350, 450, and 605° F respectively at the specimen thermocouple nearest the heater. The surface heat losses are 3.0, 3.7, and 4.5 percent for average specimen temperatures of 310, 390, and 515° F.

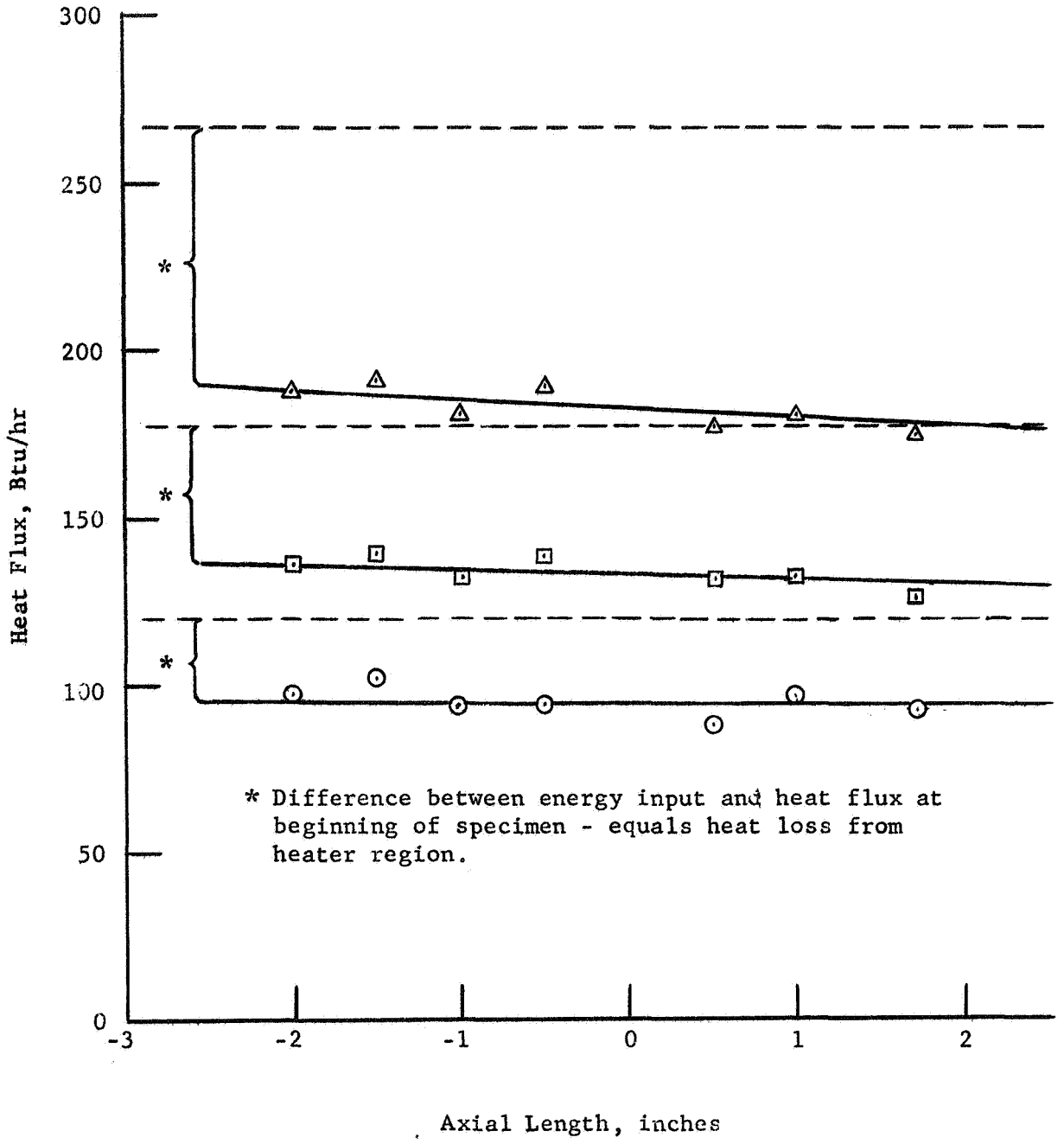

Figure E-1. The Variation of Calculated Heat Flux with Corresponding Specimen Position.

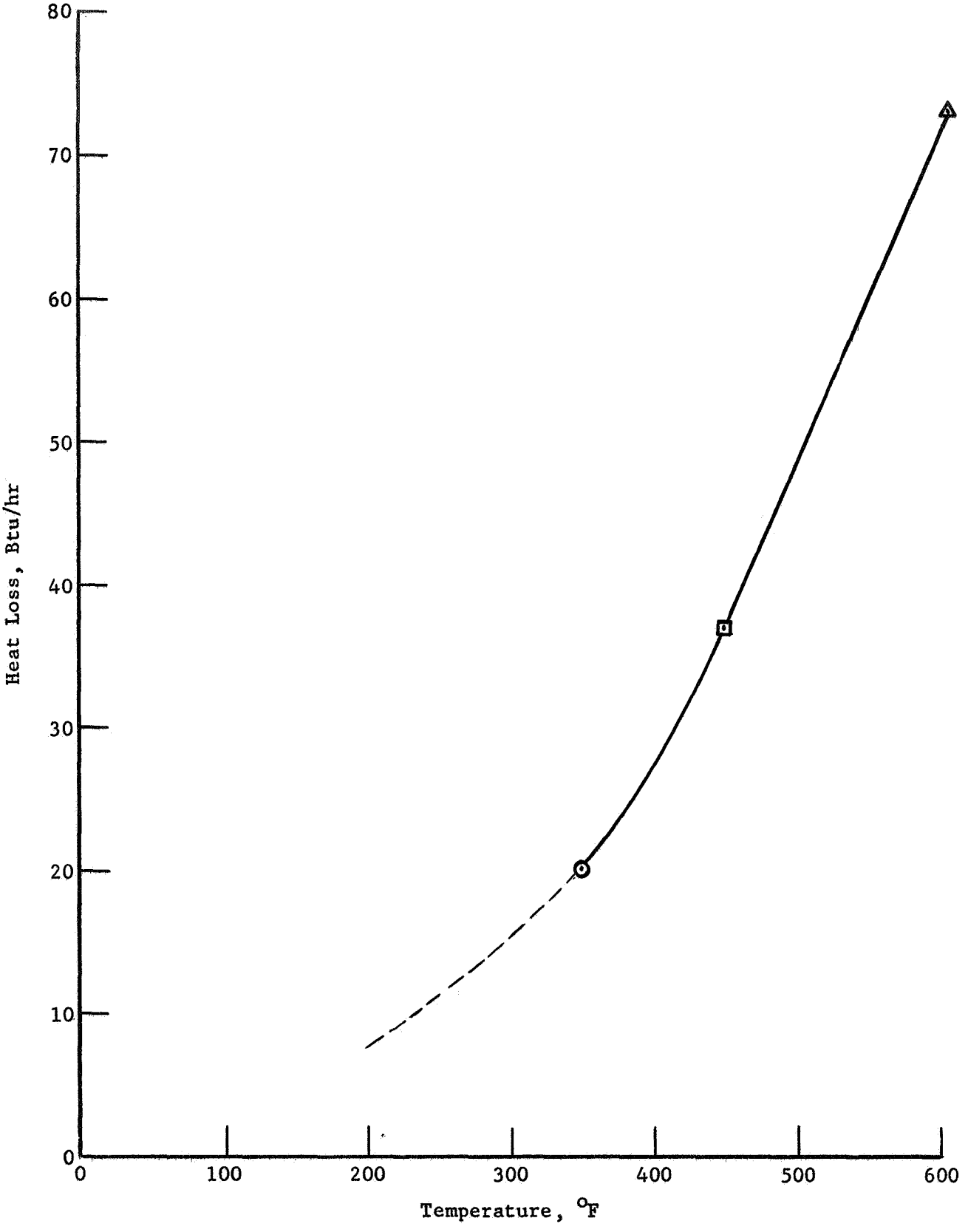

Figure E-2. The Variation of Initial Heat Loss from the Heater with Specimen Temperature.

APPENDIX F

UNCERTAINTY ANALYSIS

The uncertainty in the experimental results was estimated. The thermal contact conductance is

$$h_c = \frac{q/A}{\Delta T_j}$$

where q/A was found by

$$q/A = -k \frac{\Delta T}{\Delta x}$$

The uncertainty, δR, involved in a particular result is given as a percent of the calculated value, R, by the expansion (32)

$$\frac{\delta R}{R} = \left[\left(\frac{\delta X}{X}\right)^2 + \left(\frac{\delta Y}{Y}\right)^2 + \left(\frac{\delta Z}{Z}\right)^2 \right]^{1/2}$$

The delta terms are the uncertainties associated with their respective measured quantities such as temperature or distance. Thus, it was necessary to estimate the uncertainty corresponding to the measured quantities appearing in the above equations.

The temperatures were measured with copper-constantan thermocouples and a Leeds and Northrup 8686 millivolt potentiometer. One-half the smallest scale division on the potentiometer was 2.5 microvolts which corresponds to 0.1°F for the conditions used. According to the Appendix C, the thermocouples were accurate to $\pm$ 0.5°F over the temperature range of interest. Thus, the uncertainty in the temperature was estimated to be 0.6°F.

The temperature gradient for determination of the heat flux was found by taking the difference ,ΔT, in the adjacent temperatures recorded along the specimen and dividing it by the distance, Δx, between the thermocouples used to measure the temperatures. According to the estimated error in

the temperatures, ΔT could have been off by $\pm$ 1.2°F. Several of the runs were plotted on an expanded scale of temperature versus distance along the specimen. Analysis of these temperature gradients indicated that the temperature differences were seldom in error by more than 0.7°F. Thus, the error in ΔT was estimated to be 0.7°F.

Thermocouples were mounted in holes 0.047 inches in diameter placed 0.500 inches apart. The location of the holes was specified to be within $\pm$ 0.001 inches; however, measurements of thermocouple locations were made from X-rays of the specimens (Figure 13). Actual thermocouple locations are listed in Table F-1, indicating an uncertainty of 0.007 inches in Δx.

The thermal conductivity, k, was obtained from a graph of thermal conductivity versus temperature where the smallest scale division of k was 1 Btu/hr sq ft °F (Figure 12). The values of thermal conductivity from which the graph was plotted were experimental results. Therefore, the uncertainty associated with thermal conductivity was estimated to be 2.0 Btu/hr ft °F for the range of interest.

The uncertainty in the heat flux was determined from the following relationships

$$\frac{\delta q/A}{q/A} = \left[\left(\frac{\delta k}{k}\right)^2 + \left(\frac{\delta \Delta T}{\Delta T}\right)^2 + \left(\frac{\delta \Delta x}{\Delta x}\right)^2 \right]^{1/2}$$

$$\frac{\delta q}{q} = \left[\left(\frac{\delta k}{k}\right)^2 + \left(\frac{\delta \Delta T}{\Delta T}\right)^2 + \left(\frac{\delta \Delta x}{\Delta x}\right)^2 + \left(\frac{2\ \delta D}{D}\right)^2 \right]^{1/2}$$

Results of these expressions were found to vary from 2.0 to 5.0 percent.

The temperature difference, ΔT_j, in the thermal conductance equation was determined graphically as depicted in Figure 15. Three graphs, representative of the data, were plotted on an expanded scale where the smallest scale division for temperature was 0.5°F. Points 0.6°F above and below each data point were included to reflect the probable error in the

temperature measurements. The variations in thermocouple location (Table F-1), were included to reflect error in location. Then a line of maximum and a line of minimum feasible slope were drawn through each of the two arrays of points. These four lines were extrapolated to the interface to establish the maximum and minimum probable temperatures for each side of the interface. The maximum temperature difference, ΔT_{max}, was established by taking the average of the difference between the minimum upper and lower interface surface difference, ΔT_{min}, was determined similarly using the maximum upper and lower interface surface temperatures.

The contact conductance was calculated for each maximum and minimum junction temperature difference using the average heat flux. The uncertainty in the contact conductance was then determined as the magnitude of the deviation from the mean value presented in Table II. The uncertainty may be found for the data by locating the junction temperature difference for a given apparent pressure in Figure F-1, and reading the magnitude deviation from Figure F-2.

The uncertainty in the apparent interface pressure is determined from the expression

$$\frac{\delta P_a}{P_a} = \left[\left(\frac{\delta L}{L}\right)^2 + \left(\frac{\delta A}{A}\right)^2 \right]^{1/2}$$

The uncertainty in the load is 5 pounds and the uncertainty in the area results from a 0.001 inch uncertainty in the specimen diameter. Results of this expression vary from 0.7 to 5.6 percent for the range of loads used in this investigation.

In summary for this investigation the uncertainties ranged from 5.0 to 8.9 percent for the heat fluxes and 0.7 to 5.6 percent for the apparent load pressure.

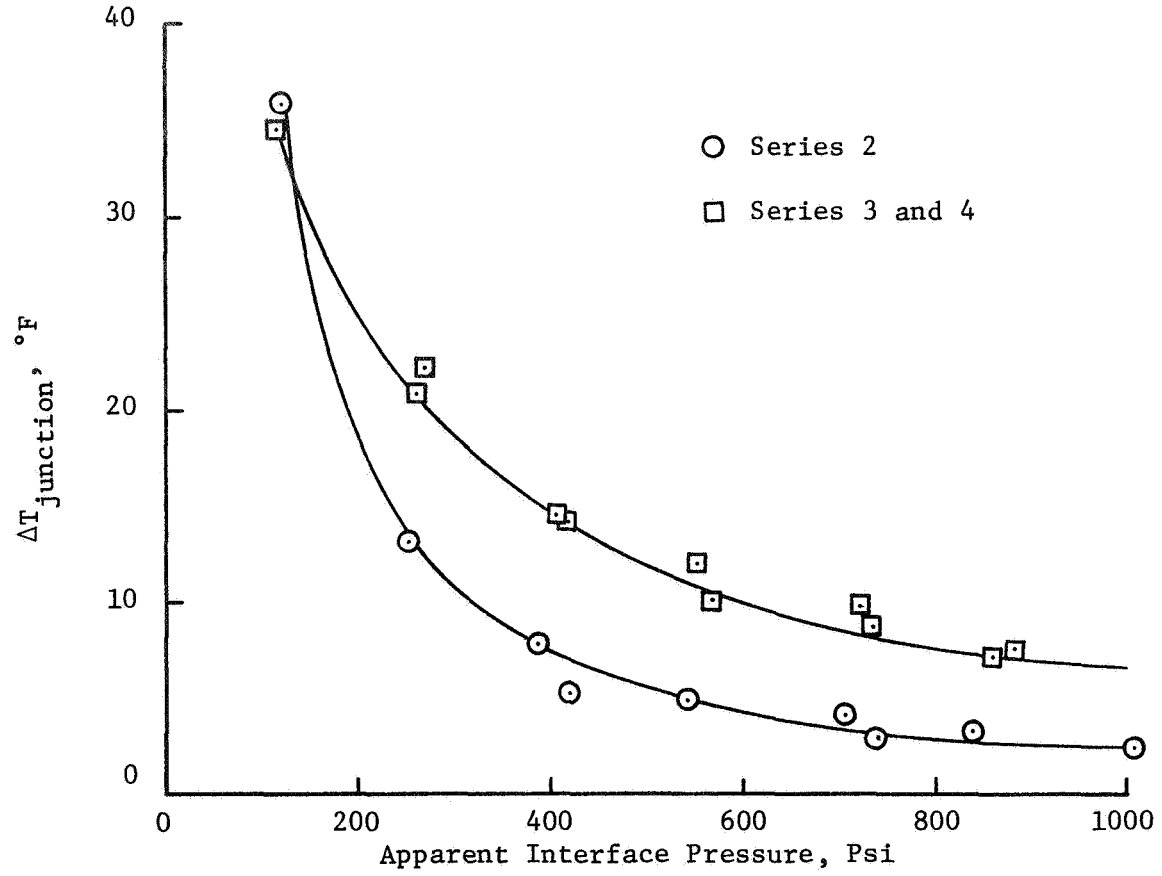

Figure F-1. The Variation of Junction Temperature Difference with Interface Pressure.

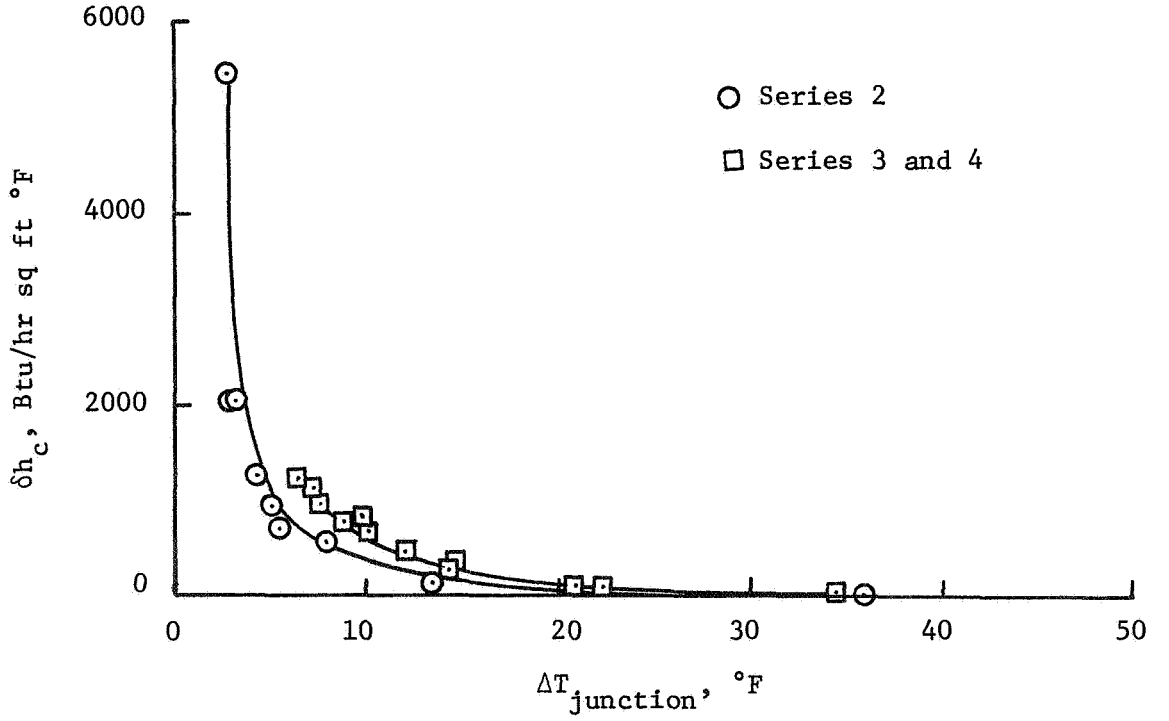

Figure F-2. The Variation of Uncertainty in Contact Conductance with Junction Temperature Difference.

TABLE F-1

MEASURED THERMOCOUPLE LOCATIONS

Specified Distance from Interface	Actual Distance from Interface	
	Source Specimen	Sink Specimen
0.250	0.246	0.245
0.750	0.751	0.745
1.250	1.258	1.253
1.750	1.764	1.742
2.250	2.272	2.248